THE 10TH WORKSHOP OF THE INTERNATIONAL LITHOSPHERE PROGRAM ILP-TASK FORCE ON SEDIMENTARY BASINS

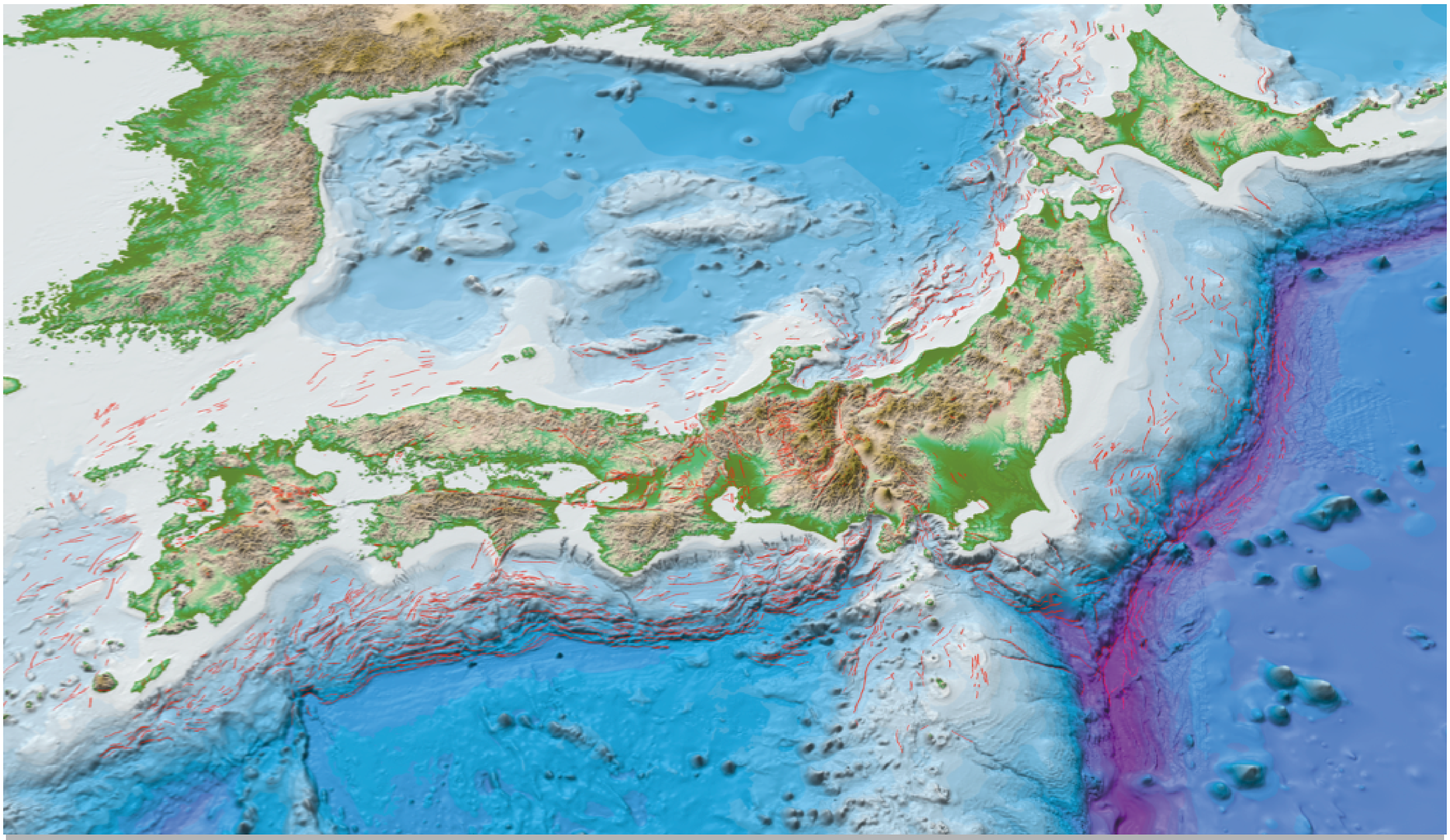

Lithosphere dynamics of sedimentary basins in subduction systems and related analogues

Abstracts with Programme

ILP Sedimentary Basin 2015 Tokyo
5-7 October
http://www.eri.u-tokyo.ac.jp/ILP2015/

Tokyo Geographical Society · JAPT · The Geological Society of Japan · Seismological Society of Japan · Japan Geoscience Union · INPEX · JAPEX · JX Nippon Oil & Gas Exploration · Mitsubishi Corporation Exploration · MODECO · JGI · GEOSYS

ILP Tokyo 2015
Lithosphere dynamics of sedimentary basins in subduction systems and related analogues
5-7 October 2015

Monday, October 5

9:00 Registration
10:00 Opening Remarks
Hiroshi SATO (Organizing Committee, ERI, Univ. Tokyo, Japan)
Kazushige OBARA (Director, ERI, Univ. Tokyo, Japan)

General Session
Chairs: Naoshi HIRATA and Frédéric GUEYDAN

10:10 O-1 Liviu MATENCO and Fadi H. NADER, Introduction on the ILP sedimentary task force science
10:30 O-2 Hiroshi SATO (keynote) , Late Cenozoic basin evolution and active tectonics of Japanese islands
11:00 O-3 Evgueni BUROV (keynote), Alexander KOPTEV, Eric CALAIS, Sylvie LEROY, and Taras GERYA, Interactions between active and passive rifting in ultra-slow extension context: Insights from 3D numerical models
11:30 O-4 Daniel GARCIA-CASTELLANOS, Quantifying the post-tectonic topographic evolution of closed basins: The Ebro basin (northeast Iberia)

11:50 Lunch break

Subduction dynamics: forearc to backarc I
Chairs: Daniel GARCIA-CASTELLANOS and Bill FRY

13:10 O-5 Armin DIELFORDER, Alfons BERGER, Marco HERWEGH, Linking megathrust earthquakes to brittle deformation and mineral vein formation in the paleoaccretionary complex of the central European Alps

13:30 O-6 Yuzuru YAMAMOTO, Shun CHIYONOBU, Nana KAMIYA, Yohei HAMADA, Saneatsu SAITO, Evolution of sedimentary basins and the basement architectures in plate subduction margin: the Miura and Boso peninsulas, central Japan

13:50 O-7 Jeroen SMIT, Jan-Diederik VAN WEES and Sierd CLOETINGH, New Definition for Avalonia's Northern Margin: insights from lower crustal velocities

14:10 O-8 LEWANDOWSKI, M., WERNER, T., VLAHOVIĆ, I., VELIĆ, I., SIDORCZUK, M., Paleomagnetic dating of incipient folding SW of the Sava–Vardar subduction zone (Karst Dinarides, Croatia)

14:30 O-9 Damien BONTÉ, Attila BALÁZS, Jan-Diederik VAN WEES, Sierd CLOETINGH, Thermal regime of back-arc region and geothermal energy

14:50 Coffee break & posters

Subduction dynamics: forearc to backarc II

Chairs: David OKAYA and Akinori HASHIMA

15:10 O-10 Frédéric GUEYDAN (keynote), Gianluca FRASCA and Jean-Pierre BRUN, Miocene tectonics of the Western Mediterranean: From mantle extensional exhumation to westward thrusting in a back-arc settings

15:40 O-11 Shigeki NAKAGAWA, Shin'ichi SAKAI, Ryo HONDA, Hisanori KIMURA, Naoshi HIRATA, Subduction of two oceanic plates beneath Kanto basin imaged by MeSO-net

16:00 O-12 Takeshi SATO, Tetsuo NO, Shuichi KODAIRA, Seiichi MIURA, Tatsuya ISHIYAMA, Hiroshi SATO, Distribution of crustal structure types and its tectonic implications in the southern part of the Japan Sea back-arc basins deduced from the seismic survey

16:20 O-13 Bill FRY, Hiroshi SATO, Tetsuya TAKEDA, Qi-fu CHEN, and Kelin WANG, Ambient noise imaging of the seismically anisotropic lithosphere below the Sea of Japan

16:40 O-14 Akinori HASHIMA, Thorsten W. BECKER, Andrew M.

FREED, Hiroshi SATO, David A. OKAYA, Hisashi SUITO, Hiroshi YARAI, Makoto MATSUBARA, Tetsuya TAKEDA, Tatsuya ISHIYAMA, Takaya IWASAKI, Influence of 3-D elastic heterogeneity on coseismic deformation due to the 2011 Tohoku earthquake

17:00 O-15 O.V. PETROV, S.N. KASHUBIN, E.D. MILSTEIN, A.V. RYBALKA, S.P. SHOKALSKY, M.L. VERBA, E.O. PETROV, Earth's crust model of the South-Okhotsk Basin by wide-angle OBS data

17:20 Posters

Tuesday, October 6

Active tectonics from shallow to deep I

Chairs: Takaya IWASAKI and Yannis PANAYOTOPOULOS

9:00 O-16 Hiroyuki TSUTSUMI, Katsushi SATO, and Atsushi YAMAJI, Late Quaternary stress field in central Japan inferred from the stress inversion of the active fault data and timing of the beginning of the modern stress state

9:20 O-17 Tatsuya ISHIYAMA, Hiroshi SATO, Naoko KATO, Susumu ABE, Permanent deformation in the overriding plate along the Japan Trench in the southern Northeast Japan

9:40 O-18 Makoto MATSUBARA and Hiroshi SATO, High-velocity lower crust along the failed rift with deep Moho

10:00 O-19 Tomoko E. YANO, Tetsuya TAKEDA, Makoto MATSUBARA, and Tatsuhiko SHIOMI, The Japan Unified High-Resolution Relocated Catalog for Earthquakes (JUICE) project for events associated with inland active faults in Japan

10:20 Coffee break & posters

Active tectonics from shallow to deep II

Chairs: Tomoko E. YANO and Hiroyuki TSUTSUMI

10:40 O-20 Takaya IWASAKI, Noriko TSUMURA, Tanio ITO, Hiroshi SATO, Eiji KURASHIMO, Naoshi HIRATA, Kazunori ARITA, Katsumi NODA, Akira FUJIWARA, Susumu ABE, Shunsuke KIKUCHI and Kazuko SUZUKI, Arc-Arc Collision Structure in the Southernmost Part of the Kuril Trench Region- Results from Integrated Analyses of the 1998-2000 Hokkaido Transect Seismic Data -

11:00 O-21 Tanio ITO, Lithospheric structures and their formation process at the northwestern border region of the Izu collision zone, central Japan

11:20 O-22 Yannis PANAYOTOPOULOS, Naoshi HIRATA, Takaya IWASAKI, Shin'ichi SAKAI, Hiroshi SATO, Fault model of the 2014

Northern Nagano earthquake: Moving towards estimation seismic hazard using the MeSO-net stations

11:40 O-23 Noriko TSUMURA, Yuu MIZUI, Tomoko EMOTO, Hiroshi FURUYA, and The Research Group for the Joint Seismic Observations at the Nobi Area, Crustal structure beneath the source region of 1891 Nobi earthquake, central Japan

12:00 Lunch break

Sedimentary and petroleum systems I/ Sedimentary basins from observation to modeling I

Chairs: Jeroen SMIT and Liviu MATENCO

13:20 O-24 Naoufal SAOUD, Mohammed CHARROUD, Said HINAJ, Mohammed DAHIRE, Souhail MOUNIR, Tafilalt Ordovician Iron Formations (IFs) Discovery, Easter Anti Atlas of Morocco: Nomenclature and Classification

13:40 O-25 Bilal U. HAQ (keynote) Inherited Landscapes, Tectonics, Eustasy and Basin Fill

14:10 O-26 Manuel PUBELLIER (keynote), Rifting, Spreading and Inversion in the South China Sea Basin; Map View

14:40 O-27 Fadi H. NADER, Rock-Fluid interactions: Numerical modelling and future perspectives

15:00 Coffee break & posters

Sedimentary basins from observation to modeling II

Chairs: Fadi H. NADER and Hiroshi SATO

15:20 O-28 Liviu MATENCO, Quantifying the evolution of sedimentary basins by coupling sedimentary fluxes with orogenic evolution

15:40 O-29 Christian GORINI (keynote) Messinian Event in the Deep Eastern and Western Mediterranean Sea: Interaction between deep processes and global sea level change

16:10 O-30 Masa KINOSHITA, Tomohiro TOKI, Possible constraints on hydrate dissociation in sedimentary basin: Sedimentation, compaction, deep-source fluid and diffusion

16:30 O-31 Motonori HIGASHINAKA, Susumu ABE, Hiroshi SATO, Tatsuya ISHIYAMA, Naoko KATO, Estimation of pre-Neogene basement in Niigata-area Japan using gravity anomalies and velocity model based on reflection and refraction seismic surveys

16:50 O-32 Susumu ABE, Motonori HIGASHINAKA, Hiroshi SATO, Tatsuya ISHIYAMA, Strategic seismic data processing for extraction of deep crustal reflectors through reconstructed velocity heterogeneity

17:10 Posters

Wednesday, October 7

Sedimentary basins from observation to modeling II/
East, SE Asia geology I
Chairs: Manuel PUBELLIER and Anne VAN HORNE

9:30 O-33 M. THIBAUT, I. FAILLE, F. WILLIEN, Advanced workflows for fluid transfer in faulted basins
9:50 O-34 Fadi H. NADER, Challenges of the Levant Basin: a typical example of frontier, off-shore, deep-water hydrocarbon basins
10:10 O-35 Tanio ITO (keynote) , Satoshi YAMAKITA and Hiroshi SATO, The Japanese island arc: geological structures and its formation processes

10:40 Coffee break & posters

11:00 O-36 Francesco ARBOIT, Khalid AMROUCH, Alan S. COLLINS, Rosalind KING and Christopher MORLEY, Determination of the tectonic evolution from fractures, faults and calcite twins on the south-western margin of the Indochina Block

11:20 Concluding remarks

11:40 Lunch break

Posters

P-1 Francesco ARBOIT, Alan S. COLLINS, Christopher MORLEY, Rosalind KING and Khalid AMROUCH, Detrital zircon age, Hf isotopic analysis and tectonic reconstruction of the Khao Khwang Fold-Thrust Belt, south-western margin Indochina terrane, central Thailand
P-2 Francesco ARBOIT, Khalid AMROUCH, Alan S. COLLINS, Rosalind KING and Christopher MORLEY, Determination of the tectonic evolution from fractures, faults and calcite twins on the south-western

margin of the Indochina Block

P-3 Nana KAMIYA, Yuzuru YAMAMOTO, Takato TAKEMURA, Deformation and paleo-geothermal structure of the Neogene forearc basin in the Boso Peninsula, central Japan

P-4 Anne VAN HORNE, Hiroshi SATO, Tatsuya ISHIYAMA, Naoko KATO, The problem with the plate boundary in the Sea of Japan

P-5 Makoto OTSUBO, Ayumu MIYAKAWA, Migration of active contractional deformation estimated from fold topographic developments along the eastern margin of the Japan Sea, northeast Japan

P-6 Ayumu MIYAKAWA, Makoto OTSUBO, Evolution of fault activity in the northeast–central Japan: Insights from crustal stress and fault orientations

P-7 Naoko KATO, Hiroshi SATO, Tatsuya ISHIYAMA, Active fault and fold systems from shallow to deep in the eastern part of Niigata basin, central Japan

P-8 Koichi YAMAUCHI, Masahiro ISHIKAWA, Hiroshi SATO, Takaya IWASAKI, Tsuyoshi TOYOSHIMA, Crust composition in the Hidaka Metamorphic Belt estimated from seismic velocity by measurements under the high P-T condition

P-9 Dong-Lim CHOI, High-resolution sequence stratigraphy of the subaqueous Nakdong Delta on the Korea Strait shelf during the Holocene transgression

O-2 Late Cenozoic basin evolution and active tectonics of Japanese islands

Hiroshi SATO

ERI, The University of Tokyo, Tokyo, Japan

1. Introduction

Late Cenozoic basin evolution, active tectonics and lithospheric structure of Japanese islands are strongly controlled by major tectonic events produced by movements of subducting slabs beneath Japanese island arcs. Lithospheric structure of Japanese islands has been revealed by recent seismic profiling using controlled source and earthquake tomography. In this paper, we introduce the new view of the late Cenozoic basin development and active tectonics based on the updated geophysical data.

2. Geological setting

Japanese islands are geologically divided into two parts (Fig. 1): NE Japan presently overriding the subducting Pacific plate (PAC: ca. 140 Ma) and SW Japan, overriding the subducting Philippine Sea plate (PHS). The subducting PHS along the Nankai trough consists of the Izu-Bonin arc and Shikoku basin. The Shikoku basin is a young (27 -15 Ma) backarc basin. Reflecting the age (and/or rate) of subducting plate, NE Japan arc shows narrower onshore width of pre-Neogene rocks. The Izu-Bonin arc is colliding with Honshu arc in the central part forming the Izu collision zone, where the upper crust of the Izu-Bonin arc has been stacked into the Honshu crust. The young PHS slab beneath SW Japan shows corrugate geometry (eg. Hirose *et al.*, 2008). The PHS subducts on the PAC and beneath the Kanto basin (Tokyo metropolitan area), PHS hit the PAC and producing unique slab-slab interaction (eg. Wu *et al.*, 2007).

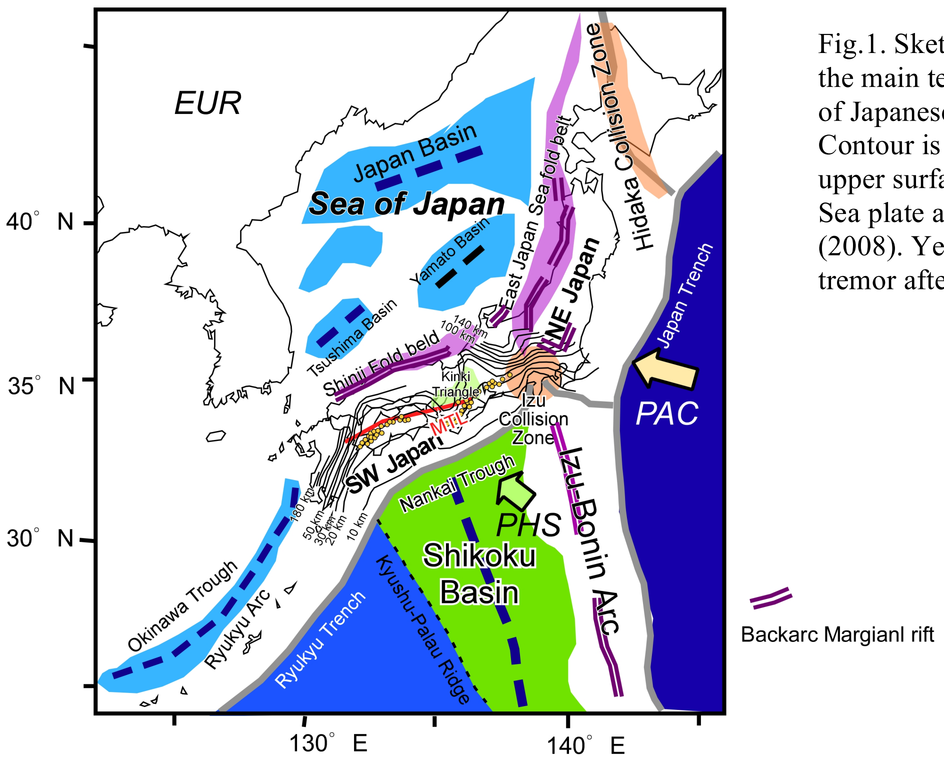

Fig.1. Sketch map showing the main tectonic features of Japanese a (Sato, 2014). Contour is depth to the upper surface of Philippine Sea plate after Hirose *et al.* (2008). Yellow circle is tremor after Obara (2002).

3. Late Cenozoic geologic evolution of Japanese islands

Formation of the Sea of Japan is large tectonic event, gave greatest impact on the structure and active tectonic features of Japanese islands (Fig. 2). Before the opening of the Sea of Japan, Japanese island arc forms almost strait geometry. Basic mode of rifting and opening was so called "double door opening" (Otofuji et al., 1994), namely, counterclockwise rotation of NE Japan and clockwise rotation of SW Japan. After the major opening the Sea of Japan, backarc marginal rift zone (Fig. 1) was developed along the southeastern margin of the Sea of Japan. These are failed rift zone, commonly 5-km-thick basin-fill accumulated on the mafic dominant crust. Between NE and SW Japan blocks, clockwise and counter clockwise rotation produced complicated rifting structures in Kanto area (Fig. 3). The opening of the Sea of Japan terminated by the collision of IBM arc system at the Izu collision zone. Soon after the termination of opening, the young Shikoku basin was hard to subduct along the Nankai trough (Kimura et al., 2005), the Shinji fold belt along the BMR located in the southern part of the Sea of Japan coast was developed in the late Miocene due to strong coupling along the Nankai trough. Along the axial part of Hokkaido, the Hidaka Mountains have been developed by EW trending conversion since the Middle Miocene, produced arc-arc collision with NE Japan and Kuril arcs. The change in the direction of the motion of PHS at 1 Ma produced major change in stress regime from NS compression to EW compression and triggered many geological events, such as the change of sense of displacement form reverse to right-lateral movement of the Median Tectonic Line (Sato et al., 2015).

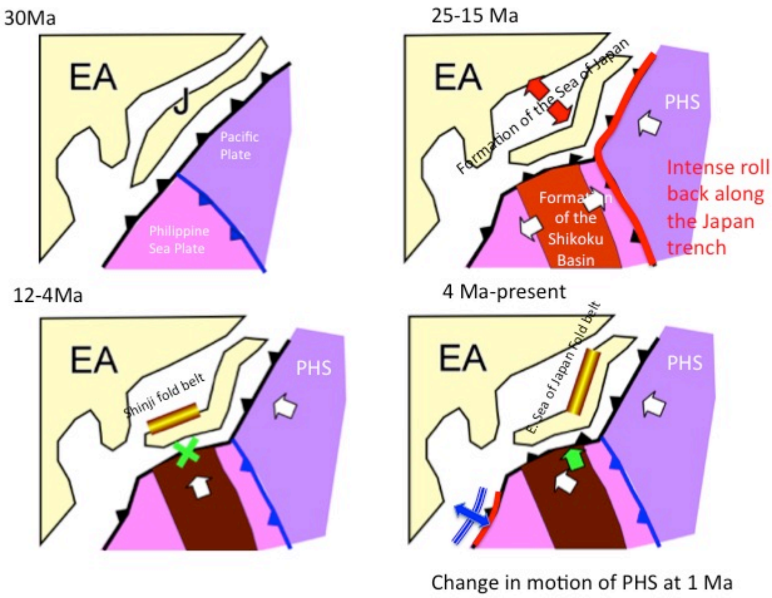

Fig. 2. Sketch map of Tectonic evolution of Japanese islands.

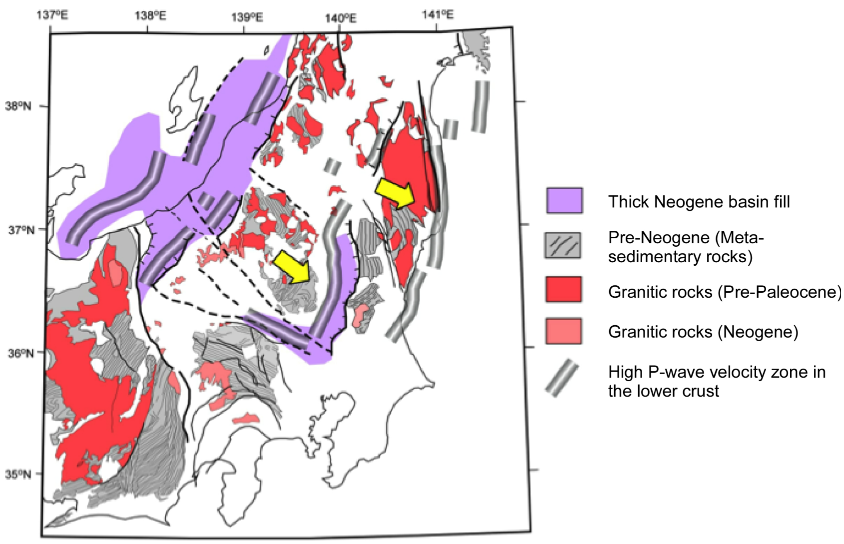

Fig. 3. Distribution of backarc rift systems in central Honshu during the opening of the Sea of Japan (Sato, 2014). Yellow arrow: direction of tectonic movement, Velocity structure of the lithosphere is after Matsubara and Obara (2011).

4. Shortening deformation along a backarc marginal rift

Late Cenozoic deformation zones in Japan may be divided into two types: (1) arc-arc collision zones like those of Izu and the Hokkaido axial zone, and (2) reactivated back-arc marginal rift (BMR) systems (Fig. 1). A BMR develops during a secondary rifting event that follows the opening of a back-arc basin. It forms close to the volcanic front and distant from the spreading center of the basin. In Japan, a BMR system developed along the Sea of Japan coast following the opening of the Japan Sea. The BMR appears to be the weakest, most deformable part of the arc back-arc system. When active rifting in the marginal basins ended, thermal subsidence, and then mechanical subsidence related to the onset of a compressional stress regime, allowed deposition of up to 5 km of post-rift, deep-marine to fluvial sedimentation. Continued compression produced fault-related folds in the post-rift sediments, in thin-skin style deformation. Shortening reached a maximum in the BMR system compared to other parts of the back-arc, suggesting that it is the weakest part of the entire system. We examined the structure of the BMR system using active source seismic investigation and earthquake tomography (Fig. 4). The velocity structure beneath the marginal rift basin shows higher P-wave velocity in the upper mantle/lower crust which suggests significant mafic intrusion and thinning of the upper continental crust. The syn-rift mafic intrusive forms a convex shape, and the boundary between the pre-rift crust and the mafic intrusive dips outward (Fig. 5). In the post-rift compressional stress regime, the boundary of the mafic body reactivated as a reverse fault, forming a large-scale wedge thrust and causing further subsidence of the rift basin. The driver of the intense shortening event along the Sea of Japan coast in SW Japan was the arrival of a buoyant young (15 Ma) Shikoku basin at the Nankai Trough. Subduction stalled and the backarc was compressed. As the buoyant basin cooled, subduction resumed, and the rate of shortening in the marginal rift decreased. The Izu collision zone provides another example of BMR deformation where a BMR zone that formed behind the Izu-Bonin arc was strongly deformed during collision, creating an asymmetric structure around the Izu-Bonin indenter. Localization of intense deformation in the BMR zone again suggests it is the weakest part of the system.

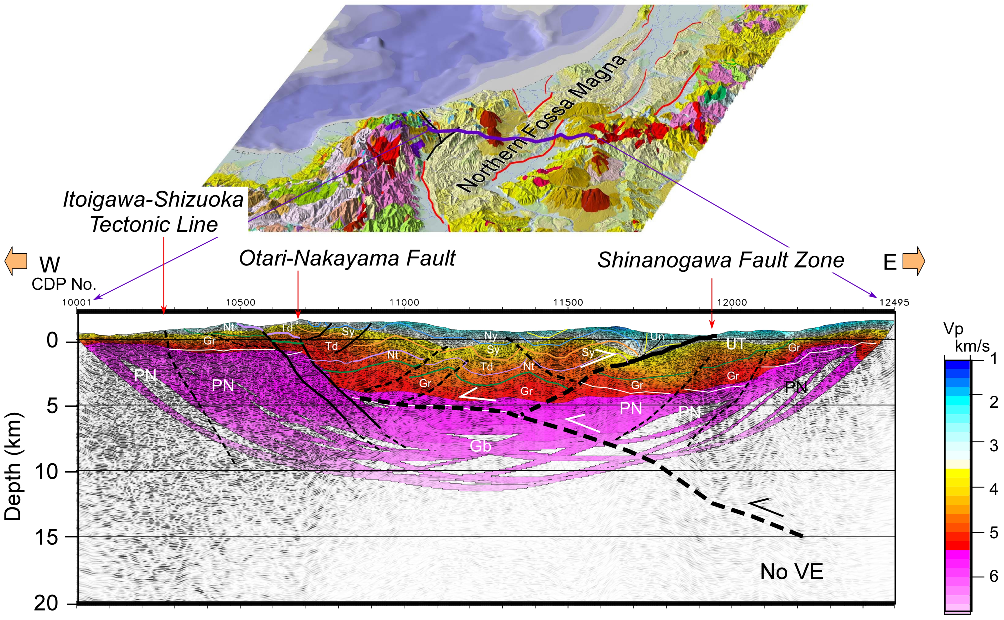

Fig. 4 Deep seismic profiling across the northern Fossa magna, failed rift (Sato, 2013).

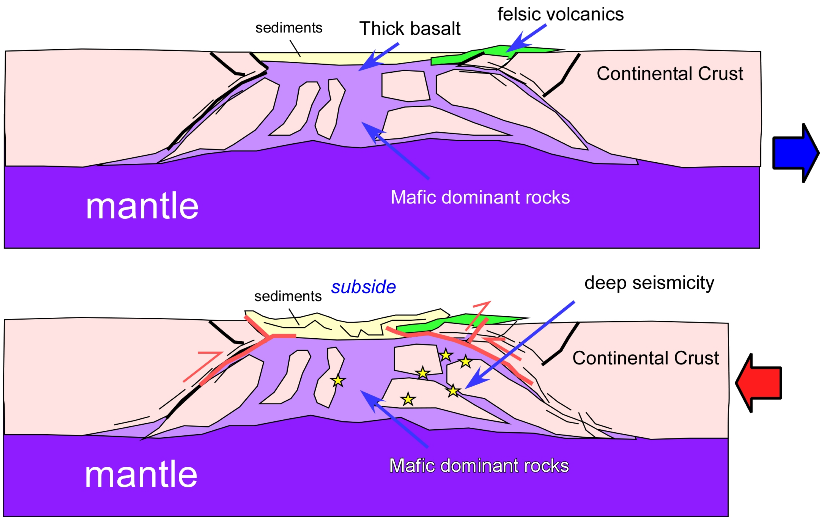

Fig. 5. Schematic diagram of the formation and shortening deformation of the aborted rift in the Niigata and northern Fossa magna (Sato, 2013).

References

Hirose, F. et al., Jour. Geophys. Res., 113, B09315, doi:10.1029/2007JB005274, 2008.

Kimura, J. et al. GSA Bulletin, 117, 969-986; doi:10.113/B25565.1, 2005.

Matsubara, M. and Obara, K., *EPS*, **63**, 663-667, 2011.

Obara, K., *Science,* **296,** 1679–1681, 2002.

Otofuji, Y. et al., *Earth and Planetary Science Letters*, **121**, 503–518, 1994.

Sato, H. et al., *Tectonophysics*, **644-645**, 58-67, 2015.

Sato, H., *The Coordinating Committee for Earthquake Prediction bulletin,* **92**, 431-433, 2014.

Sato, H., *The Coordinating Committee for Earthquake Prediction bulletin,* **90**, 516-520., 2013.

Wu, F. et al., *Geophys. Res. Lett.*, **34**, L18301, doi:10.1029/2007GL030763, 2007.

O-3 **Interactions between active and passive rifting in ultra-slow extension context: Insights from 3D numerical models**

Evgueni Burov (1,2), Alexander Koptev (1,2), Eric Calais (3,4), Sylvie Leroy (1,2), and Taras Gerya (5)

(1) Sorbonne Universités, UPMC Univ Paris 06, UMR 7193, Institut des Sciences de la Terre Paris (iSTeP), F-75005 Paris, France, (2) CNRS, UMR 7193, Institut des Sciences de la Terre Paris (iSTeP), F-75005 Paris, France, (3) Ecole Normale Supérieure, Dept. of Geosciences, PSL Research University, Paris, France, (4) CNRS, UMR 8538, Paris, France, (5) ETH-Zurich, Institute of Geophysics, Sonnegstrasse 5, 8092 Zurich, Switzerland

We reconsider previous ideas on the role of active and passive rifting processes for rifting style and basin evolution. We argue that complex brittle-ductile rheological stratification of the continental lithosphere modifies its response over the zones of plume-lithosphere interactions, converting large-scale plume-induced impact to multi-harmonic short-wavelength undulations and strain localizations that are largely controlled by far-field stresses (‘active/passive’ rifting scenario). We study these interactions using new ultra-high resolution 3D models incorporating a rheologically realistic lithosphere, phase changes and partial melting. Results demonstrate that dynamic topography in the “real” Earth exhibits strongly asymmetric small-scale 3D features, which include rifts, flexural flank uplifts and complex fault structures. We conclude from our modeling that localization of large-scale linear normal and strike-slip faults in rifted zones can be triggered and maintained by mantle flow that impacts on the base of a pre-stressed lithosphere, so that the final state of the rifted lithosphere is an indicator of the far-field stress at the time the plume arrived (Figure 1). This suggests efficient mechanism for continental rift initiation and breakup that involves passive and active rifting processes that interact with each other resulting in development of large continental rifts (e.g., Afar, Golf of Aden, Dead Sea, Baikal or East-African rift and plate-scale strike-slip faults (e.g. North-Anatolian fault). We show also that there is a significant difference in the impact of the rheological profile on rifting style in the case of dominant active rifting compared to dominant passive rifting (Figure 2). Narrow rifting, conventionally attributed to cold strong lithosphere in passive rifting mode, may develop in weak hot ultra-stretched lithosphere during active rifting, after plume impingement on a tectonically pre-stressed lithosphere. In that case, initially ultra-wide small-amplitude rift patterns focus, in few Myr, in large-scale faults that form a narrow rift. Also, wide rifting may develop during ultra-slow spreading of strong lithosphere, and “switch” to the narrow rifting upon plume impingement.

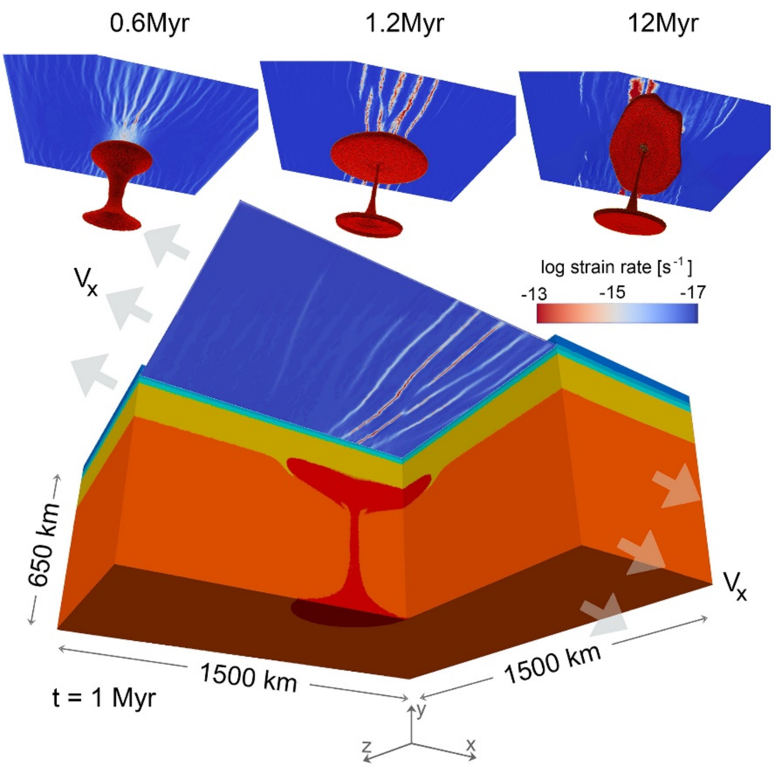

Figure 1. Combination of active-passive rifting results in fast localization of deformation

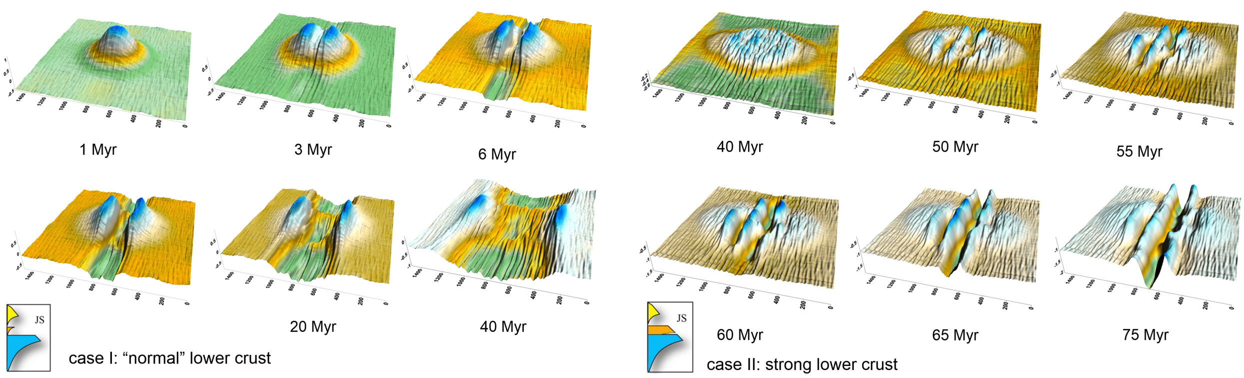

Figure 2. Surface topography in case of "normal" (left) and "strong" lower crustal composition (all other model parameters are indentical).

To further understand the mechanisms behind the interactions between the close field and far-field processes in case of realistic horizontally heterogeneous lithosphere, we have tested our models on the case of the Central East African Rift (CEAR).

This rift, lying south of the Ethiopian Rift Valley, bifurcates in two branches (eastern, magma-rich and western, magma-poor) that surround the strong Tanzanian craton. Intensive magmatism and continental flood basalts are largely present in many of the eastern rift segments, but other segments, first of all the western branch, have only very small volumes of volcanic rock. Within the Eastern rift characterized by southward progression of the onset of volcanism, the overall extension and topographic expression of the rift varies significantly from north to south: in northern Kenya the area of deformation is very wide (some 150-250 km in E-W direction), towards the south the rift narrows to 60-70 km, but further south this localized deformation is changed back into a wide deformation zone in the so-called Tanzania divergence. Widening of the Eastern branch within its southern part is associated with the impingement of the southward-propagating rift on a strong lithospheric domain of Masai block situated to east of the Tanzanian craton.

The preferred model has a plume seeded slightly to the northeast of the craton center, consistent with seismic tomography, and produces surface strain distribution that is in good agreement with observed variation of deformation zone width along eastern side of Tanzanian craton: localized above bulk of mantle material deflected by cratonic keel narrow high strain zone (Kenia Rift) is replaced by wide distributed deformations within areas situated to north (northern Kenya, Turkana Rift) and to south (Tanzania divergence, Masai block) of it.

These results (Figure 3) confirm a significant difference in the impact of the rheological profile on rifting style in the case of dominant active rifting compared to dominant passive rifting. Narrow rifting, conventionally attributed to cold strong lithosphere in passive rifting mode, may develop in weak hot ultra-stretched lithosphere during active rifting, after plume impingement on a tectonically pre-stressed lithosphere. In that case, initially ultra-wide small-amplitude rift patterns focus, in few Myr, into large-scale faults that form a narrow rift.

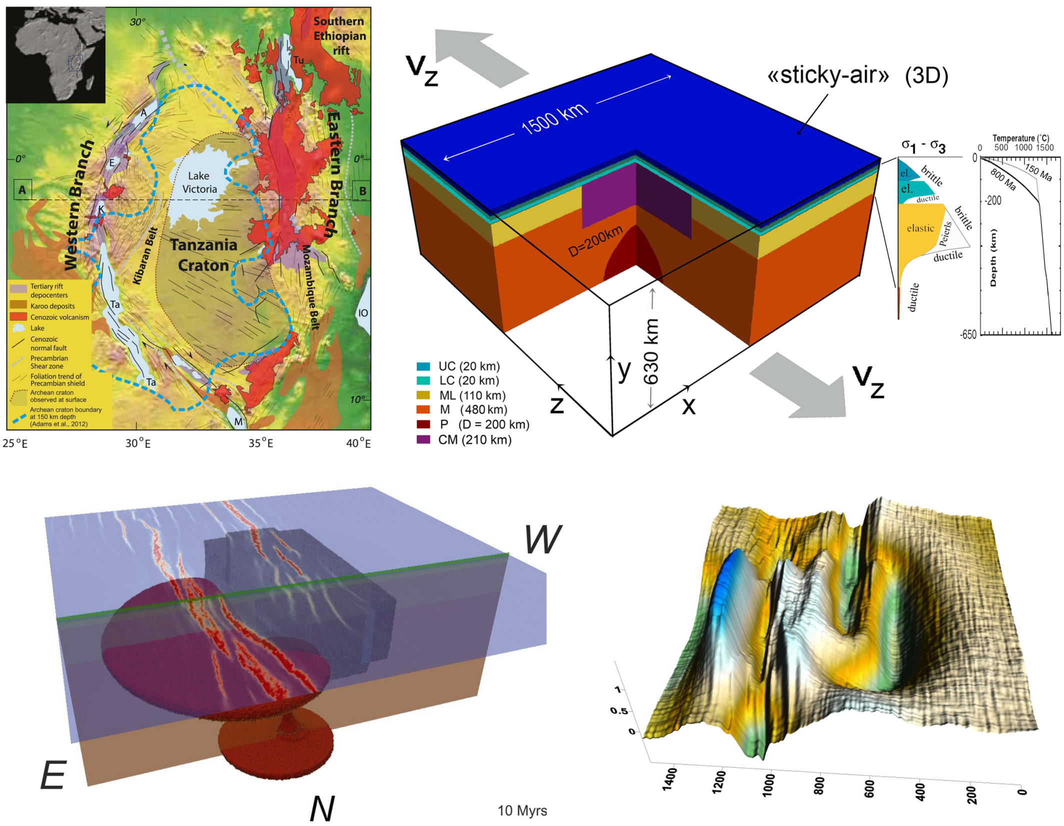

Figure 3. Application of the model to the case of CEAR. In this experiment, mantle upwelling is initialized below the a strong lithospheric heterogeneity presented by the Tanzania craton, in presence of slow (3 mm/y) passive far-filed extension in WE direction. As result mantle plume material is deviated towards one side of the craton producing a magmatic Eastern rift branch and practically amagmatic Western rift branch.

O-4 **Quantifying the post-tectonic topographic evolution of closed basins: The Ebro basin (northeast Iberia)**

Daniel Garcia-Castellanos

ICTJA-CSIC, Barcelona

Abstract:

Closed (endorheic) sedimentary basins are key recorders of the climatic, erosional, and tectonic history of their surrounding topography, playing an active role in its evolution by changing the local geomorphological base level. When these basins become exorheic, the accelerated incision along the new fluvial network can excavate excellent stratigraphic outcrops, but this often removes the uppermost infill, and essential information about the late basin history is lost. We propose estimating the opening age and past elevation of captured closed basins by combining the flexural isostatic compensation of the eroded volume with available constraints on sediment age. We use this method to constrain the post-tectonic evolution of the Cenozoic Ebro Basin in northeast Iberia. The similar results obtained for four dated stratigraphic columns show the robustness of the model and date the basin opening at 12.0–7.5 m.y. ago, with a maximum paleoelevation of the basin of 535–750 m. The isostatic rebound associated to basin erosion, up to 630 m in the center of the basin, may explain the absence of a canyon excavated by the Ebro River during the Mediterranean sea-level fall associated to the Messinian salinity crisis.

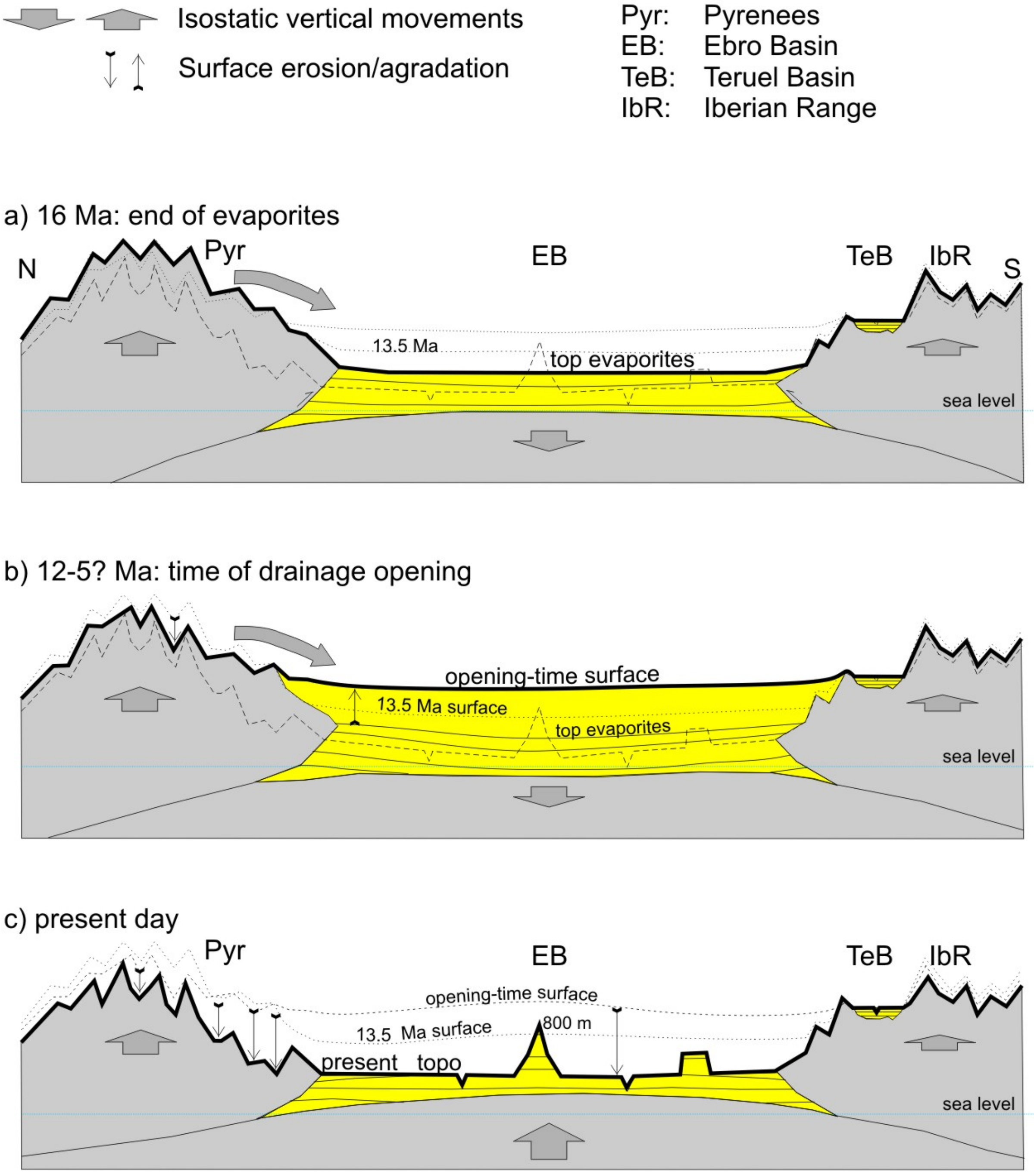

Figure 1. To determine the age of drainage opening we balance the basin volume eroded after the overfilling (between stages B and C) with the corresponding isostatic vertical motions and the sedimentation rate. A: The infilling stage when the dated stratigraphic section is being deposited in the endorheic basin. Pyr—Pyrenees; IbR—Iberian Range; B: Maximum basin infill at time *t*max when it reaches the maximum elevation and drainage opens. Dashed line shows restored position of the present topography. C: Present stage of the partially eroded and isostatically rebounded basin. The dotted line shows the present imaginary position of the surface at maximum infill.

O-5 Linking megathrust earthquakes to brittle deformation and mineral vein formation in the paleoaccretionary complex of the central European Alps

Armin Dielforder[,a], Alfons Berger[a], Marco Herwegh[a]*

[a] *Institute of Geological Sciences, University of Bern, Baltzerstrasse 1+3, CH-3012 Bern, Switzerland*

[*] *armin.dielforder@geo.unibe.ch*

Geodetic and seismological data recorded at active subduction zones suggest that megathrust earthquakes induce transient stress changes in the upper plate, which shift the wedge into an unstable state and trigger >M_w 6 aftershocks. These stress changes have, however, never been linked to geological structures that are preserved within fossil accretionary wedges, although plate interfaces of palaeo-subduction zones have been studied. The conditions under which accretionary wedges fail have therefore remained controversial. Here we show that faulting and associated vein formation in the palaeo-accretionary complex of the central European Alps record stress changes generated by the subduction earthquake cycle. Our data integrate wedge deformation over millions of years but still demonstrate the dominance of specific fracture modes at different depths within the wedge (**Fig. 1**). By combining our field observations with geochemical data (Sr, C, O), temperature constraints, and a dynamic Mohr-Coulomb wedge model (Wang and Hu, 2006), we show that early veins formed at shallow levels by bedding parallel slip during coseismic compression of the outer wedge (**Fig. 1, 2**). In contrast, subsequent vein formation occurred by normal faulting and extensional fracturing at deeper levels in response to coseismic extension of the inner wedge. Our study shows how mineral veins can be used to reveal the dynamics of outer and inner wedges, which response in opposite ways to megathrust earthquakes by compressional and extensional faulting, respectively (**Fig. 2**). We note, that coseismic fracturing implicates an increase in permeability within the hanging wall of megathrusts. Understanding how fractures are generated throughout the subduction earthquake cycle is therefore essential to better contstrain the nature of postseismic fluid flow and to assess the seismic hazard of hydraulically driven aftershocks.

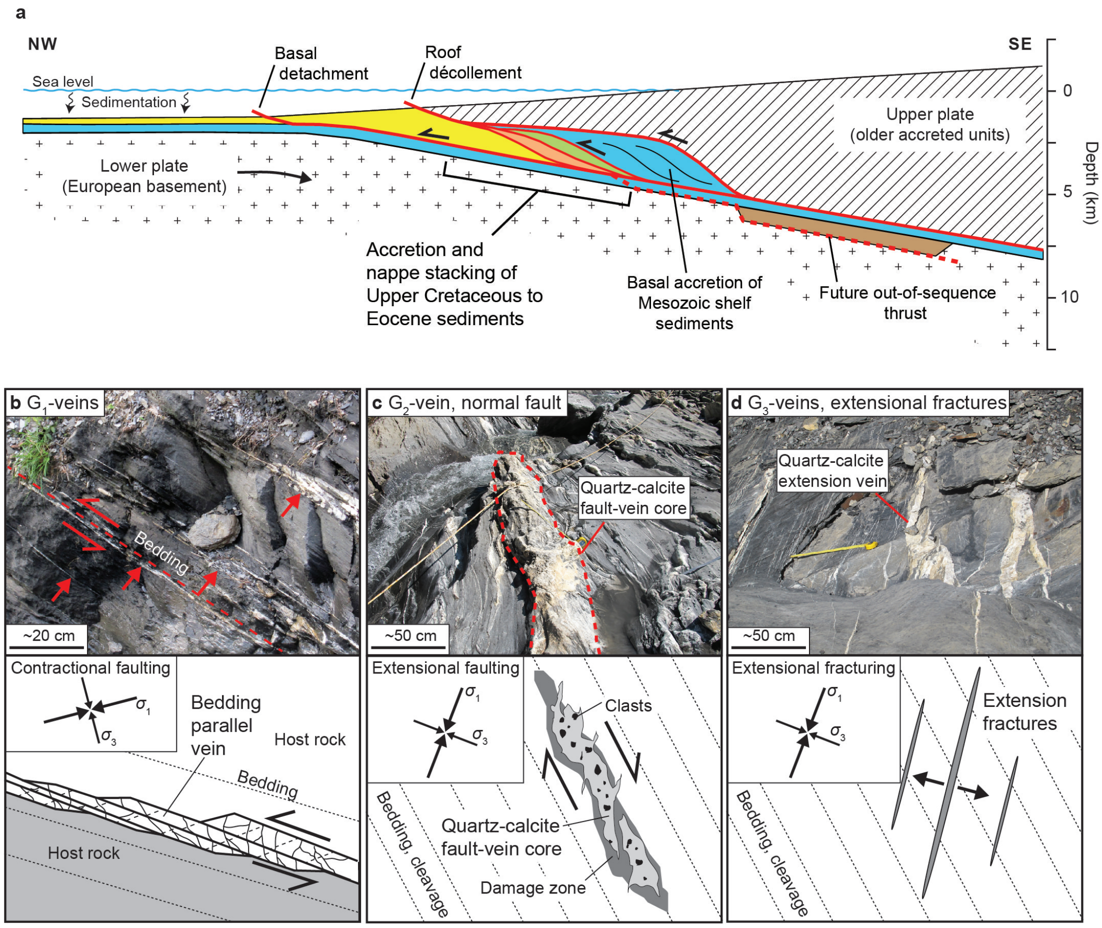

Figure 1: (a) Schematic reconstruction of the Alpine accretionary wedge in Eocene times (~40 Ma) showing the accretion of Upper Cretaceous to Eocene foreland basin deposits. The accreted sediments are buried due to activity along the roof decollement. Depths are rough estimates. Not to scale. **(b-d)** Field examples and sketches of mineral veins. **(b)** The first group of mineral veins (G_1-veins) were formed by bedding parallel shear and records contractional faulting within the wedge. **(c,d)** Later stages of vein formation (G_2- and G_3-veins) record extensional faulting (normal faulting) and extensional fracturing within the wedge. Modified from Dielforder et al. (2015).

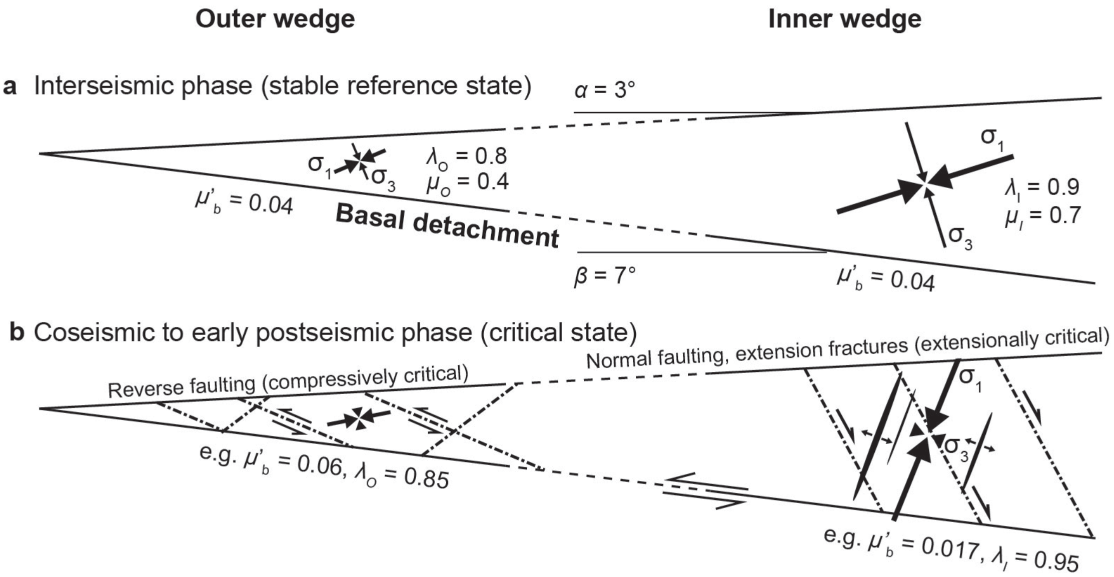

Figure 2: State of stress in a uniform cohesive wedge obtained by the dynamic Mohr Coulomb wedge model (Wang and Hu, 2006). **(a)** During the interseismic reference phase the outer and inner wedge remain stable. **(b)** During megathrust earthquakes the strength of the basal detachment below the outer wedge increases shifting the wedge into a compressively critical state and causing reverse faulting. Below the inner the wedge the strength of the basal detachment decreases. The inner wedge becomes extensionally critical causing extensional faulting within the wedge. *α* and *β* = slope angle and basal dip, respectively, μ'_b = effective coefficient of basal friction, *λ* = pore fluid pressure ratio. Subscripts *o* and *i* denote outer and inner wedge, respectively. Modified from Dielforder et al. (2015).

Dielforder, A. *et al*. Linking meganthrust earthquakes to brittle deformation and in a fossil accretionary complex. Nature Communications 6:7504, doi: 10.1038/ncomms8504 (2015).

Wang, K., Hu, Y. Accretioanry prisms in subduction earthquake cycles: The theory of dynamic Coulomb wedge. Journal of Geophysical Research 111 B06410, doi:10.1029/2005JB004094 (2006).

O-6 **Evolution of sedimentary basins and the basement architectures in plate subduction margin: the Miura and Boso peninsulas, central Japan**

Yuzuru Yamamoto, Shun Chiyonobu, Nana Kamiya, Yohei Hamada, Saneatsu Saito

Department of mathematical science and advanced technology, JAMSTEC

The Miura and Boso area, central Japan where the eastern end of the Philippine Sea Plate has been subducting beneath the North American Plate is a unique example representing plate-subduction controlled basin evolution. A simultaneous evolution of accretionary wedges/covered trench-slope basin systems and huge forearc basin capacity occurred since Middle Miocene.

The geologic architecture on the Miura and Boso area is broadly divided into two categories by existing the Hayama-Mineoka ophiolite: forearc basin in the north, and accretionary complexes and their slope cover sediments in the south. The ophiolite corresponds to the trench-slope break which divides forearc basin from the accretionary complex. The accretionary complex was subdivided into two parts: the Early to Middle Miocene Hota accretionary complex buried 2-4 km (paleomaximum temperature was estimated about 70-90 ˚C), and the Late Miocene to Early Pliocene Miura-Boso accretionary prism buried less than 1 km (about 20 ˚C). The former is composed of hemipelagic sediments and trench-fill turbidite, whereas the latter consists of volcaniclastics and hemipelagic sediments. The volcaniclastics has been derived from the Izu-Bonin island arc since Late Miocene: it moved to the present position about 12-13 Ma. Therefore, these two accretionary complexes correspond to accretionary complexes formed before and after starting Philippine Sea Plate subduction in this area. The older complex thrust up above the younger one to make an out-of sequence thrust (OST; Ishido thrust). Several other OST also developed in the older complex and represent the accretionary complex overlie the trench-slope sediments.

Several trench-slope basin sediments cover both complexes. The slope sediments on the older accretionary complex accumulated since 15 Ma and continue at least to about 7 Ma. On the other hand, the younger accretionary complex in the south was overlain by younger slope sediments since 4.2 Ma and continue to Holocene.

The forearc basin, north of the trench-slope break, start to develop since 15 Ma, approximately correspond to the timing of the Hota accretionary complex formation. Attitude of the bedding planes near the southern basin rim represent E-W trending and near-vertical steep dipping. They are generally getting to be gentler to the north, reach to subhorizontal dipping (<15˚). This means that southern rim of the forearc basin were uplifted leading to formation of much larger basin capacity. Around 3Ma, soon after starting the younger Miura-Boso accretionary prism formation, the forearc basin were deformed and eroded to make an angular unconformity, Kurotaki Unconformity. The formation of the younger accretionary complex and this unconformity was potentially due to the change of the Philippine Sea Plate convergent direction from north to NW. We show the systematic correspondence between the accretionary complexes formation and evolution of sedimentary basins in the plate subduction margin.

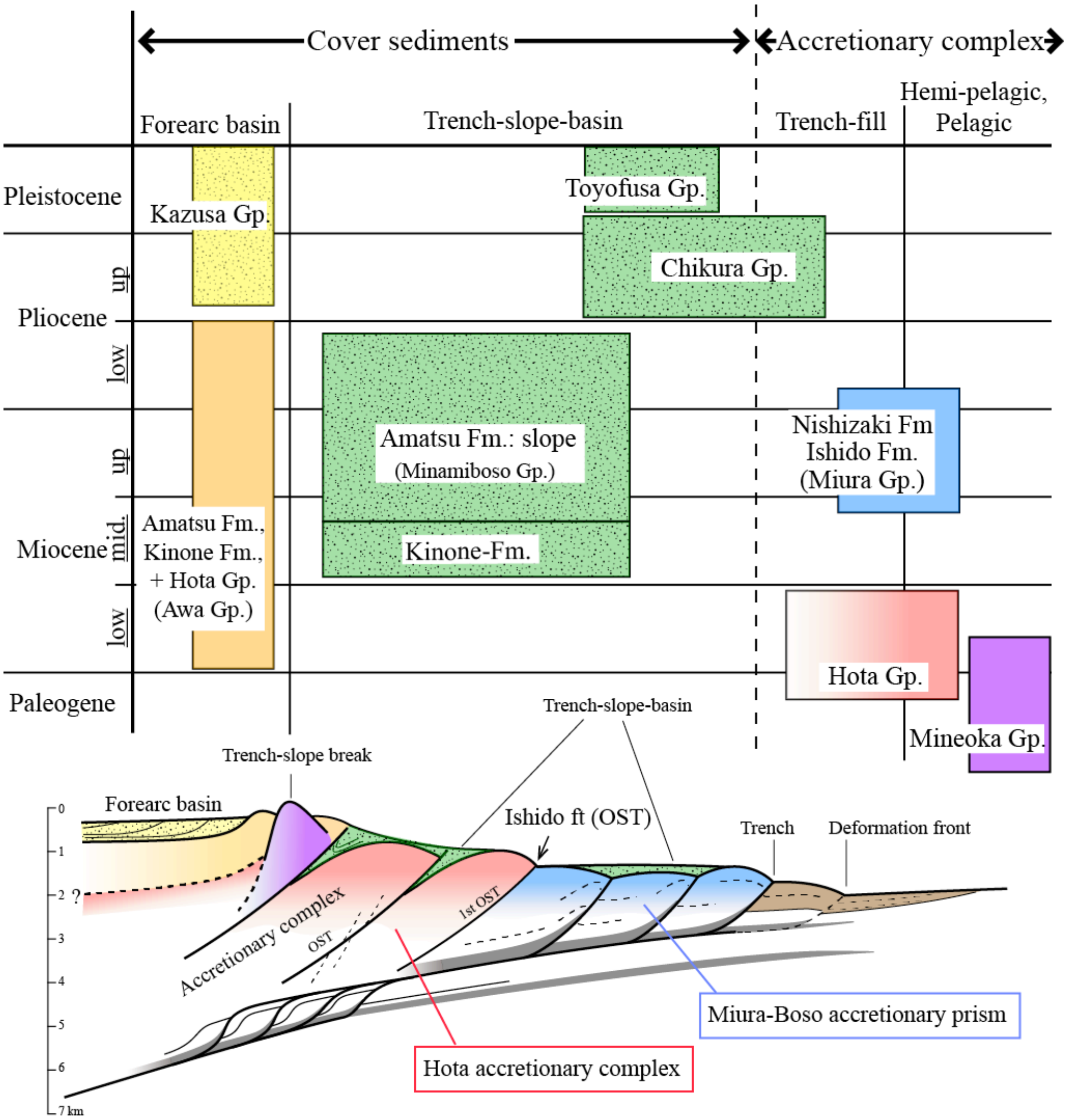

O-7 New Definition for Avalonia's Northern Margin: insights from lower crustal velocities

Jeroen Smit, Jan-Diederik van Wees and Sierd Cloetingh

Department of Tectonics, Faculty of Geosciences, Utrecht University, PO Box 80.021, 3508 TA Utrecht, The Netherlands,

The crustal seismic velocity structure of north western Europe contains a low velocity zone (LVZ) in the lower crust along the Caledonian Thor Suture Zone (TSZ), which cannot be easily attributed to the prevailing crustal domain interpretation. In this study we aim to place the identified lower crustal LVZ in a consistent crustal domain interpretation. Firstly, we introduce the geological setting of the TSZ, and current understanding of crustal terranes abutting the TSZ including Baltica and the northern Avalonian Margin. Next, we reexamine the LVZ in the TSZ and its eastern extension in the Teisseyre-Tornquist zone based on the comparison with deep seismic profiles located further east along the suture and across the Iapetus Suture in Britain.

We argue that the deep seismic velocity signatures, except for the LVZ, are well representative for different crustal domains and in agreement with earlier studies. We argue that the LVZ corresponds to the existence of a hitherto unrecognized crustal segment, separating the northern margin of Avalonia and Baltica and that it explains well the absence of Avalonia east of the Rheic suture. It follows that the Avalonian Margin is located further to the south along the southern Margin of the North German Basin, coinciding with the location of strong Late Cretaceous inversion.

Comparison with present-day examples of the Kuril Arc and Cascadia subduction zones suggests that low P-wave velocities in the lower crust are part of the accretionary complex above the subducting plate. We propose that the LVZ that separates Avalonia from Baltica is composed of the remnants of the Caledonian accretionary complex.

The newly defined Northern Margin of Avalonia and Thor Suture Zone are key elements in the reconstruction of Devonian-Carboniferous rifting of Avalonian lithosphere and the understanding of later deformation phases.

O-8 Paleomagnetic dating of incipient folding SW of the Sava–Vardar subduction zone (Karst Dinarides, Croatia)

Lewandowski, M. [1,2], Werner, T. [1], Vlahović, I. [3], Velić, I. [4], Sidorczuk, M.[5]

[1] *Institute of Geophysics, Polish Academy of Sciences, Ks. Janusza 64, 01-452 Warszawa, Poland. E-mail: lemar@igf.edu.pl*
[2] *Institute of Geological Sciences, Polish Academy of Sciences, Twarda 51/55, 00-818 Warszawa, Poland: lemar@twarda.pan.pl*
[3] *University of Zagreb, Faculty of Mining, Geology and Petroleum Engineering, Pierottijeva 6, HR-10000 Zagreb, Croatia*
[4] *Geolog d.o.o., Pančićeva 5, HR-10000 Zagreb, Croatia.*
[5] *Polish Geological Institute – National Research Institute, Rakowiecka 4, Warsaw, Poland*

1. INTRODUCTION

In this paper we focus on remagnetization phenomena of the haematite-bearing Permian redbeds and applicability of this secondary component of a natural remanent magnetization (NRM) for dating of tectonic deformation of the Karst Dinarides (Croatia), related to the collision of Adria microplate with northerly situated crustal units.

Northeasterly progression of the Adria microplate during the Late Mesozoic–Cenozoic time was associated with the Sava–Vardar subduction zone, which was active from the Late Jurassic to Palaeogene. The resulted suture is the Sava–Vardar zone, localized just south of Zagreb. However, the initiation of subduction happened earlier, in the Late Jurassic (Kimmeridgian in the Dinarides, in the Northern Calcareous Alps it happened even a bit earlier, during the Oxfordian, both evidenced by obduction of the ophiolites), and in the area of the Dinarides it was marked by significant facies variability within formerly very monotonous platform. Therefore, the Middle Jurassic represented transitional phase of tectonic peace between the extensional tectonics which was active from Permian to the end of the Early Jurassic and compressional tectonics which started in the Late Jurassic and culminated by the uplift of the Dinarides (Vlahović et al., 2005). Late Mesozoic and Cenozoic sedimentary basins, developed on the pre-Late Jurassic basement, were influenced by subduction to the NE in today's geographic coordinates. They formed several elongated parallel younger flysch basins, ranging in age from oldest in the NE, of the latest Jurassic age, to youngest in the SW of Oligocene/Miocene age as well as the Promina Basin filled with clastic-carbonate rocks during the late Palaeogene.

2. GEOLOGICAL SETTING

Our goal were Permian deposits in the Central Velebit Mt. (Croatia), which are composed of two informal lithostratigraphic units: Lower Permian clastic deposits (topic of this paper) and Middle to Upper Permian carbonates. Lower Permian clastic deposits consist mainly of pyritic sandstones, quartz conglomerates and petromictic conglomerates in the lower part and reddish-brownish sandstones and siltstones in the upper part.

Uppermost and the thickest unit of the Lower Permian clastic succession in the Central Velebit area is composed of reddish-brown siltstones and fine-grained, middle-grained to coarse-grained sandstones, in places even microbreccia greywackes. Depositional environments were probably continental and deltaic/coastal. They are gradually passing to carbonates and clastics of the Middle to Upper Permian and Triassic age. Karst Dinarides basins were formed under extensional regime until the Late Jurassic, and after that only partially influenced by ongoing subduction in the northern area, resulting mostly in reduction of sedimentary basins causing the final uplift in Cenozoic (only some temporary small basins were formed during the Late Cretaceous).

On the basis of clay minerals (Lewandowski *et al.* 2012) and CAI analyses (see Fio *et al.* 2010) the Lower Permian rocks studied in this paper should not have been exposed to the temperatures above 200–250°C.

3. METHODOLOGY

Palaeomagnetism is a well-recognized tool for reconstruction of the crustal block movements. Secondary magnetization may be applied to dating of fold structures, by a reference of identified characteristic magnetization to known palaeomagnetic poles/directions. This potential will be utilized in this study to show how NRM may be used to date incipient stage of folding at the early stages of collision between the Adria microplate and the European plate.

3. PALAEOMAGNETIC SAMPLING AND METHODS

Paleomagnetic sampling and methods, results, their discussion in terms of acquisition of NRM components, and their tectonic interpretations are described in detail in Werner *et al.* (2015). In brief we have collected ca. 160 oriented cores from two sections of Permian red siltstones and sandstones at Košna and Crne Grede (Velebit Mt., see Figs 1, 2). Both sections consist of redbed deposits, showing variety of microfacies, differing in grain sizes and mineral assemblage, although unsorted quartz grains are predominant. Clasts of the underlying Košna conglomerate were also investigated for conglomerate test. Since haematite was a main magnetic carrier, the cores were subjected to thermal demagnetization with MMTD1 thermal demagnetizer (Magnetic Measurements Ltd., UK) up to 700°C. Their NRM components were determined in the magnetic field-free space with the Model 755 Superconducting Rock Magnetometer (2G Enterprises, USA).

Two typical components of ChRM, differed by unblocking temperatures, can be fitted for thermal demagnetization paths of at least 50% of samples from each segment of the section: low-temperature component (LT – at 0–250°C) and higher-temperature component (HT – ranging from 250–350°C to 500–625°C). For a few samples HT component can be anchored at coordinate system's origin, indicative for a single-component NRM. Conglomerate test proved negative, implying acquisition of a secondary component of NRM.

5. DISCUSSION

Characteristic remanent magnetization (ChRM – HF/HT component) *in situ* is apparently similar to the Permian direction for the African plate, as expected for the Velebit Mt. coordinates from APWP for Africa (Besse & Courtillot 2002), recalculated to the present-day coordinates of the Velebit Mt. Paradoxically, this orientation is observed within the almost vertically dipping beds, i.e. before any correction for the tilted/folded structures. Consequently, ChRM must be considered secondary (as also confirmed by the negative conglomerate test) and its directional agreement with the Permian expected direction for the Velebit locality is purely coincidental (Fig. 3). The orientation of HF/HT component after 100% unfolding with plunging fold axis restored to the horizontal has no reasonable explanations for both Košna and Crne Grede sections, since their inclinations imply too high latitudes, compared to inferred equatorial position of Adria during the Permian time (e.g. Channell 1996; Muttoni *et al.* 2001; Lewandowski 2003; Cocks & Torsvik 2006). Partial unfolding of HT/HF mean ChRM direction for the Košna section was performed as clockwise rotation around 290/15 fold axis (0–100°). For angle of rotation of 65–70° it roughly coincides with Early Cretaceous–Palaeogene segment of APWP for Africa (Fig. 3). Consequently, we explain this coincidence in terms of syn-folding, Cretaceous remagnetization of the rocks at their subhorizontal position (tilted by at most 30°S). The incipient stage of folding, which we recognized and dated for the Late Cretaceous using palaeomagnetic methods, can be considered as the introduction into the final disintegration of the Adriatic Carbonate Platform, and a herald of the final uplift, which had its maximum later, in the Late Eocene/Oligocene/?Early Miocene time. Subsequent tilting, understood as an anticlockwise rotation of the beds around the axis gently plunging to the West, resulted in an almost vertical, present-day position of strata. A final geometry of the rocks under study was attained probably at the wane of the main uplift phase during the Oligocene/Early Miocene. A soft LF/LT component was acquired after the final emergence of the Velebit block. Only small (up to 10° anticlockwise) vertical axis rotation of the Velebit unit may be inferred from our data.

ACKNOWLEDGEMENTS

Research was funded by the Polish Ministry of Science and Higher Education, grant no. N N307 475238 and Croatian Ministry of Science, Education and Sport, grant 195–1953068–0242. Project "Dynarydy" of the Institute of Geological Sciences, P.A.S. is also acknowledged. The study was also partially supported within statutory activities No 3841/E-41/S/2015 of the Ministry of Science and Higher Education of Poland to the Institute of Geophysics, P.A.S.

REFERENCES

Besse, J. & Courtillot, V., 2002. Apparent and true polar wander and the geometry of the geomagnetic field over the last 200 Myr, *J. geophys. Res.*, 107(B11), 2300, doi: 10.1029/2000JB000050.

Channell, J.E.T., 1996. Palaeomagnetism and palaeogeography of Adria, in *Palaeomagnetism and Tectonics of the Mediterranean Region*, pp. 119–132, ed. Morris, A. & Tarling, D.H., Geological Society of London, Special Publication, 105.

Cocks, L.R.M. & Torsvik T.H., 2006. European geography in a global context from the Vendian to the end of the Palaeozoic, in *European Lithosphere Dynamics*, pp. 83–95, ed. Gee, D.G. & Stephenson, R.A., Geological Society, London, Memoirs, 32.

Fio, K., Spangenberg, J.E., Vlahović, I., Sremac, J., Velić, I., Mrinjek, E., 2010. Stable isotope and trace element stratigraphy across the Permian–Triassic transition: a redefinition of the boundary in the Velebit Mountain, Croatia. Chem. Geol. 278, 38–57. http://dx.doi.org/10.1016/j.chemgeo.2010.09.001.

Lewandowski, M., 2003. Assembly of Pangea: combined paleomagnetic and paleoclimatic approach, *Advances in Geophysics*, 46, 199–236.

Lewandowski, M., Werner, T., Vlahović, I., Środoń, J., Anczkiewicz, A.A., Velić, I. & Sidorczuk, M., 2012. Paleomagnetism and Thermal History of the Permian Succession of the Velebit Mt. (Dinarides, Croatia), in *Proceedings of the AGU Fall Meeting Abstracts*, San Francisco, Calif., pp. 1136.

Muttoni, G., Garzanti, E., Alfonsi, L., Cirilli, S., Germani, D. & Lowrie, W., 2001. Motion of Africa and Adria since the Permian: paleomagnetic and paleoclimatic constraints from northern Libya, *Earth Planet. Sci. Lett.*, 192, 159–174.

Ramovš, A., Hinterlechner-Ravnik, A., Kalenić, M., Karamata, S., Kochansky-Devidé, V., Mirković, M., Petkovski, P., Sremac, J., Krstić, B., Kulenović, E. & Temkova V., 1990. Stratigraphic correlation forms of Yugoslav Paleozoic. Rend. Società Geologica Italiana, 12, 359–383.

Vlahović, I., Tišljar, J., Velić, I. & Matičec, D., 2005. Evolution of the Adriatic Carbonate Platform: Palaeogeography, main events and depositional dynamics, *Palaeogeogr. Palaeoclimatol. Palaeoecol.*, 220, 333–360.

Werner, T., Lewandowski M., Vlahović I., Velić I., Sidorczuk, M. 2015. Palaeomagnetism and rock magnetism of the Permian redbeds from the Velebit Mt. (Karst Dinarides, Croatia): dating of the early Alpine tectonics in the Western Dinarides by a secondary magnetization. Tectonophysics, 651–652, 31 May 2015, Pages 199–215.

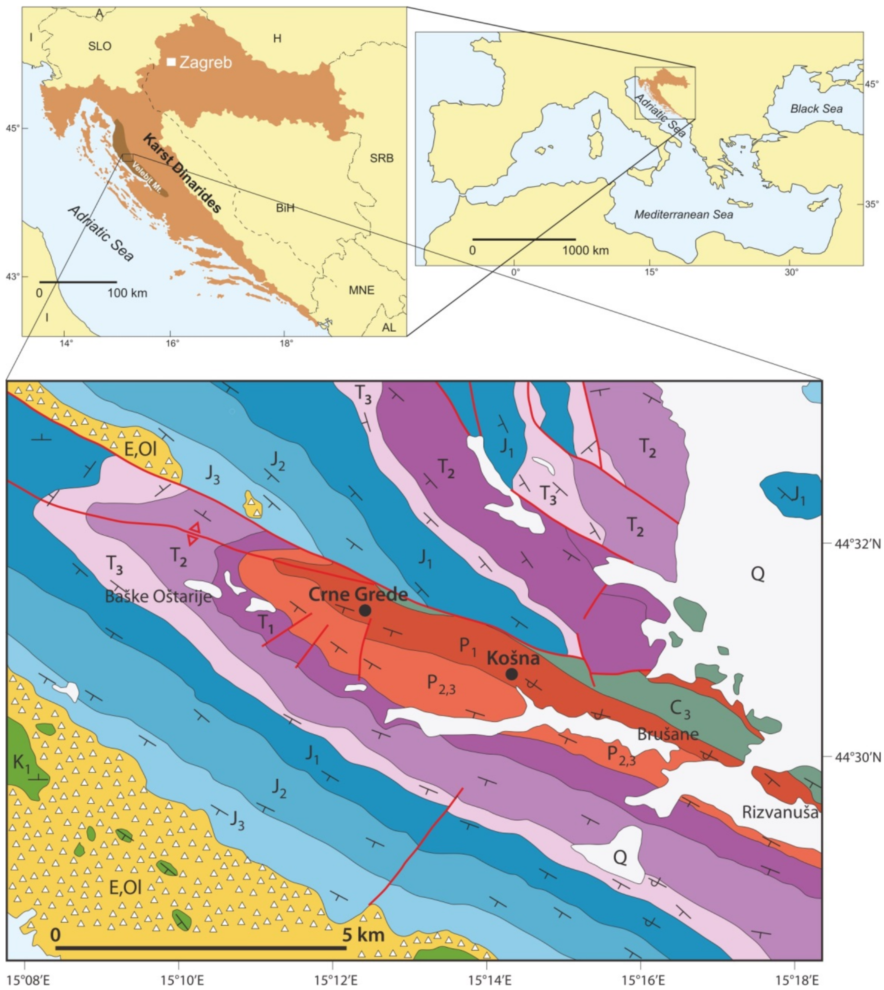

Figure 1. The location of the studied area within the Croatia. Investigated sites are marked by dots on the geological map of the area (from Werner *et al.*, 2015)

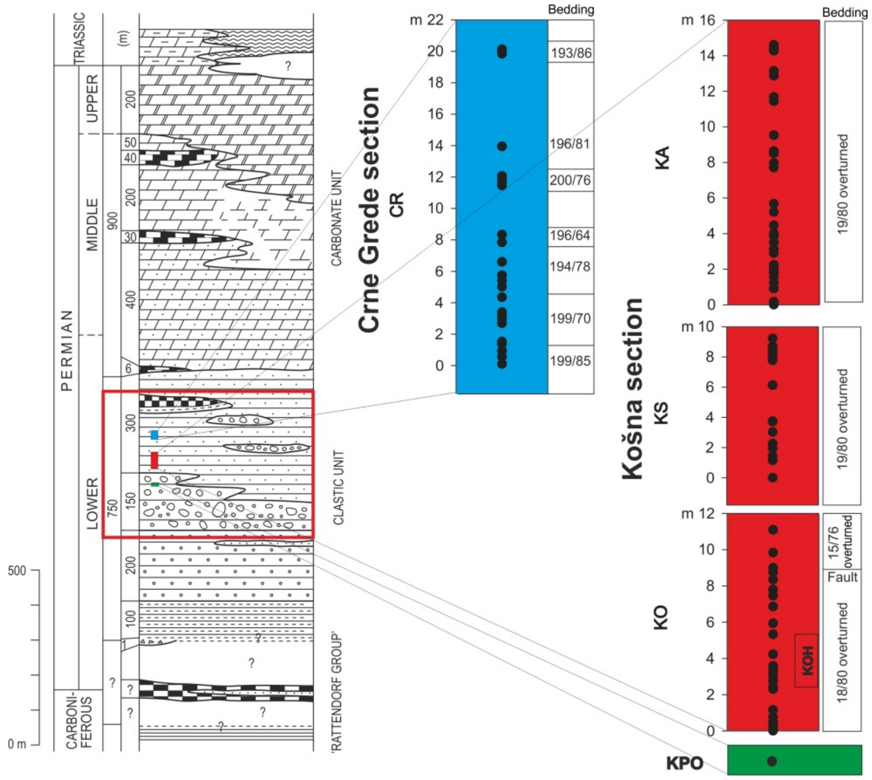

Figure 2. Sampling positions of the Crne Grede (left) and Košna (right) Permian sections within the schematic geological column of the Velebit Mt. Permian deposits (from Werner *et al.*, 2015, modified after Ramovš *et al.* 1990 and Fio *et al.* 2013). For Košna three segments were sampled (bottom – KO/KOH, middle – KS, and top – KA). In the lowermost segment KO (drill cores) and KOH (hand samples) were collected. The conglomerate section (KPO) was sampled below the lowermost Košna section.

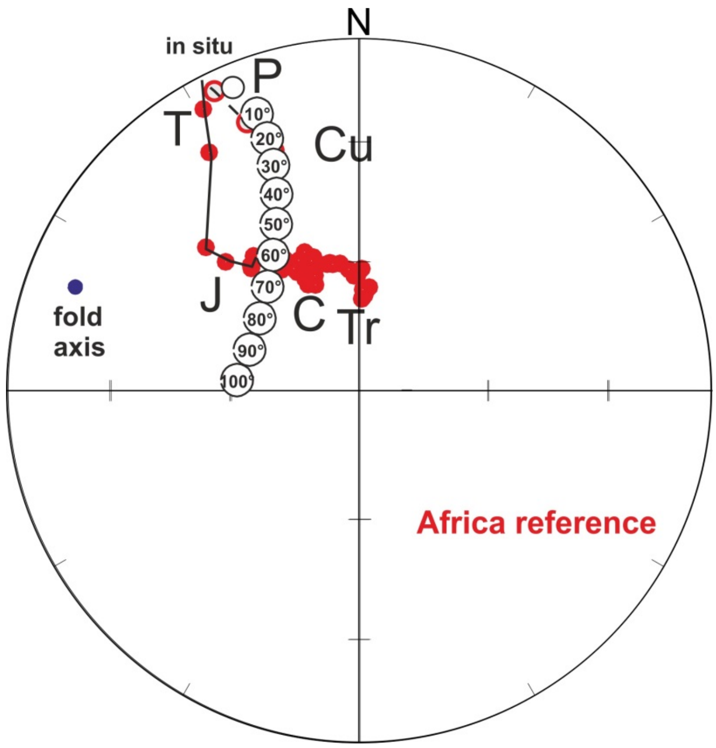

Figure 3. The model of the partial unfolding of the HT/HF mean ChRM direction for the Košna redbeds was performed as clockwise rotation around 290/15 fold axis (0–100°) (from Werner *et al.*, 2015). For the angle of rotation of 65–70° it roughly coincides with the Early Cretaceous–Tertiary segment of the APWP for Africa.

O-9 Thermal regime of back-arc region and geothermal energy

Damien Bonté[1*], Attila Balázs[1,2], Jan-Diederik van Wees[1,3], Sierd Cloetingh[1]

[1] Tectonics Group, Department of Earth Sciences, Utrecht University, Utrecht, the Netherlands
[2] Department of Geophysics and Space Sciences, Eötvös Loránd University, Budapest, Hungary
[3] TNO, Geological Survey of the Netherlands, Utrecht, the Netherlands

* d.d.p.bonte@uu.nl

Back-arc basins are all the result of tensional forces above subduction zones. With the large variety of subduction zone settings come an equally large variety of back-arc basins. From a geothermal energy perspective, these regions show an interesting convergence of elements. As a result of the active extensional setting, the lithosphere is thinned and the resulting surface heat flow measured in these regions is higher. The heat flow commonly measured and described is high (above 70-80 $mW.m^{-2}$), in comparison to the average 65.3 $mW.m^{-2}$ for the continents. Extensional settings also allow favourable stress field for the development of geothermal energy. Back-arc regions are found in two major areas, the Pacific and Europe. In the west Pacific the back-arc basins are mostly subsea behind the volcanic island arc (e.g. Japan Sea, South China Sea, and Lau Basin) but some basins are onshore (Sumatra Basins in Indonesia and Taupo Basin). In the east Pacific, in Central and South America, high heat flow has been measured in the back-arc region between the volcanic arc and the craton. In Europe, high heat flow has been measured and identified in the Tyrrhenian Sea, the Pannonian Basin, and in the Aegean Sea and western Turkey.

The aim of this work is an integrated study of the lithosphere to define the thermal regime of the back-arc regions with the objective to characterize interesting areas from a geothermal energy point of view. As such, we have selected four onshore back-arc regions. In the west Pacific, the Sumatra Basin shows very high heat flow value (> 120 $mW.m^{-2}$). In the east Pacific, to the north of the Trans-Mexican Volcanic Belt (TMVB) few heat flow measurements indicate values in excess of 70 $mW.m^{-2}$. In Europe, the Pannonian Basin and the Aegean Sea region are both of great interest. In the Pannonian Basin, the latest heat flow assessments show large areas with values in excess of 110 $mW.m^{-2}$. In the Aegean Sea region, both Greece to the west and Turkey to the east show values above 90 $mW.m^{-2}$.

These back-arc basins are related to very diverse subduction zone settings. They, however, all carry a significant potential for geothermal energy development and exploration.

O-10 **Miocene tectonics of the Western Mediterranean:From mantle extensional exhumation to westward thrusting in a back-arc settings**

Frédéric Gueydan (1), Gianluca Frasca (1,2) and Jean-Pierre Brun (2)

(1) *Géosciences Montpellier, Université Montpellier, UMR 5243 CNRS/INSU, Place E. Bataillon, CC60, 34093 Montpellier Cedex, France*
(2) *Géosciences Rennes, UMR 6118 CNRS/INSU, OSUR, Université Rennes 1, 35042 Rennes Cedex, France*

In the frame of the Africa-Europe convergence, the Mediterranean tectonic system presents a complex interaction between subduction rollback and upper-plate deformation during the Tertiary. The western Mediterranean is characterized by the *exhumation* of the largest *subcontinental mantle* massif worldwide (the *Ronda Peridotite*) and a narrow *arcuate geometry* across the Gibraltar arc within the Betic-Rif belt (the internal part being called the Alboran domain), where the relationship between slab dynamics and surface tectonics is not well understood. New structural and geochronological data are used to argue for 1/ hyperextension of the continental lithosphere allowing extensional mantle exhumation to shallow depths, followed by 2/ lower miocene thrusting. Two Lower Miocene E-W-trending strike-slip corridors played a major role in the deformation pattern of the Alboran Domain, in which E-W dextral strike-slip faults, N60°-trending thrusts and N140°-trending normal faults developed simultaneously during dextral strike-slip simple shear. The inferred continuous westward translation of the Alboran Domain is accommodated by a major E-W-trending lateral ramp (strike-slip) and a N60°-trending frontal thrust. At lithosphere-scale, we interpret the observed deformation pattern as the upper-plate expression of a lateral slab tear and of its westward propagation since Lower Miocene. The crustal emplacement of the Ronda Peridotites occurred at the onset of this westward motion.

The Miocene tectonics of the western Alboran is marked by the inversion of a continental rift, triggered by shortening of the upper continental plate and accommodated by E-W dextral strike-slip corridors. During thrusting and westward displacement of the Alboran domain with respect to Iberia, the hot upper plate, which involved the previously exhumed sub-continental mantle, underwent fast cooling.

O-11 **Subduction of two oceanic plates beneath Kanto basin imaged by MeSO-net**

Shigeki Nakagawa[1], Shin'ichi Sakai[1], Ryo Honda[2], Hisanori Kimura[3], Naoshi Hirata[1]

[1] Earthquake Research Institute, the University of Tokyo, Tokyo, Japan
[2] Hot Springs Research Institute of Kanagawa Prefecture, Odawara, Japan
[3] National Research Institute for Earth Science and Disaster Prevention, Japan

1. Introduction

Beneath the Tokyo metropolitan area, the Philippine Sea Plate (PSP) subducts and causes devastating mega-thrust earthquakes, such as the 1703 Genroku earthquake (M8.0) and the 1923 Kanto earthquake (M7.9). An M7 or greater (M7+) earthquake in this area at present has high potential to produce serious loss of life and property with even greater global economic repercussions. The Central Disaster Management Council of Japan estimates that an M7+ earthquake will cause 23,000 fatalities and 95 trillion yen (about 1 trillion US$) economic loss.

To prepare for the seismic disaster we have started a series of integrated Tokyo Metropolitan projects for disaster mitigation since 2002. The current Tokyo Metropolitan Project (Phase III) started in 2012 with a new project name as "Special Project for Reducing Vulnerability for Urban Mega-earthquake Disasters"

2. MeSO-net

During the 2nd Tokyo Metropolitan projects we have deployed the Metropolitan Seismic Observation network (MeSO-net; Hirata et al., 2009). The data from MeSO-net are continuously collected at the data management center in the Earthquake Research Institute (ERI), the University of Tokyo, with a sampling rate of 200 Hz. The data are 3-componnent accelerogram with a full scale of +/- 1,500 gal for horizontal and +/-500 gal for vertical component and the effective dynamic range is 135dB at 40Hz. Available frequency range is from 0.05 to 85 Hz, which is good for travel time analysis of body waves to ambient noise analysis for surface waves.

We have successfully operated MeSO-net for about 7 years without serious malfunction. We collect more than 150 TB continuous ground motion data with more than 100K earthquakes including the 2011 Tohoku-oki earthquake and all its aftershocks. The data are used many studies (e.g., Nakagawa et al., 2010; Ishibe et al., 2015; Denolle et al., 2014) and currently prepared for disclosing both in continues and event-by-event format.

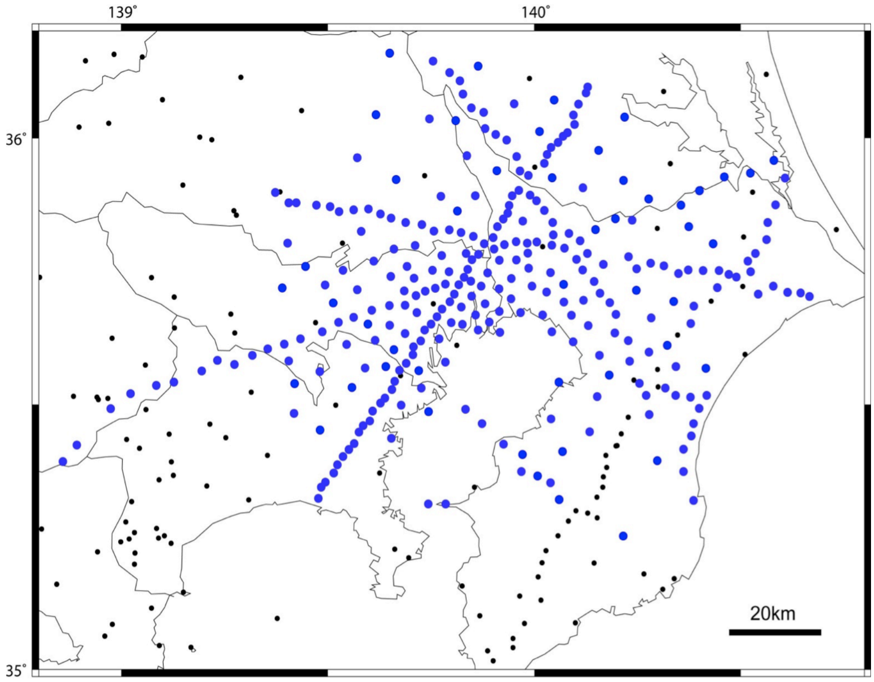

Figure 1. Metropolitan Seismic Observation network (MeSO-net)

3. Tomography

We selected events from the Japan Meteorological Agency (JMA) unified earthquake catalogue so that sufficient number of event is clearly recorded with a good signal-to-noise ratio. Data of MeSO-net were edited into event data by the selected catalogue. We picked the P and S wave arrival times manually. The total number of stations and events for tomography are 496 and 1,958, respectively. We applied the double-difference tomography method [Zhang and Thurber, 2003] to the dataset and estimated the velocity structure and hypocenters simultaneously. We used 287,190 (P wave) and 246,843 (S wave) absolute arrival times, and 656,375 (P wave) and 580,792 (S wave) differential travel times. We use hypocenters routinely determined by Hi-net, NIED, as initials for the tomography. The velocity structure used in location by Hi-net [Ukawa et al., 1984] is used as an initial velocity structure for the current tomography.

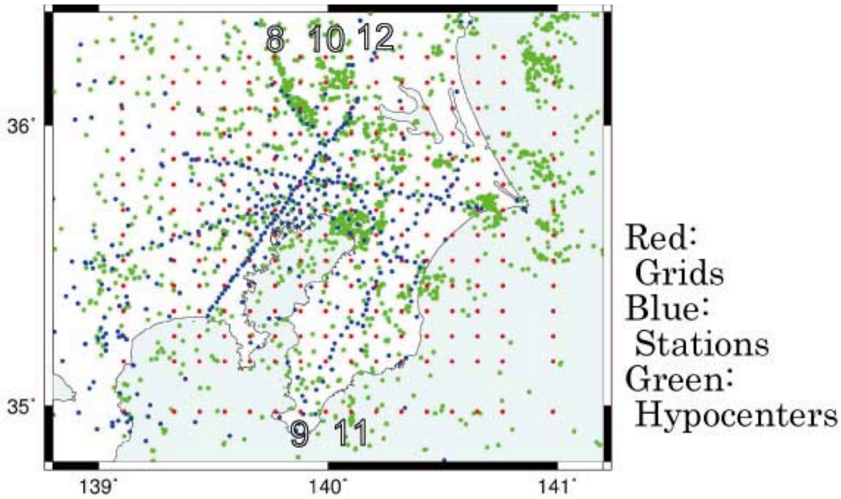

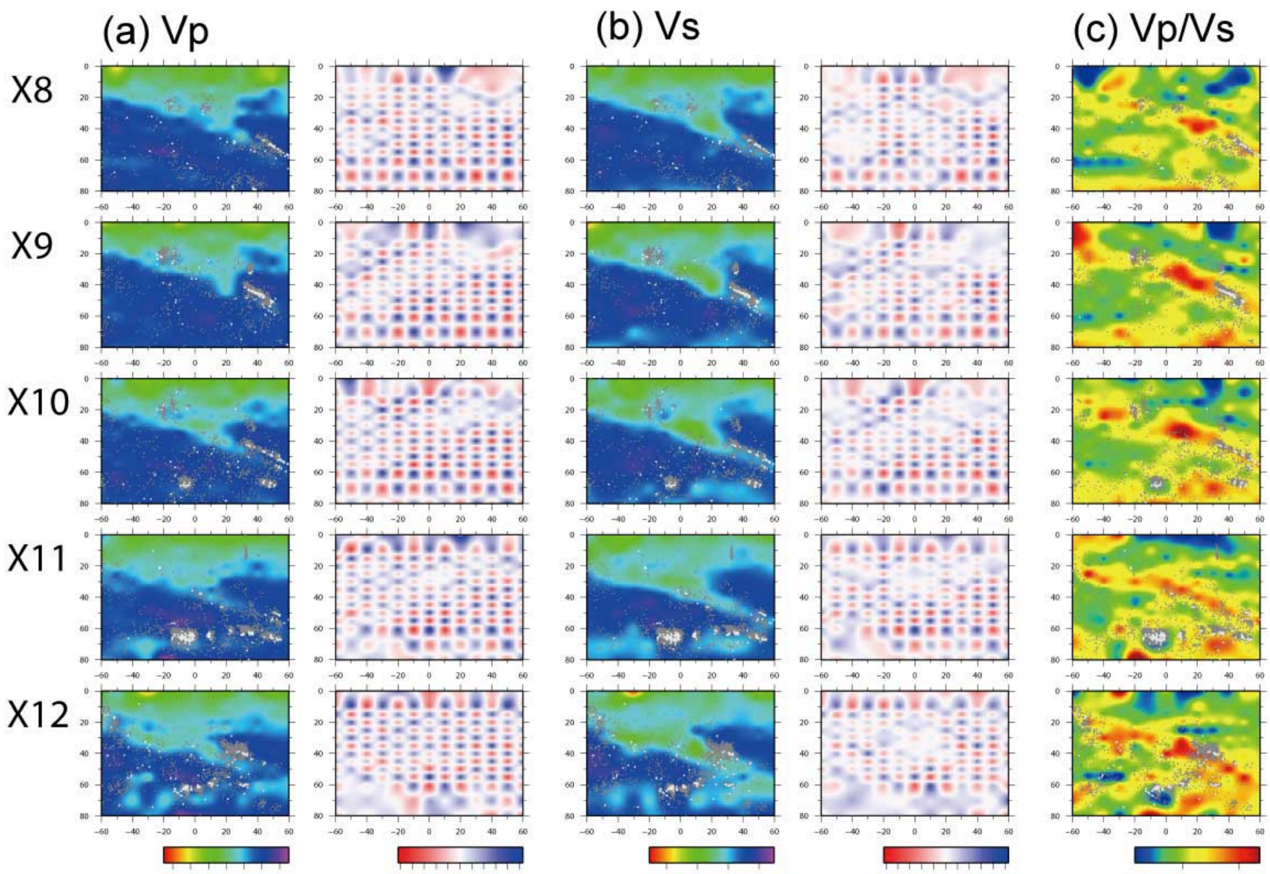

Fig. 2 Vertical sections of (a) Vp, (b) Vs, (c) Vp/Vs along the north –south trending lines in (d). Left and right of (a) and (b) show velocity and checker board resolution test, respectively. White dots indicate relocated events. Gray dots show seismicity between 2005 and 2010.1.

The grid nodes are located every 10 km in horizontal directions inside the studied area, and every 5 km in vertical direction between 0 to 60 km, and every 10 km from 60 to 80 km (Fig. 2(d)). The weighted root mean square travel time residual was reduced from 0.4133 s to 0.1128 s after 12 iterations.

To verify the model resolution, we construct a checkerboard pattern with ±5% velocity perturbation and calculated synthetic travel times. The synthetic data were inverted from the initial 1-D model. We find that the central part of the study region, except for the region off the coast of the Boso Peninsula, are well resolved at depths between 10 km and 70 km as shown in Figure 2. A detailed image of tomograms shows that PSP hits Pacific plate at a depth of 50 km beneath northern Tokyo bay. A variation of velocity along the oceanic crust suggests dehydration reaction to produce seismicity in a slab, which may related to the M7+ earthquake.

4. Discussion

Using MeSO-net data, we obtain P- and S- wave velocity tomograms which show a clear image of Philippine Sea Plate (PSP) and Pacific Plate (PAP). A depth to the top of PSP, 20 to 30 km beneath northern part of Tokyo bay, is about 10 km shallower than previous estimates based on the hypocenter distribution (Ishida, 1992). Distribution of P- and S- wave velocity distribution along the subducting oceanic plate suggest hydrate and dehydrate reactions of rocks in the crust and mantle suggesting area of seismically active area in the Tokyo Metropolitan area.

5. Concluding remarks

We have deployed 296 seismic stations in the Tokyo metropolitan area, which provides us with data for clearer tomographic image than ever obtained before. We modeled a configuration of the Philippine Sea plate (PSP) and the Pacific plate. The upper boundary of the PSP is about 10 km shallower than previously estimated. We have proposed potential areas of the coming M7+ events on the PSP upper boundary and in PSP slab. The 2011 M9.0 Tohoku-oki event promotes seismicity in the Kanto region. The seismic activity is about 6 times as high as that before March 11, 2001, which results higher probability of the M7+ event in the Tokyo metropolitan area if the activation lasts for a decade.

Acknowledgements
This study was supported by the Special Project for Reducing Vulnerability for Urban Mega Earthquake Disasters of MEXT, Japan and the Earthquake Research Institute cooperative research program.

O-12 **Distribution of crustal structure types and its tectonic implications in the southern part of the Japan Sea back-arc basins deduced from the seismic survey**

Takeshi Sato[1], Tetsuo No[1], Shuichi Kodaira[1], Seiichi Miura[1], Tatsuya Ishiyama[2], Hiroshi Sato[2]

1: Research and Development Center for Earthquake and Tsunami (CEAT), Japan Agency for Marine-Earth Science and Technology (JAMSTEC), Yokohama, Japan
2: Earthquake Research Institute, University of Tokyo, Tokyo, Japan

The Japan Sea, located between the Asian continent and Japan Island Arcs, is a back-arc basin in the northwestern Pacific. The sea mainly comprises some basins (e.g., Japan, Yamato, and Tsushima Basins) and the major topographic high (Yamato Rise) (Figure 1). It has been inferred from geophysical, geological, and petrological data that the back-arc opening of the Japan Sea was initiated by crustal rifting separated Japan Island arcs from the Asian continent in the Early Oligocene, with subsequent the ocean floor spreading in the Late Oligocene (e.g., Tamaki et al., 1992). This opening lasted somewhere in the middle Miocene (e.g., Otofuji et al., 1985; Sato, 1994). After this opening stopped, from 3.5 Ma, in the eastern and southwestern margin of the Sea, the crustal shortening by a strong compression occurred (Tamaki, 1988; Sato, 1994). Because of this back-arc opening and this crustal shortening, the deformation such as active faults and folds has developed and large earthquakes with magnitudes-7 class repeatedly occurred in these margins (e.g., Okamura et al., 2007). It is quite likely that the crustal deformation in the Japan Sea has a relevance to the back-arc opening process. However, we have little information concerning with a crustal structure formed by the back-arc opening and crustal deformation by strong compression. To obtain this information, we have been carrying out active-source seismic surveys using ocean bottom seismographs (OBSs) and multi-channel streamer system (MCS) to cover the eastern margin of the Japan Sea.

In this study, we will present the crustal structures in the southern part ranging from the northern and central Yamato Basin in the back-arc basin to the continental shelf (e.g., Sato et al., 2014) (Figure 1, Lines 1-3), and will compare these structures with that in the northern part of the Japan Sea (No et al., 2014). Additionally, we will discuss about the relationship of the back-arc opening process and the distribution of the crustal deformation in the southern part.

In the southern part of the Japan Sea, the crustal structure of the Yamato Basin has characteristics of the thicker oceanic crust because the distribution of the P-wave velocity resembles that of a typical oceanic crust (White et al., 1992) and because the crust is thinner than that of the Korean Peninsula (Cho et al., 2006) or the northeastern Japan island arc (Iwasaki et al., 2001). The crustal structure of the continental shelf suggests a rifted continental crust because the P-wave velocity in the crust resembles that of the Korean Peninsula and the northeastern Japan Island arc and because the crustal thickness is less than that of this peninsula or this arc (Cho et al., 2006; Iwasaki et al., 2001).

These crustal structure types of the southern part of the Japan Sea differ from those of the northern part (No et al., 2014). In the northern part of the Japan Sea, the crustal structure is divided into three types; the oceanic crust in the southern Japan Basin, the thicker oceanic crust in the transition area from the basin to the continental shelf, and the rifted continental crust in the continental shelf (No et al., 2014). Moreover, in spite of the same crustal type of the thicker oceanic crust in the southern and northern parts, the crust of the Yamato Basin in the southern part is thicker than that in the transition area in the northern part. These might show that the southern part is different from the northern one in the back-arc opening process and might have an effect on the deformation by the crustal shortening.

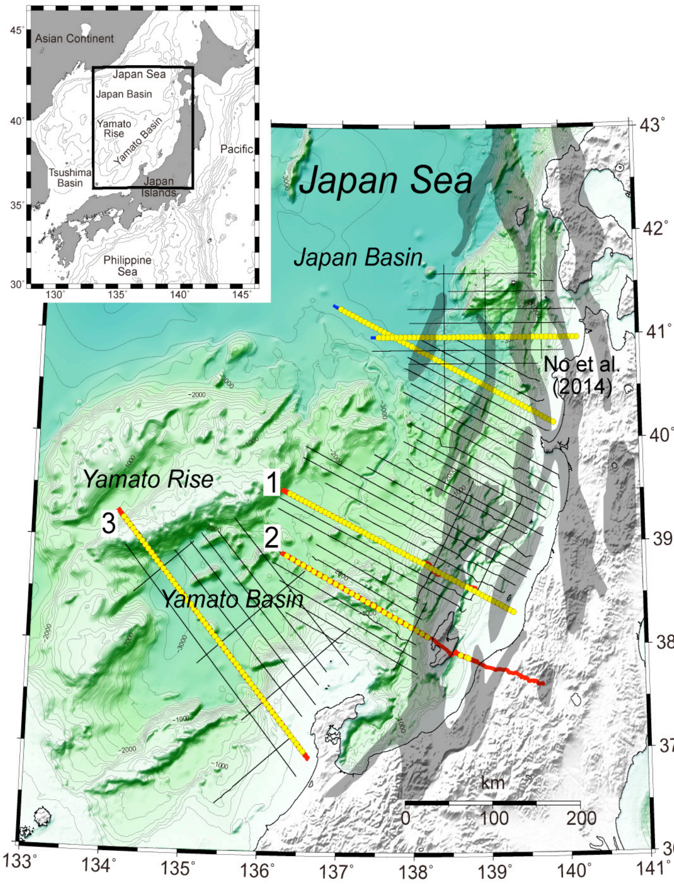

Figure 1: Map of the bathymetry around the survey area in the eastern and southwestern margin of the Japan Sea and of the survey lines. Gray area shows deformation zone (Okamura et al., 2007).

Reference:

Cho, H.-M., C.-E. Baag, J.M. Lee, W.M. Moon, H. Jung, K.Y. Kim, and I. Asudeh, Crustal velocity structure across the southern Korean Peninsula from seismic refraction survey, *Geophys. Res. Lett.*, 33 (L06307), doi:10.1029/2005GL025145, 2006.

Iwasaki, T., W. Kato, T. Moriya, A. Hasemi, N. Umino, T. Okada, K. Miyashita, T. Mizogami, T. Takeda, S. Sekine, T. Matsushima, K. Tashiro, and H. Miyamachi, Extensional structure in northern Honshu Arc as inferred from seismic refraction/wide-angle reflection profiling, *Geophys. Res. Lett.*, 28, 2329–2332, 2001.

No, T., T. Sato, S. Kodaira, T. Ishiyama, H. Sato, N. Takahashi, and Y. Kaneda, The source fault of the 1983 Nihonkai–Chubu earthquake revealed by seismic imaging, *Earth Planet. Sc. Lett.*, 400, 14–25, 2014.

Okamura, Y., T. Ishiyama, and Y. Yanagisawa, Fault-related folds above the source fault of the 2004 mid-Niigata Prefecture earthquake, in a fold-and-thrust belt caused by basin inversion along the eastern margin of the Japan Sea, *J. Geophys. Res.*, 112, B03S08, doi:10.1029/2006JB004320, 2007.

Otofuji, Y., T. Matsuda, and S. Nohda, Opening mode of the Japan Sea inferred from the palaeomagnetism of the Japan Arc, *Nature*, 317, 603–604, 1985.

Sato, H., The relationship between late Cenozoic tectonic events and stress field and basin development in northeast Japan, *J. Geophys. Res.*, 99(B11), 22261–22274, 1994.

Sato, T., T. No, S. Kodaira, N. Takahashi, and Y. Kaneda, Seismic constraints of the formation process on the back-arc basin in the southeastern Japan Sea, *J. Geophys. Res. Solid Earth*, 119,

1563–1579, doi:10.1002/2013JB010643, 2014.
Tamaki, K., Geological structure of the Japan Sea and its tectonic implications, *Bull. Geol. Survey Japan*, 39, 269–365, 1988.
Tamaki, K., K. Suyehiro, J. Allan, J. C. Ingle Jr., and K. A. Pisciotto, Tectonic synthesis and implications of Japan Sea ODP Drilling, In Tamaki, K., K. Suyehiro, J. Allan, M. McWilliams, et al. *Proc. ODP, Sci. Results*, 127/128, Pt.2 College Station, TX Ocean Drilling Program, 1333–1348, 1992.
White, R. S., D. P. McKenzie, and R. K. O'Nions, Oceanic crustal thickness from seismic measurements and rare earth element inversions, *J. Geophys. Res.*, 97(B13), 19683–19715, 1992.

O-13 Ambient noise imaging of the seismically anisotropic lithosphere below the Sea of Japan

Bill Fry#, Hiroshi Sato, Tetsuya Takeda, Qi-fu Chen, and Kelin Wang
#GNS Science, New Zealand

The development of the lithosphere beneath the Sea of Japan is poorly understood, with ongoing debate between traditional pull-apart and fan-shaped evolution. We attempt to provide more refined images of this active area by investigating the surface wave and shear wave velocity structure of the Sea of Japan based on dispersion measurements made on broad-band, cross-correlated ambient noise. Work is ongoing, however, we will present preliminary results.

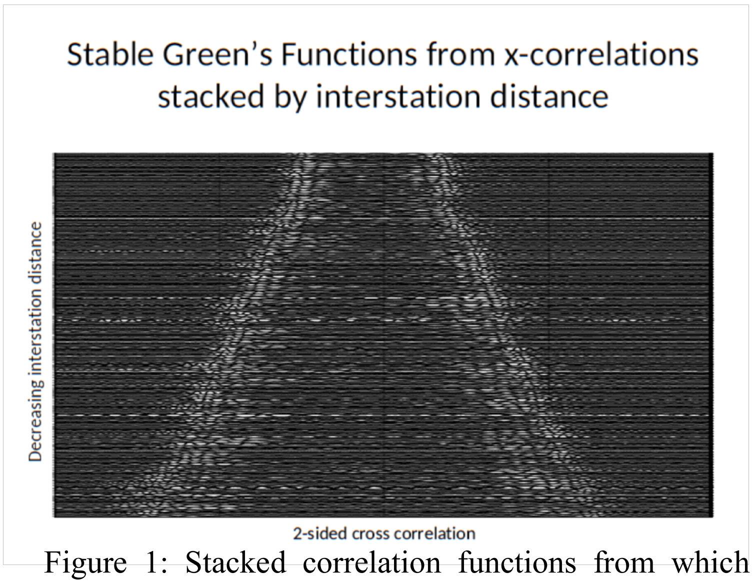

Figure 1: Stacked correlation functions from which dispersion is measured.

It has been shown that the Green's Function between two seismometers can be estimated by stacking the cross correlation functions of ambient noise recorded at each of the stations. Stacking cross correlations from each station pair statistically requires that incoherent energy propagating off the great-circle path between the stations interferes destructively; coherent energy that propagates directly between the receivers is isolated and enhanced. Continuous data from terrestrial broadband stations surrounding the sea are filtered, cross correlated on a day-by-day basis, and then stacked. We first cut seismic recordings to 1-day files. The signals are then decimated to 1 Hz and the trend is removed by subtracting the best-fit line from the signal and the signals are tapered. We deconvolve the instrument responses, leaving a record of ambient velocity recorded at the site. The data are then spectrally whitened in a frequency band between 0.008 and 0.33 Hz (3 to 125 second periods). The whitening lessens the effects of spectral peaks that result from earthquakes and dominant oceanic microseismic peaks. We perform the cross correlation for the vertical component of each day of recording for each station pair. Because the particle motion of Rayleigh waves is recorded on the radial and vertical components, by looking at the vertical component, we are isolating the Rayleigh wave signal. The cross correlation functions are then stacked for each station pair. With a sufficient number of stacked correlations, the stacked-function becomes stable in our frequencies of interest (Figure 1).

In this talk, we present the results of dispersion measurements at discrete periods between 20 and 50 seconds, sampling from about 15 to 100km in depth. We determine group velocities from the Green's Functions by applying multiple-filtering an manually selecting the frequency bandwidth from which the time of arrival of the maximum energy is observed (Figure 2). We make a maximum of 245 velocity estimates at 20s and only 93 estimates at 50s (Figure 3).

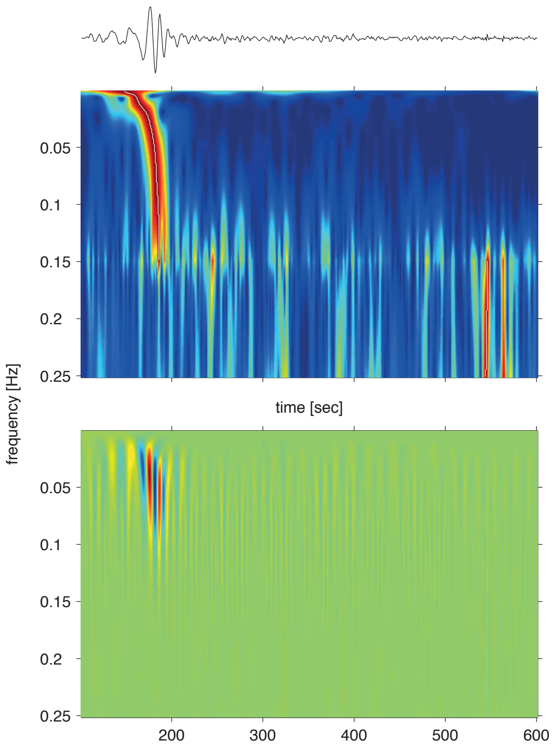

Figure 2: Frequency-time analysis showing spectrogram at bottom and the multiple-filtered signal at top.

The resulting interstation dispersion curves are inverted for 2D isotropic and anisotropic Rayleigh wave structure at discrete periods. The relative sparseness of the data requires significant regularization and damping of the inversion problem to generate a stable solution. Ongoing efforts are aimed at increasing the available data for our inversions. We present results for 20s, 25s, 30s, and 50s (Figure 4).

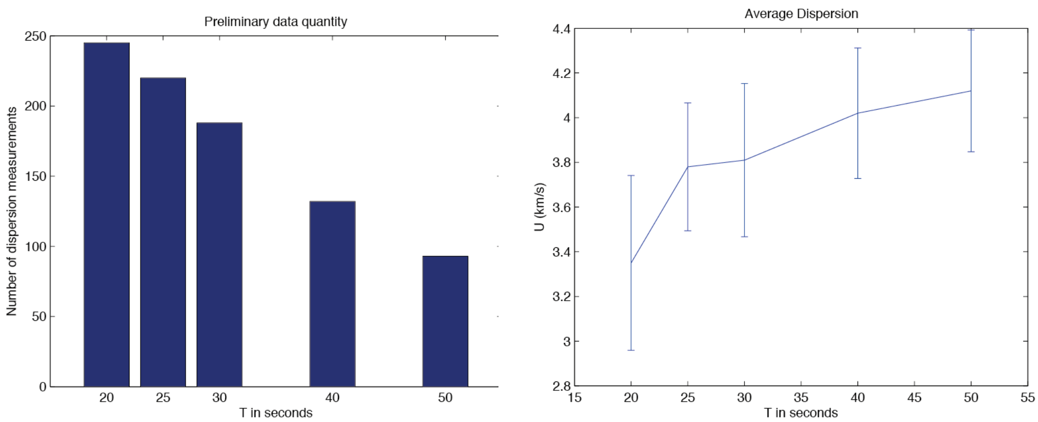

Figure 3: Left) Histogram showing the number of data measured at discrete periods. Right) Average group velocity (U) resulting from the measurements.

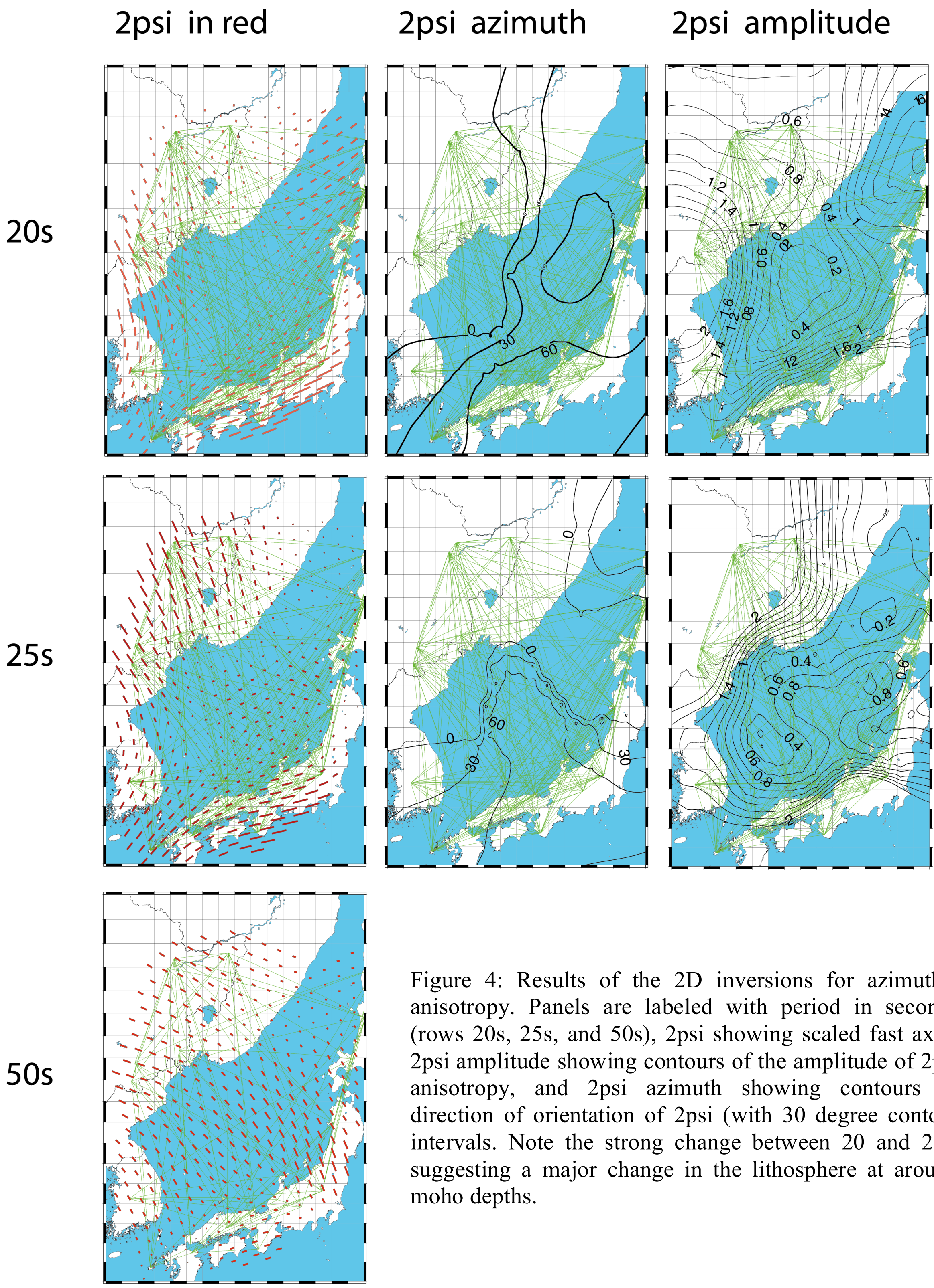

Figure 4: Results of the 2D inversions for azimuthal anisotropy. Panels are labeled with period in seconds (rows 20s, 25s, and 50s), 2psi showing scaled fast axes, 2psi amplitude showing contours of the amplitude of 2psi anisotropy, and 2psi azimuth showing contours of direction of orientation of 2psi (with 30 degree contour intervals. Note the strong change between 20 and 25s, suggesting a major change in the lithosphere at around moho depths.

In a second stage of inversion, the 2D isotropic inversion results are combined at each spatial node to create a "1D" dispersion curve. We use a linearized, iterative process to model the 1D dispersion at each node for depth dependent shear wave velocities. The 1D models are then combined to form at 3D model of shear wave velocity.

We image slow shear-wave anomalies under the central basin and relatively fast velocities under the Yamamoto and Japan Basins and offshore of the western Japan shelf (Figure 5). Current estimates of azimuthal aniostropy from our inversions are poorly constrained due to sparse data distribution. We currently have insufficient resolution to map anisotropy on terrestrial areas. Ongoing efforts are aimed at refining anisotropy estimates by increasing data density from noise correlations by increasing the spatial coverage of our database. Our work is very much ongoing and our most recent sotropic and anisotropic models will be presented. We are in the process of actively increasing our resolution by including data from the 55 station NECsaids array deployed in eastern China.

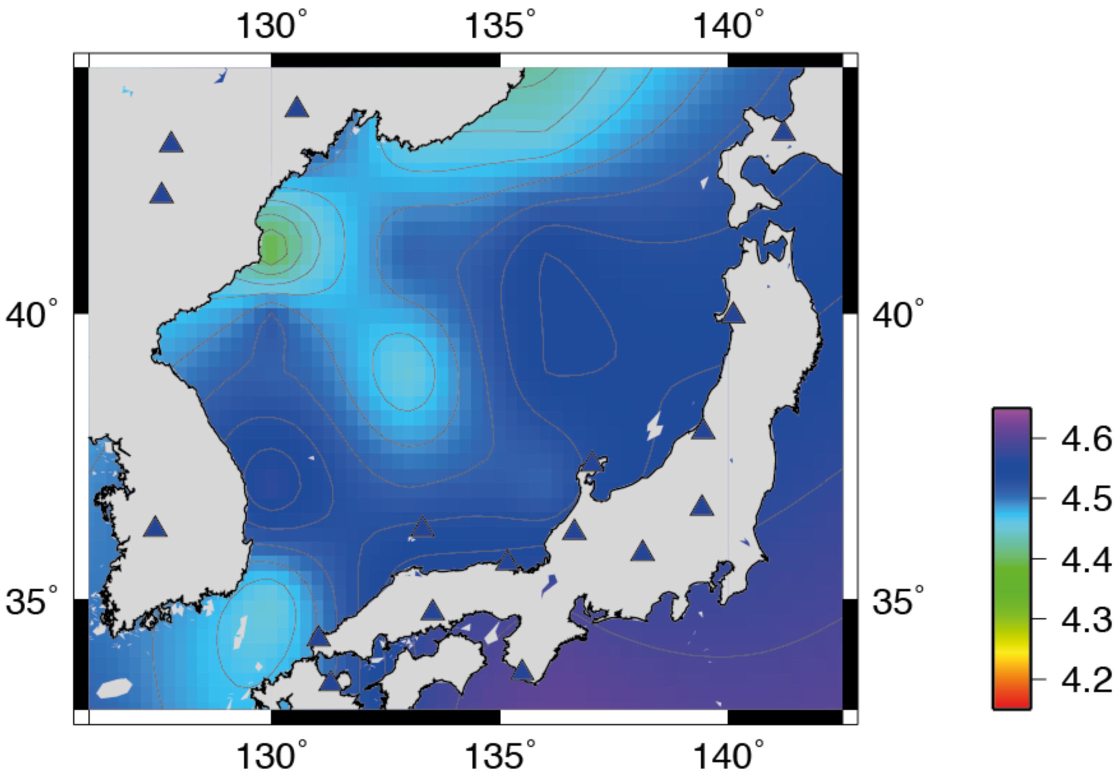

Figure 5: Horizontal section through our 3D Vs model at 50km depth. Slow velocities exist in the strait between Korean and Japan as well as in the central Sea of Japan.

O-14 **Influence of 3-D elastic heterogeneity on coseismic deformation due to the 2011 Tohoku earthquake**

Akinori Hashima[1], Thorsten W. Becker[2], Andrew M. Freed[3], Hiroshi Sato[1], David A. Okaya[2], Hisashi Suito[4], Hiroshi Yarai[4], Makoto Matsubara[5], Tetsuya Takeda[5], Tatsuya Ishiyama[1], Takaya Iwasaki[1]

[1]Earthquake Research Institute, the University of Tokyo, [2]University of Southern California, [3]Purdue University, [3]GSI of Japan, [5]NIED

The 2011 M9 Tohoku mega-thrust earthquake caused broad deformation in lithosphere and the mantle and abrupt change in seismicity. Surface deformation due to the 2011 Tohoku earthquake was detected by over 1200 land based GPS stations and several seafloor stations, which reflect elastic structure under the Japan region. Using these observations as constraints, we investigate the effects of heterogeneous elastic moduli under Japan on the inversion for coseismic slip. For this purpose, we construct a 3-D finite element model (FEM) that incorporates the geometry of the Pacific and Philippine sea slabs and crust-mantle layering. Effects of elastic structures are examined by comparing analyses of following three structure models: (a) homogeneous half-space model, (b) two-layered model considering crust-mantle structure (rigidity of 35 and 65 GPa, respectively), (c) crust-mantle model with cold slab (85 GPa). The patterns of inverted slip distribution are basically similar for all three models, but the amount of maximum slip is not simply related to average rigidity of structure models: it increases from 37 m in homogeneous model to 40 m in two-layered model and then falls to 38 m in slab model. These characteristics can be understood by separately observing the behavior of the onshore (far field) and offshore (near field) displacements. We found the following two contradicting effects: (1) In the far field, relatively lower rigidity in the shallow part decreases the amount of displacement for the same slip. This can be explained by the decrease in seismic moment. (2) In the near field or just above the thrust, relatively lower rigidity in the shallow part increases the amount of displacement for the same slip amount. This is because the stiffer (less deformable) footwall requires more movement of the hanging wall to accommodate the slip. Comparing the computed displacements with three structure models, we found that crust-mantle layering is more effective on far field while slab effect is more prominent in the near field.

O-15 Earth's crust model of the South-Okhotsk Basin by wide-angle OBS data

O.V. Petrov[1], S.N. Kashubin[1], E.D. Milstein[1], A.V. Rybalka[1], S.P. Shokalsky[1], M.L. Verba[1], E.O. Petrov[1]

[1] – Russian Geological Research Institute (VSEGEI), Saint-Petersburg, Russian Federation, vsgdir@vsegei.ru

Deep seismic studies with ocean bottom seismometers (OBS) and 3-component wave field registration along the near north-south line in the Sea of Okhotsk were a framework for the depth models reflecting the position and geometry of the main interfaces in the crust and upper mantle, as well as distribution of P-wave velocity values (Vp), velocity ratio (Vp/Vs), and density (σ) (see. Fig.).

New geophysical data reflect the geology of the southern area of the Sea of Okhotsk region, including structures of the South Okhotsk Borderland, the South Okhotsk Basin, and the Kuril Island Arc. All geostructures have individual arrangement of structural and physical parameters, enabling to identify the sedimentary cover, upper, middle, lower crust, and upper mantle.

South Okhotsk Borderland and the Kuril Island Arc have the most complete set of crustal layers. Sections of these domains include three layers in the consolidated crust (upper, middle, and lower crust) and two in the sedimentary cover. Crustal thickness in these structures is 22÷26 km, with an insignificant proportion of the sedimentary cover. Crustal thickness in the South Okhotsk Basin, which separates the borderland and the island arc, is much smaller (14-16 km). Thickness of the sedimentary layer is increased here, thickness of the upper crust is significantly reduced. Velocity and density parameters corresponding to a lower crust were not detected. Common features of the deep structure have certain symmetry with respect to the axe of the mantle dome, whose arch is located below the South Okhotsk Basin, as shown in Fig. However, this symmetry is not complete. That is observed in some reduction of the total crustal thickness of the Kuril Island Arc and is accompanied by an increase in the proportion of mafic varieties and by growth of lateral heterogeneity of that part of the section. Thickness of the velocity and density anomalous layer in the uppermost mantle is also asymmetric.

Architecture of the Earth's crust and upper mantle, shown in megacomplex structure, enables to typify crust in the distinguished large geological structures. Crust of the South Okhotsk Borderland is characterized as a "typical" three-layered consolidated crust and developed sedimentary layer despite the reduced crustal thickness (about 25 km). Entire set of features can confidently attribute the South Okhotsk Borderland crust to be of a continental type. Crust of the Kuril Island Arc is symmetrically arranged on the other side of mantle dome and is close to that of the borderland in macroparameters. The difference of the island-arc crust from the borderland crust is only in more complex lateral zoning related to volcanic processes. Since, the decisive argument for attributing of the continental crust is not its thickness but the presence of a "granite layer" in crustal structure, this criterion enables to attribute the strongly stretched crust of the South Okhotsk Basin to the continental type, where the upper "felsic" part is preserved.

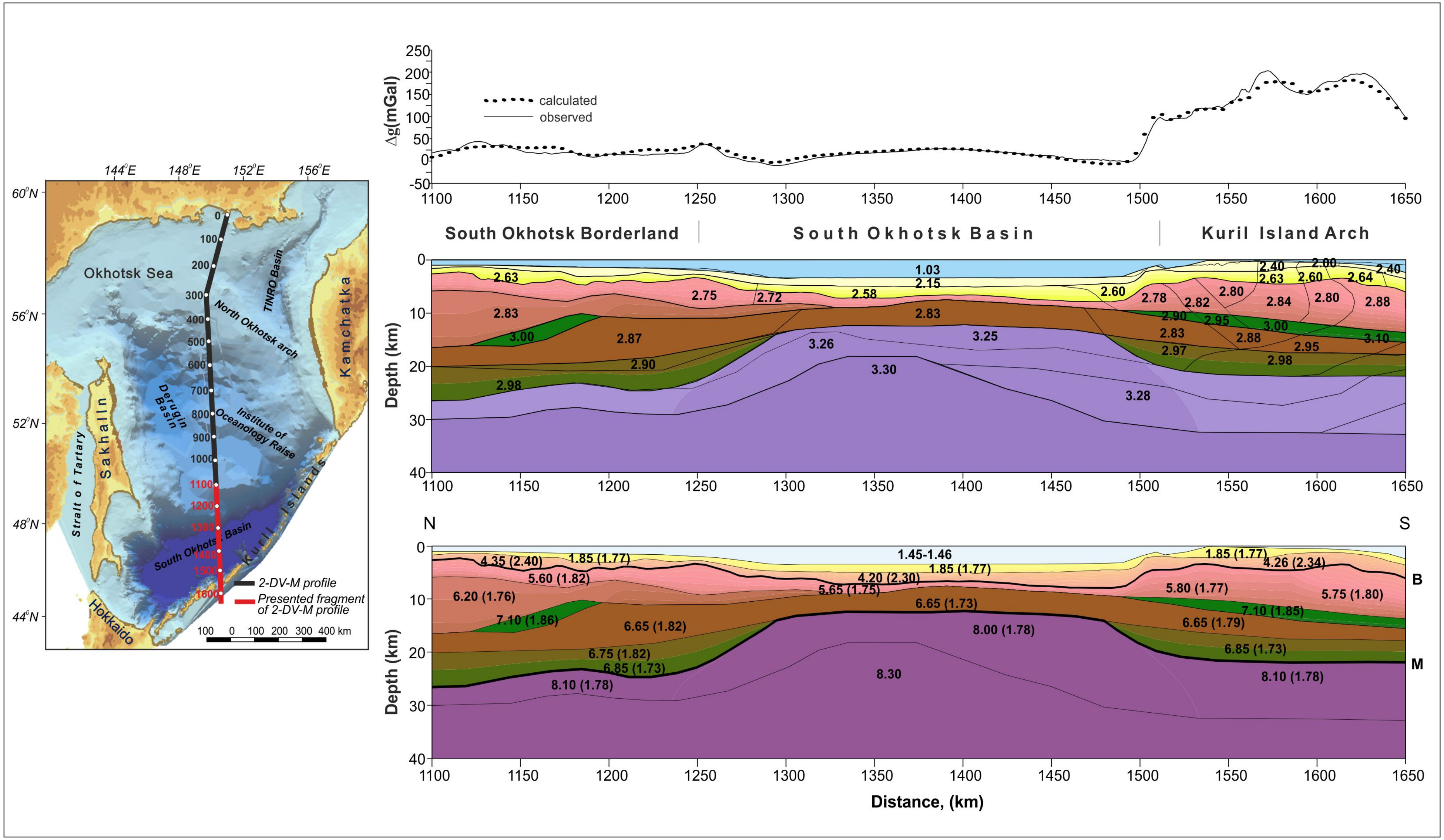

Fig. Velocity (bottom) and density (top) models of the Earth's crust and upper mantle of the South Okhotsk Basin. Densities in the section are given in g/cm^3, P-wave velocities in km/s, Vp/Vs ratios are in parentheses.

O-16 Late Quaternary stress field in central Japan inferred from the stress inversion of the active fault data and timing of the beginning of the modern stress state

Hiroyuki Tsutsumi, Katsushi Sato, and Atsushi Yamaji

Division of Earth and Planetary Science, Graduate School of Science, Kyoto University, Kyoto 606-8502, Japan, tsutsumh@kugi.kyoto-u.ac.jp

Introduction

The crustal stress field is one of the most important parameters required to understand tectonics, but the secular variation or stability of tectonic stress is not adequately understood for the time scales of 10^3–10^5 years. The geophysical data reveal stress fields on the time scales of 10^0–10^2 years, whereas the geological data reveal stress fields over longer periods, usually 10^5 years or longer. Active faults are the clues that will help in filling the gap between the time scales of geophysical and geological observations. Central Japan is suitable for crustal stress-field analyses on different time scales because it contains one of the world's highest-quality geophysical and geological data sets.

Permanent regional strain in central Japan has been induced mainly by active faults, which form a dense network in the region (Figure 1). Since the 1995 Kobe earthquake, most of the long and fast-slipping faults in the region have been studied extensively through a national active-fault-research program, which has produced one of the most comprehensive active-fault data sets in the world. Therefore, non-Andersonian faults have gradually become clear; reverse and strike-slip faults are interlaced in this region. Active faulting and its relation to the stress field in central Japan have been a topic of debate [*Huzita,* 1968; *Okada and Ando*, 1979], but the coexistence of faults with different senses of motion makes inference difficult without the inclusion of a special type of stress-tensor inversion.

In this study, we apply the method of *Sato* [2006], who developed a special type of stress-inversion method to deal with the incomplete fault-slip data, to the active fault data to derive the regional stress field in central Japan. We show that central Japan is under an ESE–WNW compressional stress field with a small stress ratio and that the regional stress field has been uniform and stable over the past ~10^5 years.

Tectonic setting

To the east of the Japanese islands, the Pacific plate is subducted westward beneath the North American and Philippine Sea plates (Figure 1). Along the Nankai trough, the Philippine Sea plate has been subducting northwestward since the Pliocene or mid-Pleistocene. In the study area, i.e., the eastern part of the southwest Japan arc, north-trending reverse faults and northwest-trending left-lateral and northeast-trending right-lateral strike-slip faults are densely distributed. The offsets of dated geomorphic features indicate slip rates in the order of 10^{-1} to 10^0 mm/yr for such faults. The area has experienced one reverse-slip and four strike-slip earthquakes that ruptured the surface since the 1891 Nobi earthquake. Geodetic and seismological data show that the Japan arc is subject to an approximate E–W compression

[*Mazzotti et al.,* 2001; *Townend and Zoback*, 2006; *Terakawa and Matsu'ura*, 2010].

Data and results

After the 1995 Kobe earthquake, the Headquarters for Earthquake Research Promotion (HERP) of the Japanese government selected approximately 100 inland active faults and conducted extensive geological and paleoseismological studies to assess their seismic potential effectively. We compiled the fault-slip data from 37 active faults selected by HERP in the Chubu and Kinki districts. We examined the data from paleoseismic trench walls, natural outcrops, and seismic reflection profiles in published reports and maps. Therefore, we catalogued reliable fault orientations and slip senses at 169 sites along 37 faults.

The fault-slip data set used in this study had a few deficits. Slickenside striations were observed to determine the rakes of slip vectors at only 11 sites out of 169. We obtained the "complete" data for 11 sites, and the remaining sites produced "sense-only" data, which have the rake uncertainties of 90° or 180°. The stress-inversion method proposed by *Sato* [2006] was employed to determine the stress conditions that explain the mixed set of the complete and sense-only data.

A reverse faulting-stress regime with an ESE–WNW-trending σ_1-axis was found to clarify almost all the data. The stress ratio, $\Phi = (\sigma_2 - \sigma_3) / (\sigma_1 - \sigma_3)$, was determined to be 0.09, which means that the magnitude of σ_2 is approximately equal to that of σ_3.

Discussion

Despite the large variation of fault orientations, stress inversion revealed that almost all the active faults in the study area are clarified by the reverse-faulting stress regime with ESE–WNW-trending σ_1-axis. The theoretical slip directions of the faults calculated with this optimal stress were consistent with all the data except for five of them. The optimal stress ratio of 0.09 indicates that σ_2 and σ_3 have similar values. Such a state of stress allows the coexistence of reverse and strike-slip faults, provided that they have different fault orientations. Their coexistence puzzled previous researchers who inferred the stress field from active faults in Japan because they assumed Andersonian faulting [*Huzita,* 1968; *Okada and Ando*, 1979]. Consequently, they neglected the coexistence of reverse and strike-slip faults or they had to infer spatially or temporarily complicated stress fields.

Although the ESE–WNW compression determined from active faults in this study is generally the same as that proposed by *Huzita* [1968], we demonstrated that a single state of stress explains the fault-slip data from all sites except five of them. This means that the stress field in central Japan has been uniform and that the active faults have slipped in the same directions over the past $\sim 10^5$ years. From the coexistence of reverse and strike-slip faults, we predicted that non-Andersonian, oblique-slip faulting is common in this region although the rakes of slip vectors were observed for only 10 of 37 faults.

The reactivation of the pre-existing planes of weakness gives rise to the non-Andersonian faulting of planes with a wide variety of orientations. *Kano* [2002] suggested that a few active faults are present in such planes in the Mesozoic accretionary complex in the northern part of the study area. For example, the left-lateral Yanagase fault (Figure 1) reactivated a kink plane of a map-scale chevron fold. Similarly, the right-lateral Hanaore fault (Figure 1) lies along the axial surface of a fold structure [*Kano*, 2002]. *Ito*

[2006] obtained the apatite fission track ages of ~20 Ma for dykes intruded along the Yanagase fault, which provides a minimum age constraint for the fault. *Murakami and Tagami* [2004] conducted the zircon fission-track analysis of pseudotachylyte sampled from the Nojima fault (Figure 1). They suggested that the Nojima fault was already initiated at ~56 Ma. Therefore, a few active faults in central Japan reactivated the pre-existing faults under the present-day stress regime.

Slip on the active faults catalogued in this study reflects the average stress regime in the late Quaternary. The inverted stress state determined in this study is principally consistent with that obtained by geodetic and seismological data [*Mazzotti et al.*, 2001; *Townend and Zoback*, 2006; *Terakawa and Matsu'ura*, 2010], suggesting that the stress state in central Japan has been uniform and stable for the past ~10^5 years.

The current stress state appears to have started at ~1 Ma in southwest Japan. *Doke et al.* [2012] complied the data on the timing of the initiation of fault movement with the same sense as in the late Quaternary and demonstrated that most of the active faults in southwest Japan reactivated in the past ~1.5 Ma. The Median Tectonic Line had moved as a reverse fault until ~1Ma forming pairs of elongated fault-block mountains and sedimentary basins in eastern Shikoku and western Kinki, and since then it has moved as a right-lateral strike slip fault [*Sangawa*, 1977; *Sato et al.*, 2015]. The Kiso Range, a fault-block mountain range in central Japan, started to shed gravels to the surrounding basins at ~0.8 Ma, suggesting that the mountain had attained considerable relief by that time [*Moriyama and Mitsuno*, 1989]. The Rokko Mountains with the highest peak at 931 m have uplifted at least ~500 m since 1 Ma, because 1-Ma-old marine clay is found at an elevation of 500 m asl. These data suggest that the current E–W–compressional stress regime in southwest Japan has initiated at ~1 Ma and the faults have moved with the current slip sense.

This abstract is based on [Tsutsumi, H., Sato, K., and Yamaji, A., 2012, Stability of the regional stress field in central Japan during the late Quaternary inferred from the stress inversion of the active fault data, Geophysical Research Letters, 39, L23303, doi: 10.1029/2012GL054094.] with an additional discussion on the onset of the modern stress state. Please refer to the paper for the references in this abstract.

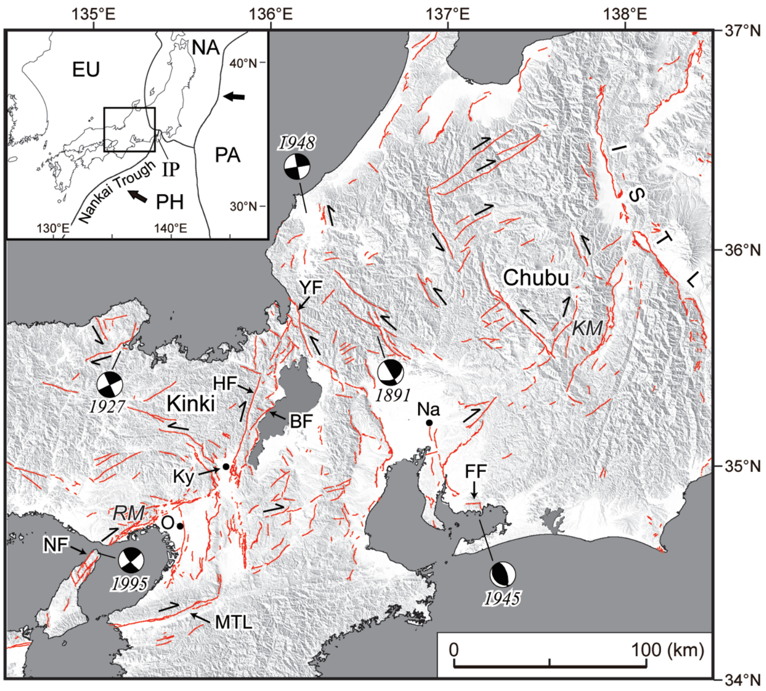

Figure 1. Tectonic setting and distribution of active faults in the Kinki and Chubu districts of central Japan, modified from *Tsutsumi et al.* [2012]. The active fault traces (red lines) are from *Nakata and Imaizumi* [2002], and black arrows denote major strike-slip faults. Focal-mechanism solutions for historical surface-rupturing earthquakes are also shown: 1891 Nobi, 1927 Kita-Tango, 1945 Mikawa, 1948 Fukui, and 1995 Kobe earthquakes. Active faults and mountain ranges mentioned in the text are Biwako-seigan fault: BF, Fukozu fault: FF, Hanaore fault: HF, Nojima fault: NF, Yanagase fault: YF, Kiso Range, KM, and Rokko Mountains, RM. Other abbreviations are Itoigawa–Shizuoka tectonic line: ISTL, Nagoya: Na, Osaka: O. Inset shows the plate-tectonic setting of Japanese islands. Eurasian plate: EU, Izu Peninsula: IP, North American plate: NA, Pacific plate: PA, Philippine Sea plate: PH. Thick arrows denote convergence directions between the Pacific and North American plates and between the Philippine Sea and Eurasian plates.

O-17 Permanent deformation in the overriding plate along the Japan Trench in the southern Northeast Japan

Tatsuya Ishiyama[1+], Hiroshi Sato[1], Naoko Kato[1], Susumu Abe[2]

[1]Earthquake Research Institute, University of Tokyo, 1-1-1 Yayoi, Bunkyo-ku, Tokyo 113-0032, Japan , [2] JGI, Inc., Japan
+ Corresponding author

Discrepancy between geodetic and geologic rates of strains in the overriding plate is a key issue to understand processes and mechanisms to accommodate its permanent deformation and strain budgets in arc-subduction systems over repeated seismic cycles (Baker et al., 2013). In this study, we estimated across-arc distribution of permanent strain rates accommodated within overriding plate in the southern Northeast (NE) Japan above the subducting Pacific plate, based on onshore and offshore, deep to shallow seismic reflection data, and rates of fault slip determined by offsets of geomorphic features or stratigraphic horizons identified of drilled shallow boreholes. Structure of subduction deformation front is comprised by gently tapered accretionary wedge and moderately dipping, Cretaceous and older inactive crustal wedge that forms structural backstop and >1500 m high east-facing large escarpment on the continental slope (Ishiyama et al., 2012). To the west of this escarpment, Normal-faulting aftershocks of the 2011 Tohoku-oki earthquake (M9.0), consistent with dense networks of north to northeast trending normal faults that deforms continental shelf deposits, are interpreted as reactivation of Pre-Neogene extensional rift system in the overriding plate inferred by seismic tomography (Ishiyama et al., 2012). Inland active structures within the overriding plate of the NE Japan is characterized by north to northeast trending active thrusts that deform Neogene deposits. Estimated strain rates accommodated by active faults and folds, most of which are reactivated Miocene normal faults, are an order of 10^{-8}/yr for each structures, 1/10 of geodetic strain rates observed before the 2011 Tohoku-oki earthquake (Figure 1). Across-arc distribution of permanent geologic strain rates in middle to late Quaternary clearly shows peak in back-arc region with 10 times higher rates than fore-arc region, similar to millennial strain rates (Sato, 1989). These shorter wavelength strain distribution is overprinted by longer-wavelength rates of uplift and subsidence estimated by fluvial incision and borehole stratigraphy, clearly showing across-arc patterns of significant negative peak (i.e., subsidence) in back-arc and relatively uniform distribution in fore-arc region. Area with rapidly subsiding and shortening in the NE Japan back-arc is underlain by relatively higher Vp lower crust, presumably associated with rapid extension during the opening of the Sea of Japan. In contrast, area with uniform and lower uplift rate is underlain by crustal thickening caused by magmatic underplating during late Cenozoic volcanisms.

References

Baker, A., Allmendinger, R. W. Owen, L. A. and Rech, J., 2013, Permanent deformation caused by subduction earthquakes in northern Chile, Nature Geoscience, 6, 492–496.

Ishiyama, T., Sugito, N., Echigo, T., and Sato, H., 2012, Rare normal faulting earthquake induced by subduction megaquake: example from 2011 Tohoku-oki earthquake, EGU General Assembly, EGU2012-4208.
Ishiyama, T., Sato, H., Kasaya, T., Kodaira, S., and Abe, S., 2012, Structural characters of the Japan Trench subduction zone over the March 2011 Mw 9.0 Tohoku-Oki earthquake rupture based on seafloor geomorphology and reprocessed multichannel seismic reflection data, AGU fall meeting, T13A-2581.
Matsubara, M. and K. Obara, The 2011 Off the Pacific Coast of Tohoku earthquake related to a strong velocity gradient with the Pacific plate, Earth Planets Space, 63, 663-667, 2011.
Matsubara, M., K. Obara and K. Kasahara, 2009, High-Vp/Vs zone accompanying non-volcanic tremors and slow slip events beneath southwestern Japan, Tectonophysics, 472, 6-17.
Sato, H., 1989, Degree of deformation of late Cenozoic strata in the Northeast Honshu Arc, Memoirs of the Geological Society of Japan (in Japanese with English abstract), 32, 257-268.

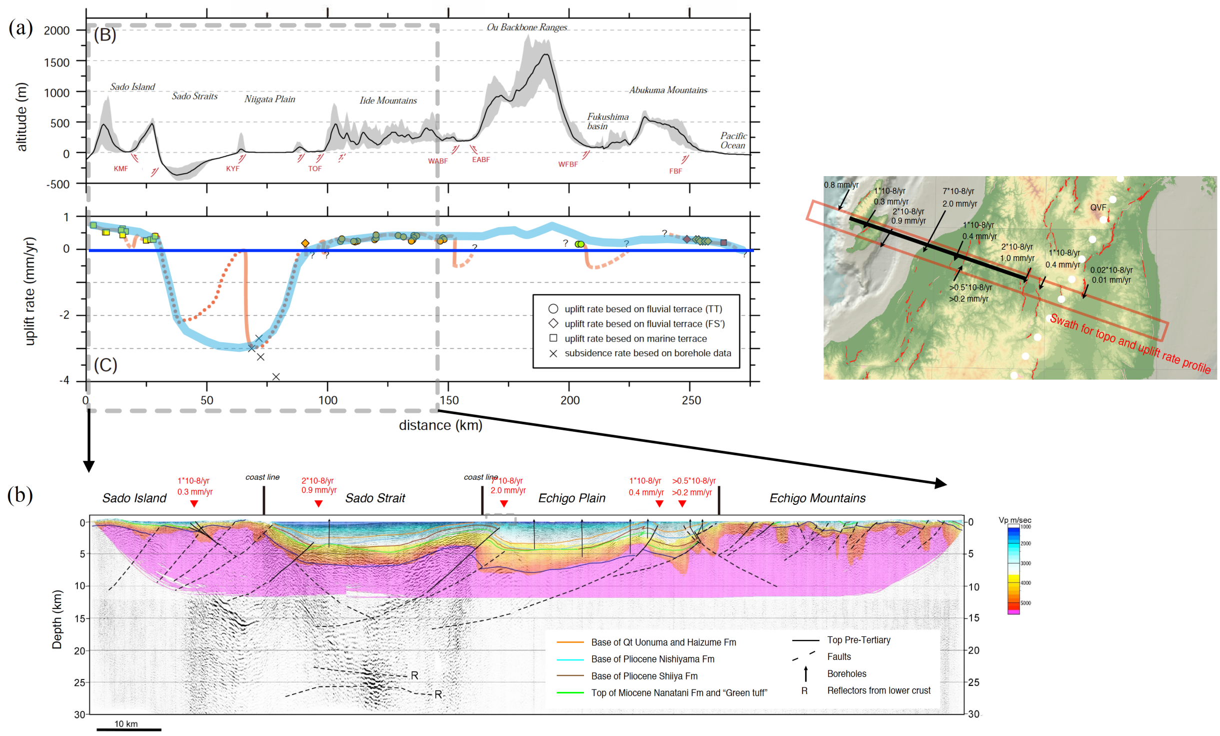

Figure 1 (a) Topography (top) and distribution of uplift and subsidence rate across the southern NE Japan estimated from river incision and borehole stratigraphy. (b) Deep seismic reflection profile from the Sea of Japan to west of the volcanic front (Sato et al., 2010).

O-18 **High-velocity lower crust along the failed rift with deep Moho**

Makoto Matsubara[1] and Hiroshi Sato[2]

1) National Research Institute for Earth Science and Disaster Prevention (NIED)
2) Earthquake Research Institute (ERI), the University of Tokyo (UTokyo)
mkmatsu@bosai.go.jp

1. Introduction

P-wave seismic velocity is well known to be up to 7.0 km/s and over 7.5 km/s in the lower crust and in the mantle, respectively. A large velocity gradient is the definition of the Moho discontinuity between the crust and mantle. In this paper, we investigates the configuration of Moho discontinuity defined as an isovelocity plane with large velocity gradient derived from our fine-scale three-dimensional seismic velocity structure beneath Japanese Islands using data obtained by dense seismic network with the tomographic method (Matsubara and Obara, 2011). The Philippine Sea and Pacific plates are subducting beneath these continental plates. We focus on the Moho discontinuity at the continental side. Among the northeastern Honshu island, there are many failed rifts formed at the Japan Sea opening around 15 Ma. The failed rift is filled with the sediments and felsic rocks in the shallow basin and is attached with mafic dominant rocks at the bottom of the crust (Sato, 2013). We investigate the relationship with velocity structure, Moho depth and failed rift.

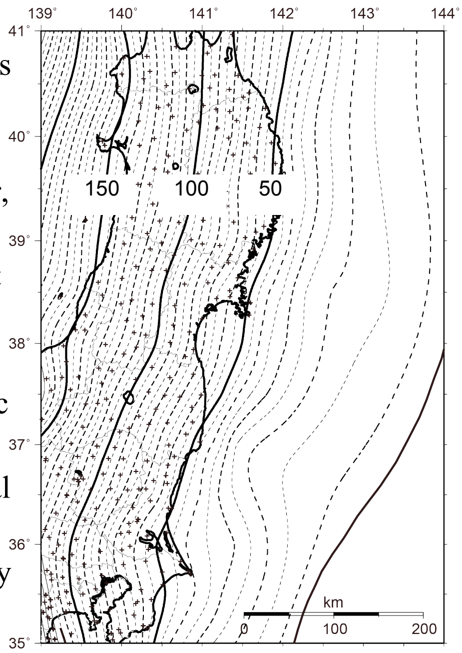

Fig. 1: Depth contour of the upper boundary of the subducting Pacific plate. Thick, thick broken, and thin broken contor lines denote the depth interval of 50, 10, and 5 km, respectively.

2. Seismic tomography

We conduct seismic tomography using arrival time data picked by NIED Hi-net, including earthquakes off the coast, outside the seismic network around the source region of the 2011 Tohoku-oki Earthquake. For these offshore events, we use the centroid depth estimated from moment tensor inversion by NIED F-net. After the Tohoku-oki Earthquake we also used the centroid depth estimated from seismograms of high-sensitivity accelerometers operated by NIED with moment tensor inversion (Asano et al., 2011).

The target region, 20-48°N and 120-148°E, covers the Japanese Islands from Hokkaido to Okinawa. A total of manually picked 4,622,346 P-wave and 3,062,846 S-wave arrival times for 100,733 earthquakes recorded at 1,212 stations from October 2000 to August 2009 is available for

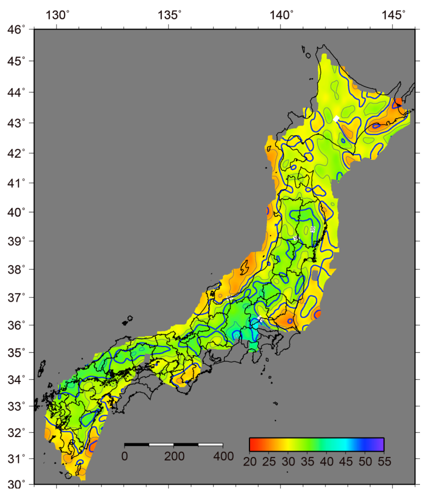

Fig. 2: Contour map of 7.2 km/s isovelocity plane defined as Moho discontinuity.

use in the tomographic method. In the final iteration, we estimate the P-wave slowness at 458,234 nodes and the S-wave slowness at 347,037 nodes. The inversion reduces the root mean square of the P-wave traveltime residual from 0.455 s to 0.187 s and that of the S-wave data from 0.692 s to 0.228 s after eight iterations (Matsubara and Obara, 2011). After the Tohoku-oki earthquake, we also used arrival time data from many aftershocks determined by moment tensor inversion (Asano et al., 2011) composed of 1,089,228 P- and 593,191 S-wave arrival times from 4,384 events outside of the seismic network.

Centroid depths are determined using a Green's function approach (Okada et al., 2004) such as in NIED F-net. For the events distant from the seismic network, the centroid depth is more reliable than that determined by NIED Hi-net, since there are no stations above the hypocenter.

We determine the upper boundary of the Pacific plate based on the velocity structure and earthquake hypocentral distribution (Fig. 1). The upper boundary of the low-V oceanic crust corresponds to the plate boundary where thrust earthquakes are expected to occur. Where we do not observe low-V oceanic crust, we determine the upper boundary of the upper layer of the double seismic zone within high-V Pacific plate. We assume the depth at the Japan trench as 7 km.

3. Data and method

We calculate the P-wave velocity gradients between the vertical grid nodes. The largest velocity gradient is 0.078 (km/s)/km at velocities of 7.2 and 7.3 km/s. In this study, we define the iso-velocity plane of 7.2 km/s as the Moho discontinuity. However, it is difficult to identify the Moho discontinuity of the Eurasian plate where the lower crust of the Eurasian plate contacts with the subducting oceanic crusts of the Pacific and Philippine Sea plates since there is no mantle high-velocity material. We discuss the Moho discontinuity above the upper boundary of these subducting oceanic plates with consideration of configuration of plate boundaries of prior studies (Shiomi et al., 2008; Kita et al., 2010; Hirata et al, 2012) (Fig. 2).

4. Moho configuration

The Moho discontinuity deepens over 35 km in the collision zone like Kanto Mountains, the volcanic underplating zone as the Tohoku backbone range, and non-tension region like Chugoku Mountains. These regions associated with deep Moho are characterized by the crustal seismicity within the depth range from 20 to 30 km. The iso-depth contour of 35 km beneath the southwestern Japan is consistent with that derived from the receiver function method (Shiomi et al. 2006). There are nonvolcanic tremors and short-time slow slip events (SSE) beneath the southwestern Japan (eg. Obara, 2002). Matsubara et al. (2009) consider that the tremors and SSEs occur along the contact zone of Moho discontinuity beneath the Eurasian plate and the subducting Philippine Sea plate beneath southwestern Japan. Our Moho model is consistent with this since they exist along the southern edge of the Moho discontinuity of the continental Eurasian plate.

The Moho discontinuity shallower than 30 km depth is distributed within the tension region like northern Kyushu and the tension region at the Cretaceous like the northeastern Kanto district. These regions have low seismicity. Positive Bouguer anomaly beneath the northeastern Kanto district indicates that the ductile material with large density in lower crust exists at the shallower portion and that the crust is aseismic.

5. Deep Moho and high-velocity structure along the failed rift

High velocity zones within the lower crust are found east off the Kanto beneath the Pacific Ocean, off northwestern Honshu beneath the Japan Sea, and across Honshu Island (Fig. 3). These zones are consistent with low-V zone within the upper crust and the deep seismicity within the mid crust. Sato (2013) estimated that these zones are the aborted rift deformed by the shortening formed at the Japan Sea opening.

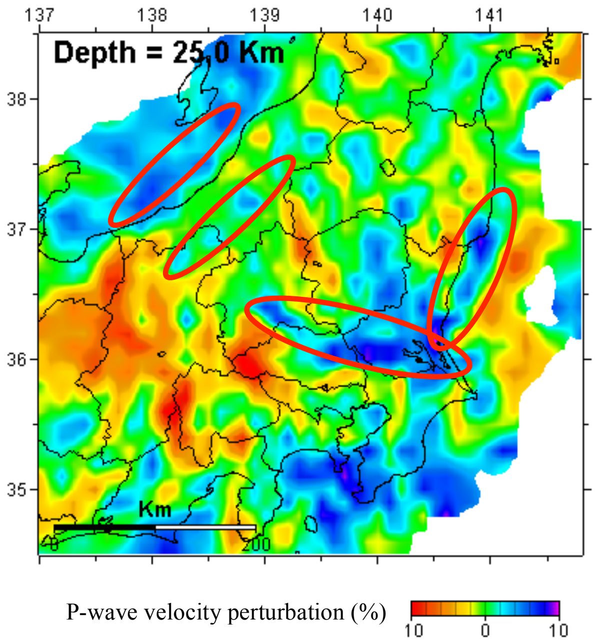

Fig. 3: P-wave velocity perturbation at a depth of 25 km. Red zones are the high-V lower crust.

Reference:

Asano, Y. et al., Spatial distribution and focal mechanisms of aftershocks of the 2011 off the Pacific coast of Tohoku Earthquake, Earth Planets Space, 63, 675-679, 2011.

Hirata, N. et al.: A new tomographic image on the Philippine Sea Slab beneath Tokyo -Implication to seismic hazard in the Tokyo metropolitan region, Abstract T11C-06, AGU, 2012.Kita et al., 2010.

Matsubara, M. et al., High-Vp/Vs zone accompanying non-volcanic tremors and slow-slip events beneath southwestern Japan, Tectonophysics, 472, 6-17, 2009.

Matsubara M. and K. Obara : The 2011 off the Pacific coast of Tohoku Earthquake related to a strong velocity gradient with the Pacific plate, Earth Planets Space, 63, 663-667, 2011.

Okada Y. et al., Recent progress of seismic observation networks in Japan -Hi-net, F-net, K-NET and KiK-net -,Earth, Planets and Space, 56, xv-xviii, 2004.

Obara, K., Nonvolcanic Deep Tremor Associated with Subduction in Southwest Japan, Science, 296, 1679-1681, 2002.

Sato, Recent deep seismic profiling in the Niigata fold-and-thrust belt, central Japan, Rep. Coord. Comm. Earthq. Pred., 90, 516-520, 2013.

Shiomi, K. et al., Moho Depth Variation beneath Southwestern Japan Revealed From the Velocity Structure Based on Receiver Function Inversion, Tectonophys., 420, 205-221, 2006.

Shiomi, K. and J. Park, Structural features of the subducting slab beneath the Kii Peninsula, central Japan: Seismic evidence of slab segmentation, dehydration, and anisotropy, J. Geophys. Res., 113, B10318, 2008.

O-19 The Japan Unified High-Resolution Relocated Catalog for Earthquakes (JUICE) project for events associated with inland active faults in Japan

Tomoko E. Yano[1] , Tetsuya Takeda[1], Makoto Matsubara[1], and Tatsuhiko Shiomi[1]

1) National Research Institute for Earth Science and Disaster Prevention (NIED)
t.yano@bosai.go.jp

1. Introduction

We have completed the first version of catalog by Japan Unified High-resolution Relocated Catalog for Earthquakes (JUICE) project for the Japan Islands. The objective of the JUICE project is to provide a high-resolution earthquake catalog for understanding the tectonic processes, estimating seismogenic zones along the active faults, and evaluating active faults. The first version of this new earthquake catalog contains relocated hypocenters where the shallow (> 40 km) earthquakes up to M6.5 occurred from year of 2001 to 2013 using hypoDD (Waldhauser & Ellsworth, 2000), the Double-Difference method, to obtain high-resolution earthquake locations.

Some studies have attempted to understand the seismogenic zone by calculating D90, the depth above which 90 % of the earthquakes occurred (e.g. Omuralieva et al., 2012). However for even more detail, such as, investigating seismogenic depth along the active fault is required to analyze into very fine scale. NIED High-Sensitivity seismic observation (Hi-net) has launched in 2000 and we now acquire more than 14 years of data observed at about 800 locations. Since Hi-net is designed to detect small signals from microearthquakes and their stations are distributed to equidistance (about 20 km) spaced in the borehole from 100 m to over 3,500 m in depth, both quantity and quality of data enable us to relocate over 1,000,000 events and these events are now confined into appropriate clusters and lines by hypoDD. We also apply our new earthquake catalog for determine the cutoff depth of D95, the depth above which 95 % of the earthquakes occurred from the surface.

2. Data and method

We collect hypocenter information of size of M0.0 to M6.5 occurred down to 40 km in depth from year of 2001 to 2013 from NIED Hi-net hypocenter catalog, Hi-net P and S-wave arrival data, and waveform data. Using information, we generate two different datasets; (1) a dataset of differential travel time calculated from P- and S-wave arrival data, hereafter referred to as “Catalog data”; (2) a dataset of differential travel time determined by cross-correlating to waveforms, hereafter referred to as “Cross-correlation data”. We apply these two differential travel time data to hypoDD for high-resolution hypocenter locations (Fig. 1).

To treat the big datasets to recalculate their hypocenters, we define grid spaces (n = 1673) as shown in Figure 2. Each grid space contains no more than 3,000 events and is used to parallelize the relocation calculation. Both datasets, “Catalog data” and “Cross-correlation data”, are based on the records observed as long as their station locations are within the range wider than 0.5˚ x 0.5˚ of its grid space. Results after relocation does not show the strong correlation with neither their grid sizes nor their shape.

3. Result and discussions

Total of over 1,000,000 events are relocated for JUICE project. Since their locations are now confined into appropriate clusters and lines to each other, the new catalog makes easier to distinguish events related particular fault system. For instance, learning from previous study(e.g. Omuralieva et al., 2012), the cut off depth of where most earthquake occurred can be useful to understand the variation of seismogenic zone. Since the resolution of our new catalog is high enough that we can now calculate the cutoff depth where 95 % of earthquake occurred (D95) (Fig.3) rather than D90. A gray range in the figure shows that D95 are only calculated when there are more than or equal to 50 events within the each grid range otherwise masking a solid gray in the figure. D95 shows mainly around 15 km under Japan island while there the strong spatial variation throughout Japan island. It is worthwhile to note that the new event catalog used for D95 contains not only hypocenters located within the crust but also some hypocenters corresponding to inter-plate and intra-slab events. This contamination will mislead seismogenic zone to be deeper than it suppose to be. In our presentation, we will show the new JUICE catalog and its applications.

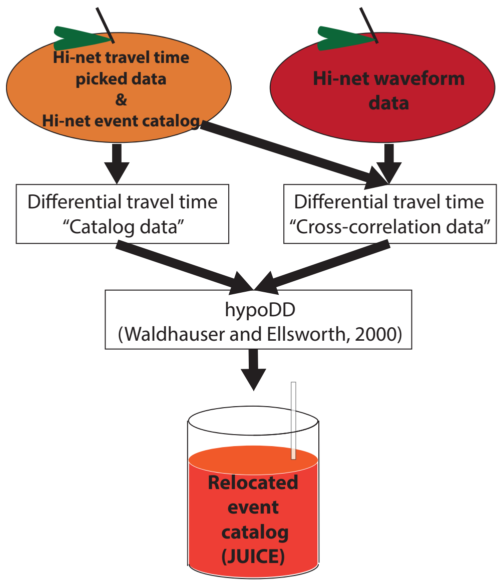

Figure 1: Process flowchart of JUICE project is shown. First, routinely determined Hi-net event catalog and corresponding waveforms observed at Hi-net stations are obtained. Second, we prepare two kinds of data sets: 1. The differential travel time data determined by arrival time routinely picked by Hi-net team; 2. The differential travel time data which are determined by waveform cross-correlation; 3. hypoDD (Waldhauser and Ellsworth, 2000) are applied to these data sets prepared in step 2. Finally, the results are evaluated and adopted to the relocated event catalog.

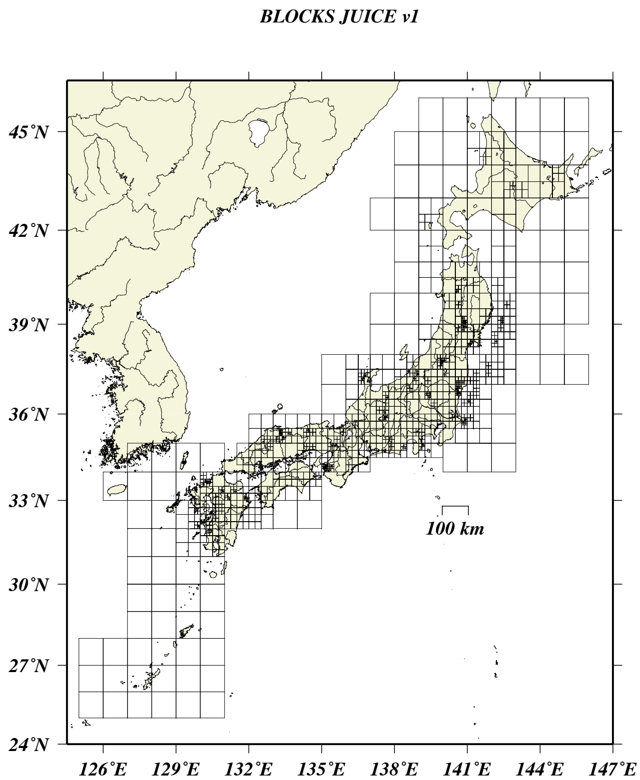

Figure 2: Grid spaces (n = 1673) are defines as the areas used to parallelize the relocation calculation (fig. 2). Each grid space contains no more than 3,000 events. Both datasets, “Catalog data” and “Cross-correlation data”, are prepared based on the records observed at these stations as long as their station location is within the range wider than 0.5° x 0.5° of its grid space.

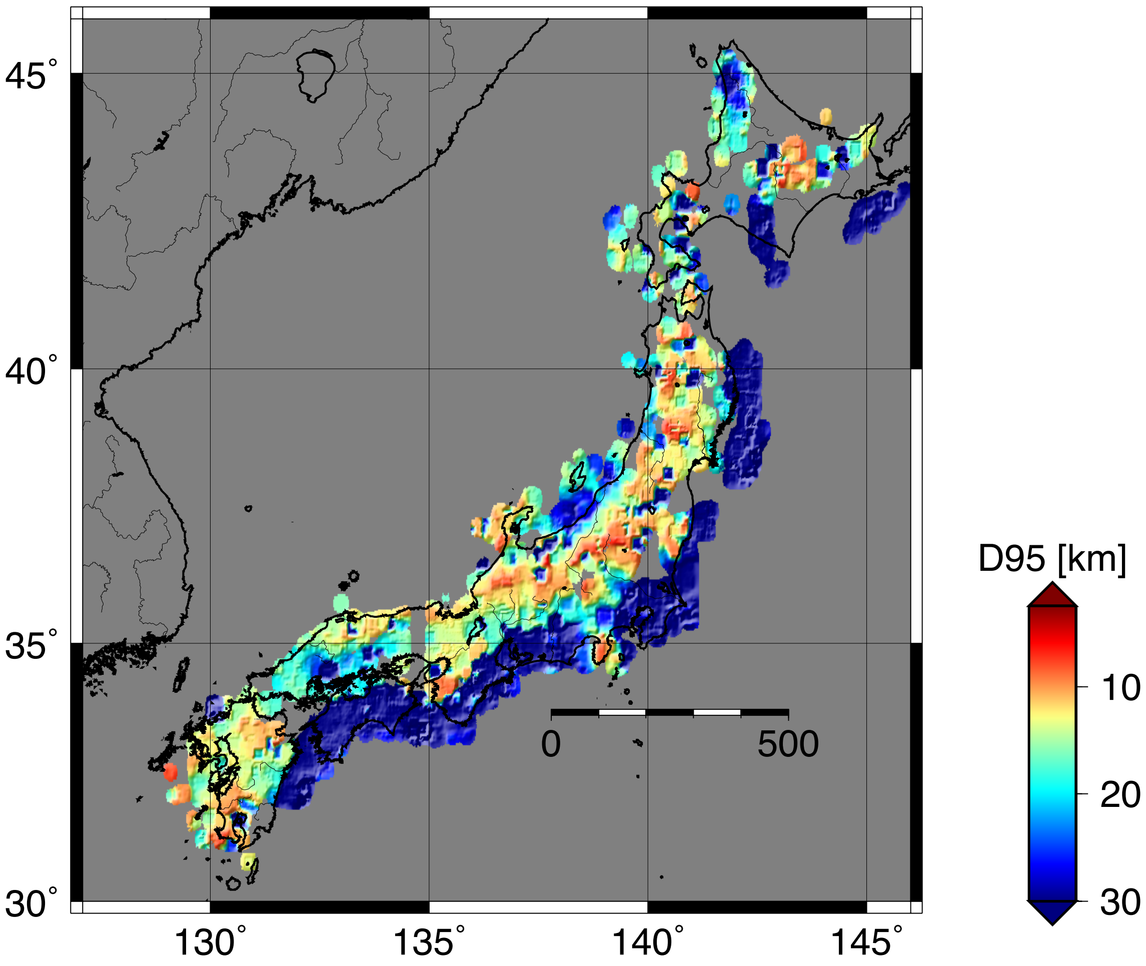

Figure 3: A map of preliminarily D95 to demonstrate an example of applying the new earthquake catalog from JUICE project.

References

Omuralieva, A. M., Hasegawa, A., Matsuzawa, T., Nakajima, J., & Okada, T. (2012). Lateral variation of the cutoff depth of shallow earthquakes beneath the Japan Islands and its implications for seismogenesis. *Tectonophysics, 518*.

Waldhauser, Felix, & Ellsworth, L. William. (2000). A Double-Difference Earthquake Location Algorithm: Method and Application to the Northern Hayward Fault, California. *Bulletin of the Seismological Society of America, 90*(6), 1353-1368.

O-20 **Arc-Arc Collision Structure in the Southernmost Part of the Kuril Trench Region- Results from Integrated Analyses of the 1998-2000 Hokkaido Transect Seismic Data -**

Takaya Iwasaki(1), Noriko Tsumura(2), Tanio Ito(3), Hiroshi Sato(1), Eiji Kurashimo(1), Naoshi Hirata(1), Kazunori Arita(4), Katsumi Noda(5), Akira Fujiwara(5), Susumu, Abe (5), Shunsuke Kikuchi(1) and Kazuko Suzuki(7)

(1) Earthquake Research Institute, the University of Tokyo, (2) Graduate School of Science, Chiba University, (2) Heisei Teikyo University, (3) The Hokkaido University Museum, Hokkaido University, (3) JGI, Inc., (4) JAPEX, (1) Schlumberger Ltd.

1. Introduction

The Hokkaido Island, located in the southernmost part of the Kuril trench region, has been under a unique tectonic environment of arc-arc collision (Fig. 1(a)). Due to the oblique subduction of the Pacific (PAC) plate, the Kuril forearc sliver started to collide against Northeast (NE) Japan arc from the east at the time of middle Miocene to form complicated structures in the Hidaka collision zone (HCZ), as characterized by the westward obduction of the crustal rocks of the Kuril arc (the Hidaka metamorphic belt (HMB)) along the Hidaka main thrust (HMT) and a thick foreland fold-and-thrust belt.

In and around the HCZ, a series of seismic reflection/refraction experiments were undertaken from 1994 to 2000, which provided important structural features including crustal delamination in the southern HCZ (Arita et al., 1998; Tsumura et al., 1999; Ito et al., 2000) and a thick fold-and-thrust belt with velocity reversals (low velocity layers) in the northern HCZ (Iwasaki et al., 2004). Reprocessing/reinterpretation for these data sets, which started in 2012, is aimed to construct a more detailed collision model through new processing and interpretation techniques. In this paper, we present a revised collision structure model from the A multi-disciplinary project of the 1998-2000 Hokkaido Transect, crossing the northern part of the HCZ in EW direction.

2. Processing and Analysis

The seismic expedition of the Hokkaido Transect is composed of a 227-km seismic refraction/wide-angle reflection profile extending from the hinterland to the fold-and-thrust and three seismic reflection lines whose total length is 130 km (Fig. 1(b)). These reflection lines were designed to almost coincide with the wide-angle line in the HCZ to ensure the complimentary analysis. In the seismic reflection processing, we applied the CRS (Common Reflection Surface Method)/MDRS (Multi-dip Reflection Surface Method) processing to the reflection data to improve the deeper image under the HCZ. Intensive refraction/wide-angle reflection analyses were also undertaken both for the dense seismic reflection data as well as seismic refraction/wide-angle reflection data to revise the shallower structure (<5-10 km) around the collision front and constrain physical properties (seismic velocities) in the deeper part (> 20-30 km) of the HCZ. A large amount of travel time data of the first arrival and later phases were used in determining the shallower structure by seismic tomography method (Zelt and Barton, 1998) and forward modelling by ray tracing (Iwasaki, 1988). The estimation of seismic velocity in deeper part was based on the amplitude modelling by asymptotic ray theory (eg. Cerveny, 1985).

(a) (b)

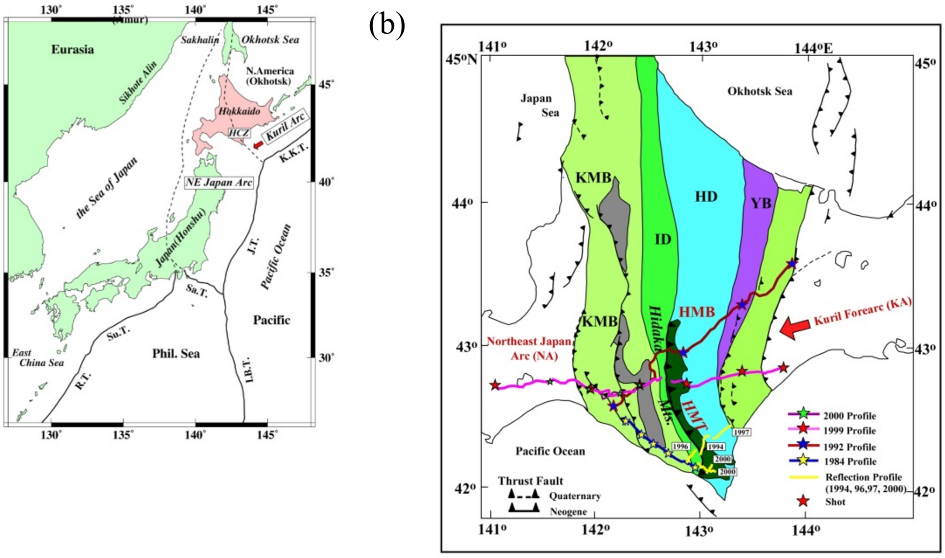

Fig.1 (a) Tectonic map around Japan. (b) Geology of Hokkaido Island and locations of seismic expeditions. The Refraction/wide-angle reflection experiment of the Hokkaido Transect is shown by a pink line. A series of seismic reflection survey were also undertaken in the central part of this line.

3. Results

3 (a) Shallow Structure

We conducted travel time tomography to both the refraction/wide-angle reflection data from 10 dynamite shots and reflection data from 10 dynamite and 78 small-charge dynamite/ vibroseis shots. In total, 44,616 travel time data were inverted. This model, which is almost consistent with the previous from the forward modelling by Iwasaki et al. (2004), shows a very thick (~10 km) sedimentary package in the fold-and-thrust belt. Also, beneath the hinterland, 5-7 km thick undulated sedimentary layers are found. Complicated geometry of the sedimentary layers 40-50 km east of the HMT may correlate active fault systems developed in the Tokachi plain. Between these thick sediments, namely just beneath the HMB, a crystalline crust is almost outcropped, which corresponds to high Vp and high Vp/Vs material corresponding to obducted middle/lower crustal materials. The forward modelling by ray-tracing to the reflection data set revealed the uppermost geometry of the HMT. West of the HMT, gently eastward dipping layering was found at a shallower depth (< 8 km), probably representing to fragments of Cretaceous subduction/arc complexes or deformation interfaces branched from the HMT. The seismic velocity beneath this layering is rather high (6.3-6.4 km) as compared with the upper crust in Japan (5.8~6.2 km/s).

3(b) Deeper Structure

The CRS/MDRS processing for the reflection data provided clearer images of the westward obduction of the upper half of the crust (including upper part of the lower crust) of the Kuril arc and the deformation of shallow structural packages within the fold-and-thrust belt. The obduction starts at a depth of 27-30 km (Fig. 2). Below the obducted part of the crust, there exists a 10-km thick reflective zone, expressing the deformation associated with the collision process.

The most important finding in the present processing is a series of reflection events imaged at a 30-45 km depth below the obducted crust. These events, showing gradual increase in dip to the east, are probably representing the lower crust and Moho within the NE Japan arc descending down to the east under the collision zone.

Refraction/wide-angle reflection analysis revealed the very complicated structure above the descending NE Japan arc. Eastward dipping strong reflectors with a contrast of 0.5-1 km/s are distributed in a depth range of 10-35 km in the HCZ. The Moho depth east of the HMT is about 25-30 km.

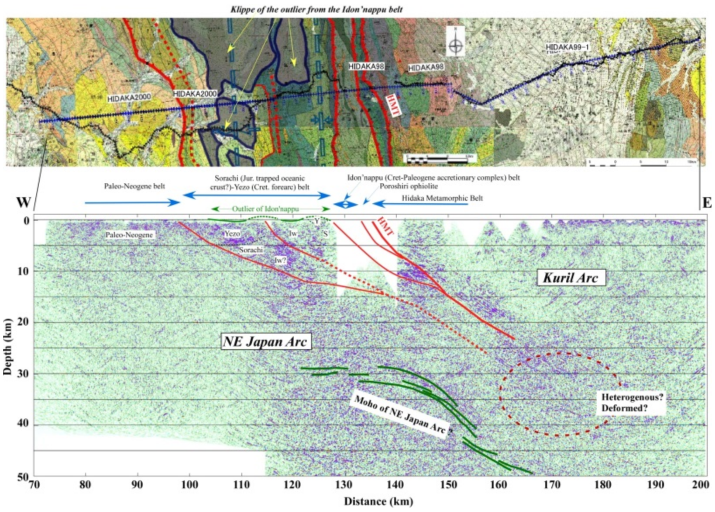

Fig.2. Seismic images of the Hidaka Transect by CRS/MDRS method.

Our result shows that the subducted NE Japan arc meets the Kuril arc 20-40 km east of the HMT at a depth of 20-30 km. The Moho east of the HMT is not clear but our data provide no evidence for a shallow Moho (< 30 km) as indicated by tomography studies. Weak but coherent phases observed at far offsets (120-180 km) on the wide-angle reflection line are explained as reflection from the lower crust of the Kuril arc, PmP and Pn from the NE Japan arc.

4. Discussion

Seismic reflection image in the southern HCZ reprocessed by almost the same techniques confirms a clear crustal delamination, where the upper 23-km of the Kuril arc crust is thrust up along the HMT while the lower part of the crust descends down to the subducted PAC plate (Ito et al., 2013; Tsumura et al., 2014). Our result, on the other hand, obduction of the Kuril arc crust starts at a deeper depth of 27~30 km. If the metamorphic rocks east of the HMT along our profile are the same crustal materials (shallower than 22-23 km depth) as in the case of the southern HCZ, the deeper crustal portion originally situated at 23-27~30 km depth must exist in the western side of the present HMT. The very strong reflectors found west of the HMT might result from the mixture of upper crustal (low velocity) materials of the NE Japan arc and middle/lower crustal (high velocity) materials of the Kuril arc.

5. Conclusions

(1) Integrated processing and analysis to seismic refraction/reflection data in Hidaka region provided new constraints on the deformation style of HCZ.
(2) CRS/MDRS techniques succeeded in imaging the obduction of the Kuril forearc upper crust and geometry of downgoing NE Japan arc.
(3) Refraction/wide-angle reflection analysis delineated a detailed structure beneath the HMT and the hinterland and highly heterogeneous deformation at middle/lower crustal levels of 15-35 km depths.
(4) Eastward and westward dipping reflectors with high velocity contrast at 15-35 km depths may represent merging of lower velocity materials (upper crust of the NE Japan Arc) and higher velocity materials (middle/lower crust of the Kuril Arc) at the collision front.

References

Arita, K., Ikawa, T., Ito, T., Yamamoto, A., Saito, M., Nishida, Y., Satoh, H., Kimura, G., Watanabe, T., Ikawa, T and Kuroda, T., 1998. Crustal structure and tectonics of the Hidaka Collision Zone, Hokkaido (Japan), revealed by vibroseis seismic reflection and gravity survey, *Tectonophysics*, **290**, 197-210.

Cerveny, V., The application of ray tracing to the propagation of shear waves in comlex media, *in Seismic Shear Waves Part A: Theory*, edited by Dhor, G., pp1-124, Geophysical Press, London-Amsterdam, 1985.

Ito, T., 2000. Crustal structure of the Hidaka collision zone and its foreland fold-and-thrust belt, Hokkaido Japan (in Japanese with English abstract), *J. Japanese Assoc. Petrol. Technol.* **65**, 103– 109.

Ito, T., Tsumura, N., Iwasaki, T., Arita, K,. Kurashimo, E., Sato, H., Hirata, N., Noda, K., Fujiwara, A., Abe, S., Kikuchi, S. & Suzuki, K., 2013. Reinterpretation of the lithospheric structure beneath the Hidaka collision zone, Hokkaido, Japan 1. Outline, 2013 Fall Meeting, American Geophysical Union, San Francisco, T33A-2610.

Iwasaki, T., 1988. Ray-tracing program for study of velocity structure by ocean bottom seismographic profiling (in Japanese), *J. Seismol. Soc. Jpn.*, **41**, 263-266.

Iwasaki, T., Adachi, K., Moriya, T., Miyamachi, H., Matsushima, T., Miyashita, K., Takeda, T., Taira, T., Yamada, T. & Ohtake, K., 2004. Upper and middle crustal deformation of an arc-arc collision across Hokkaido, Japan, inferred from seismic refraction/wide-angle reflection experiments, *Tectonophysics*, **388**, 59-73..

Tsumura, N., Ikawa, H., Ikawa, T., Shinohara, M., Ito, T., Arita, K., Moriya, T., Kumura, G. and Ikawa, T, 1999, *Geophys. Res. Lett.*, **26**, 1057-1060.

Tsumura, N., Iwasaki, T., Ito, T., Sato, H., Kurashimo, E., Hirata, N., Arita, K., Noda, K., Fujiwara, A., Abe, S., Kikuchi, S. & Suzuki, K., 2014., Reinterpretation of the Lithospheric Structure beneath the Hidaka Collision Zone, Hokkaido, Japan 1. Outline, 16-th SEISMIX International Symposium **(**International Symposium on Multi-scale Seismic Imaging of the Earth's crust and Upper Mantle), Castelldefels, Barcelona, Spain, P34.

Zelt, C.A., Barton, P.J., 1998. Three-dimensional seismic refraction tomography: a comparison of two methods applied to data from the Faeroe Basin. *J. Geophys. Res.* **103**, 7187–7210.

O-21 **Lithospheric structures and their formation process at the northwestern border region of the Izu collision zone, central Japan**

Tanio Ito

Teikyo Heisei University, Mailing Address Nakano 4-41-2, Nakano-ku, Tokyo

Several seismic profiling studies have been made widely from the Central Japan Alps to the southwestern foot of the Mt.Fuji cross the Median Tectonic Line, the Southern Japan Alps, the Itoigawa-Shizuoka Tectonic Line, and so-call "the South Fossa Magna" . Their main purpose are to reveal the lithospheric structures at the northwestern border region of the Izu collision zone and their formation process since Middle Miocene. The significant results of the studies are summarized as follows:

1. Most materials of the colliding Izu arc on the Philippine Sea Plate (PHS) have been subducting beneath the Japanese island arc since middle Miocene. Only three buoyant huge blocks were exfoliated from the upper crust of the Izu arc and have accreted to the Japanese island arc. Thus nearly 50-km thick materials derived from the Izu arc have been underplated to the Japanese island arc.
2. The initial stage of the colliding process produced two major left-lateral faults: the southern segment of the Itoigawa-Shizuoka Tectonic Line (ISTL) and the Akaishi Tectonic Line (ATL). The former was originally formed as a major thrust in the subduction zone of the PHS, and then changed into a high-angle left-lateral fault associated with the colliding process. The latter displaced the structure of the Outer zone at about several tens km in a left-lateral slip sense. Its northern extension cut the gently dipping original Median Tectonic Line (MTL) and newly constructed the present high-angle MTL. In that sense, the present MTL is a part of the ATL.
3. The Outer zone exhibits extraordinary structures only between the new MTL and the northern part of the southern segment of the ISTL. That is, the verging direction is opposite to that of the accretionary complexes in the Outer zone in southwest and central Japan. This suggests the Outer zone there has been overturned by the collision.
4. At the present northwestern border region of the Izu collision zone, the active faults in the Fujikawa-kako fault system are spraying directly from the upper surface of the PHS at about several km in depth. Their vertical slip rate is estimated to be about 4 mm / year. Considering that the fault system forms a small-scale nappe structure in the shallower part, their net slip rate must be more than the vertical one.

O-22 Fault model of the 2014 Northern Nagano earthquake: Moving towards estimation seismic hazard using the MeSO-net stations.

Yannis Panayotopoulos, Naoshi Hirata, Takaya Iwasaki, Shin'ichi Sakai, Hiroshi Sato (ERI, Univ. Tokyo)

On November 22, 2014 a destructive earthquake with a local magnitude (M_{JMA}) of 6.7, struck Northern Nagano prefecture in Honshu, Japan. The earthquake, which we will refer to as the 2014 Northern Nagano Earthquake, occurred at local time 22:08:17 (UTC+9) and its hypocenter was located by the Japan Metrological Agency (JMA) at a depth of 4.59 km, a few km east of Hakuba village (Fig. 1). Due to its proximity to the Itoigawa-Shizuoka Tectonic Line the main shock is inferred to have occurred on the Kamishiro fault segment of the Northern ISTL (Japan Meteorological Agency, 2014). The ISTL is a prominent inland fault system which extends across Honshu Island from Itoigawa City on the Sea of Japan to Shizuoka City on the Pacific Ocean. It divides Honshu Island into NE and SW parts (e.g., Yabe, 1918). The ISTL is a key feature controlling the evolution of the Northern Fossa Magna (NFM) rift basin (Sato, 1994) since its creation in early Miocene. The NFM basin is part of a Miocene rift system that developed in the final stages of the opening of the Sea of Japan (25-15 Ma)(Otofuji et al., 1985; Yamaji, 1990). The area to the west of NFM is occupied by Pre-Neogene basement rocks, which consist of Mesozoic accretionary complex and granitic rocks and which are generally referred as the "inner zone" (Kano et al., 1990; Taira, 2001)(Fig. 2). The basin itself is filled mostly with more than 6-km-thick Miocene marine sediments and displays significant folding on a NE-trending axis. The stratigraphy of the basin is represented by a sequence of volcanic and volcanoclastic rocks, distal to proximal turbidities, and shallow marine to fluvial sediments (Kato, 1992). The basin has undergone shortening deformation since the Pliocene (3 Ma) (e.g. Sato, 1994) due to compressional inversion of a formerly extensional stress regime (e.g. Williams et al., 1989; Sato 1996).

We used data recorded at 42 stations of the local seismographic network in order to locate 2118 earthquakes that occurred between November 18 and November 30, 2014. In order to accurately estimate hypocenters, we assigned low Vp velocity models to stations within the Northern Fossa Magna (NFM) basin which lies to the east of the Kamishuiro fault to account for large lateral crustal heterogeneities across the fault. We relocated the hypocenters inside a 3D velocity model using the double difference method and observed several distinct clusters of hypocenters along the fault. We have split the fault into 5 segments from south to north and correlated the observed surface deformation caused by the main shock with surface geology and the aftershock clusters (Fig. 3). The dip of the source fault steepens where the deeper extension of the Kamishiro fault reaches the bottom of the NFM basin and merges with the deeper extension of the Otari-Nakayama fault. We interpret this geometry to be evidence of shortcut thrusting in the footwall of the Otari-Nakayama fault relative to the Kamishiro fault. We identify a prominent seismic activity gap in the area of the main shock near the center of the fault where the InSAR data indicate significant deformation, and increased seismic activity to the north where deformation is low. We interpret the InSAR observations by assuming large coseismic slip in the area of low aftershock activity and small coseismic slip in the areas of high seismicity to the north.

In addition, the 2014 Northern Nagano earthquake was the first and largest event from the Itoigawa-Shizuoka Tectonic Line (ISTL) to be well recorded by MeSO-net stations. Our proposed fault model can be used to understand the Kanto Basin seismic amplification from a forthcoming large M7+ earthquake on the ISTL. Finally, the recordings on MeSO-net stations are essential for calibrating the estimated absolute long period (1-10 sec) amplitudes in a study of ground motion prediction from Virtual Earthquakes (Denolle et al., 2014). The present study is supported by Ministry of Education, Culture, Sports, Science and Technology (MEXT) of Japan, under its Earthquake and Volcano Hazards Observation and Research Program and Special Project for Reducing Vulnerability for Urban Mega-earthquake Disasters.

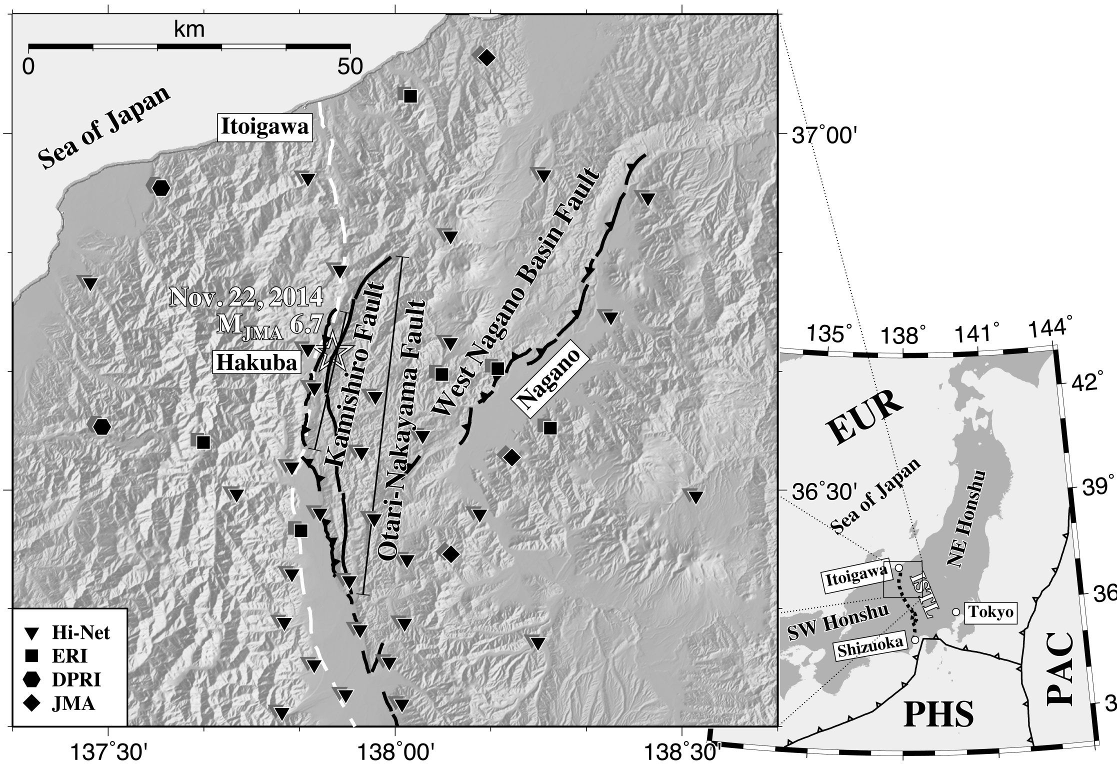

Fig. 1. Location map of the Kamishiro fault and Otari-Nakayama fault and distribution of stations of the permanent earthquake observation network in the area of study. Inverted triangles: stations of the High Sensitivity Seismograph Network of Japan (Hi-Net); Squares: stations operated by the Earthquake Research Institute of Tokyo University (ERI); Hexagons: stations operated by the Disaster Prevention Research Institute of Kyoto University (DPRI); Diamonds: stations operated by the Japanese Meteorological Agency (JMA). White dashed line: approximate boundary of the Northern Fossa Magna Rift basin at 0 km depth mapped from surface geology (Geological Survey of Japan, 2003) and tomography studies (Panayotopoulos et al. 2014).White boxes indicate toponyms in the vicinity of the ISTL, Itoigawa: Itoigawa city; Hakuba: Hakuba village; Shizuoka: Shizuoka city; Tokyo: Tokyo metropolitan area. PHS: Philippine Sea Plate; PAC: Pacific Plate; EUR: Eurasia Plate. White open star: epicenter of the 2014 Northern Nagano Earthquake determined by JMA.

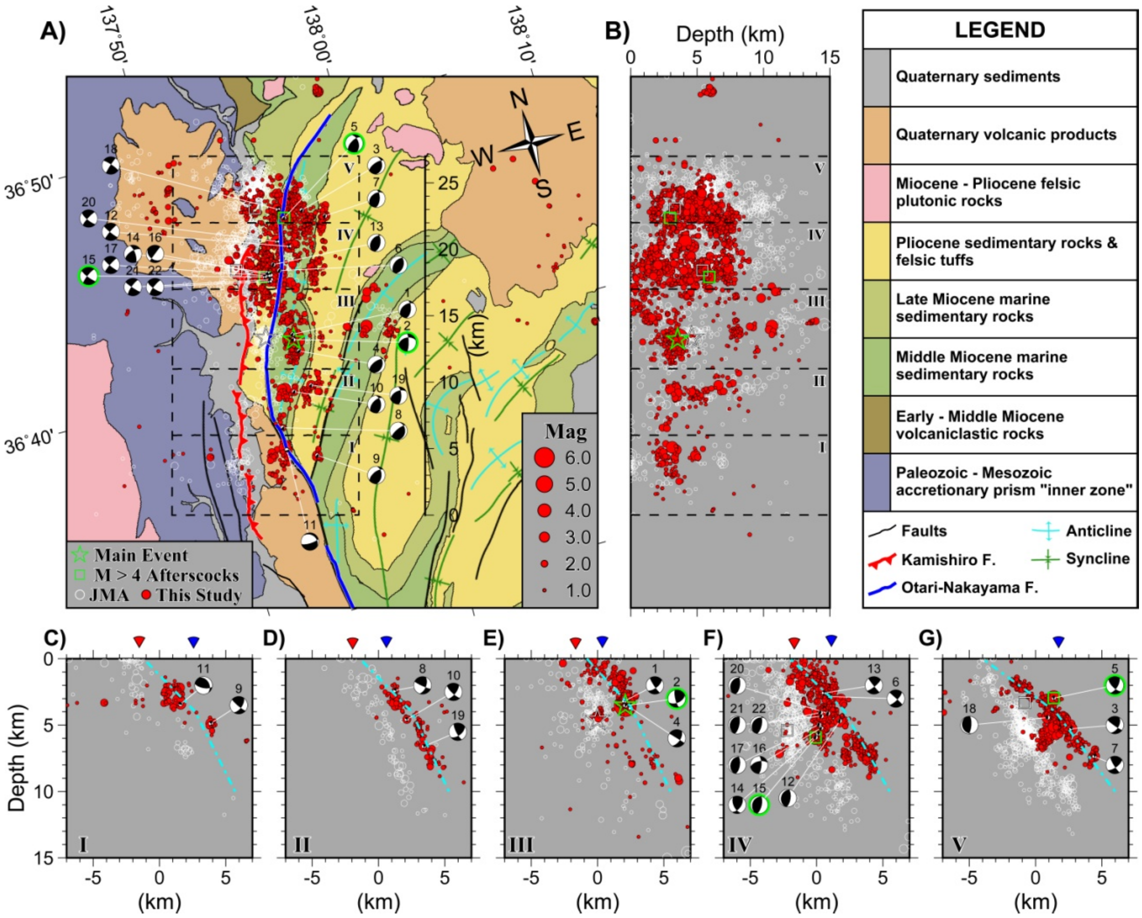

Fig.2. JMA-UEC hypocenter locations and double difference (DD) relocated hypocenter locations from this study correlated with surface geology. a) Plot of JMA-UEC epicenters (white rings) and DD relocated epicenters (red circles) overlaid on a simplified geological map (after Editorial Committee of Civil Engineering Geologic Map of Kanto, 1996). Red line: surface trace of the Kamishiro fault. Blue line: surface trace of the Otari-Nakayama fault. Focal mechanism solutions for the first major foreshock (earthquake 1), the main shock (earthquake 2) and major aftershocks (earthquakes 3 to 22) plotted showing the lower hemisphere. b) Cross-section of all hypocenters along the Kamishiro fault from South to North. Note the absence of hypocenters at approximately 4 to 7 km depth inside segments II and III. c~g) Cross-sections across the Kamishiro fault from South to North. The clustering of the DD relocated hypocenters appears to occur on a SE-dipping line whose angle to the surface shallows to the north. Focal mechanism solutions for the first major foreshock (earthquake 1), the main shock (earthquake 2) and major aftershocks area plotted showing the back hemisphere (earthquakes 3 to 22).

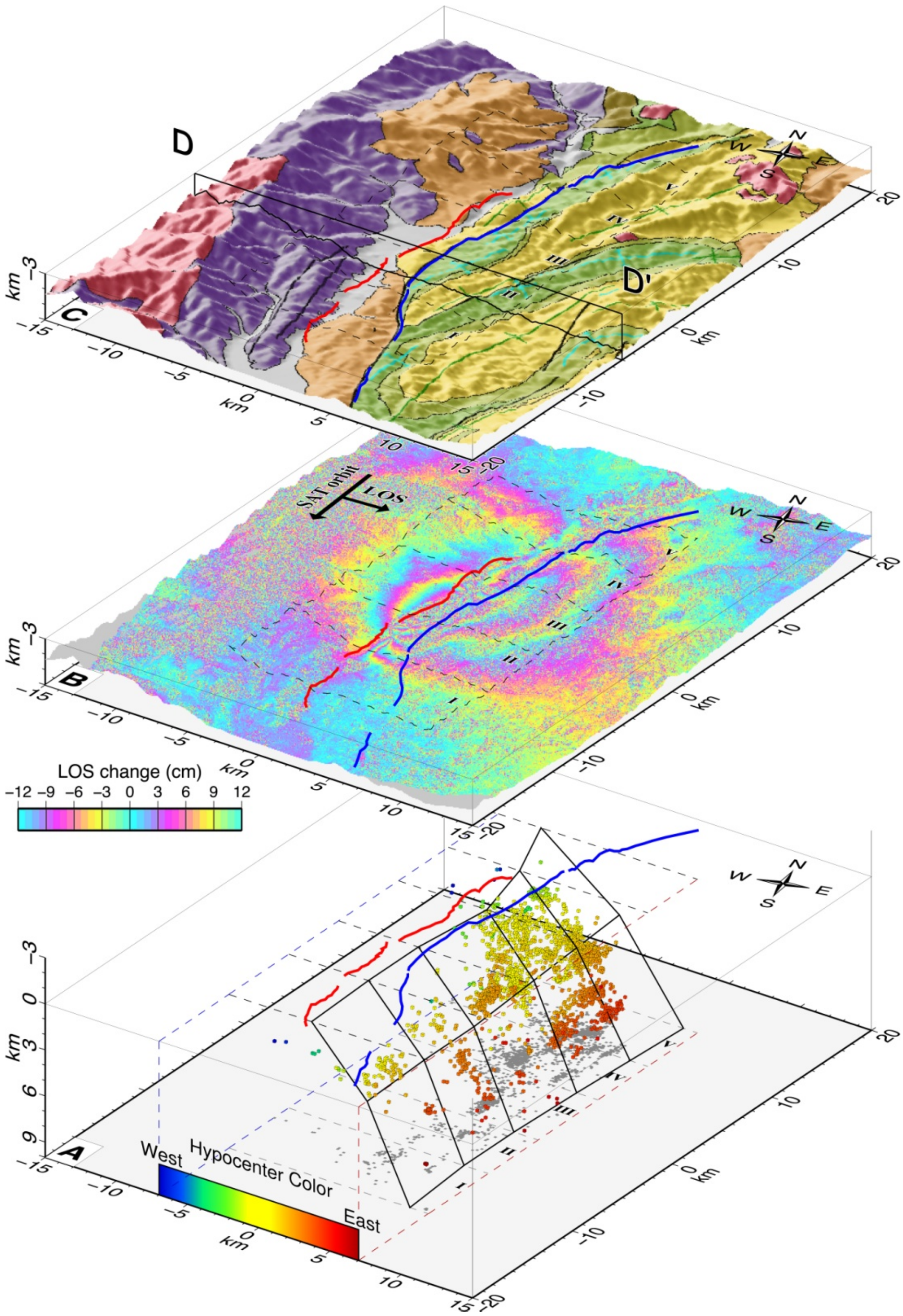

Fig.3. Correlation of the fault model to the observed crustal deformation and surface geology-topography. Red line: surface trace of the Kamishiro fault. Blue line: surface trace of the Otari-Nakayama fault a) 3-D fault model derived by the clustering the DD relocated hypocenters. b) InSAR plot analyzed by GSI from ALOS raw data of JAXA, METI superimposed on a topographical relief map (Geospatial Information Authority of Japan, 2014). Satellite data suggests a maximum upward deformation of 1m to the east of the fault trace and a maximum downward deformation of 20 cm to the west of the fault trace in segment III. c) 3-D map of the surface geology and topography along Kamishiro fault. See Fig. 2 for geological map legend. Segments IV and V at the northern end of the Kamishiro fault form blind thrusts which have been covered by Quaternary volcanics.

O-23 Crustal structure beneath the source region of 1891 Nobi earthquake, central Japan

Noriko Tsumura[1], Yuu Mizumi[1], Tomoko Emoto[2], Hiroshi Furuya[3], and The Research Group for the Joint Seismic Observations at the Nobi Area[4]

1. Graduate school of Science, Chiba University, Japan, 2. Suncoh Consultants Co. Ltd., Japan
3. Itochu Oil Exploration Co. Ltd., Japan, 4. Earthquake Research Institute, the University of Tokyo, Japan

1. Introduction

Central Japan is characterized by the region where active faults occur densely. Further a mega-kink which has NW-trending hinge zone was formed by the crustal scale bending of the Japanese island arc in association with the opening of the Japan Sea. As several active faults, such as, the Yanagase and the Yoro faults are running along the hinge zone, and the Neodani fault in the northeastern limb close to it, the locations, histories, and activities of these faults must be deeply related to the crustal structure established during the opening of the Japan Sea [Kano, 2002].

Recently it was found that the hinge zone is running above the subsurface axial part of the NW-plunging broad and huge antiformal undulation made by the Philippine Sea plate (PSP) 's upper surface [Hirose et al., 2008].

This correspondence among three kinds of the structures mentioned above suggests essential relationship between the subducting PSP and the overlying crustal structures in the northwestern part of Central Japan.

Since it is important to know whole crustal structure there and the location of the PHS upper surface for understanding the deformation system of the study region, several kind of seismic observations were conducted by universities and research institutes of Japan during the period from 2009 to 2014.

2. A linear seismic array observation across Neodani Faults Zone

Three seismic station lines were settled with an interval of approximately 1km and each length is about 30km. These seismic lines intersected at high angle with Neodani Faults Zone (NFZ), where the largest inland Nobi earthquake occurred in 1891. The location of the linear array stations was shown by open squares in Fig.1. In October 2009, Chiba and Gifu Universities, and NIED carried out 8 dynamite shots and 2 vibrator shots for a seismic reflection survey (asterisks of Fig.1). These shots were recorded by our array stations with sampling frequency of 200Hz.

We applied a conventional reflection method to the linear array data. Since derived NMO images show laminated reflections from the deeper part, we estimated crustal velocity by forward modeling using the travel times of the reflected waves.

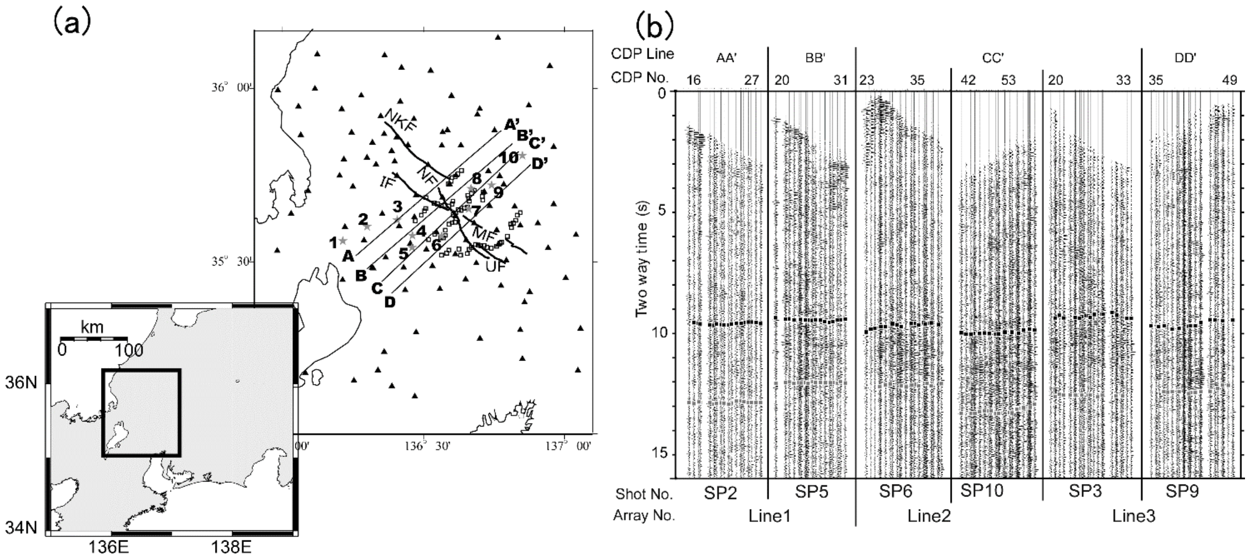

Fig.1 (a) A temporary seismic stations(triangle) and linear array stations(square) settled in and around Neodani Faults Zone (NKF, NF, UF,IB, MF: indicate active faults, Nukumi, Neodani, Umehara, Ibigawa and Mugigawa faults, respectively). Asterisks and thin lines show the shots for seismic reflection survey and CDP lines. (b) NMO reflection profiles along the CDP lines, AA',BB',CC',and DD'. Shot numbers were given in Fig.1 (a) by numerals.

3. A temporary seismic observation in the Northern Mino-district

A temporary dense seismic observation for local earthquakes (triangles of Fig.1) were conducted in and around the NFZ Spatial intervals of the temporary stations were quit shorter than that of the routine seismic stations and it makes us possible to clarify a detailed attenuation structure beneath the study area.

We used a joint inversion method in which the 3-dimensional attenuation structure, source effects, and site effects are deconvolved (Tsumura et al., 2000). P-wave velocity spectra of 131 events recorded at 99 stations were used for the inversion. Amplitude spectra were calculated by FFT for a time window of 1.0 s, beginning from the P arrivals. The total number of amplitude spectra was 7065.

4. Results and Interpretation

Applying a reflection analysis, we found significant reflections with duration of 2s around 10s two way travel time (Fig.1 (b)). Based on comparisons with other seismic reflection profiles, these events were interpreted to come from the laminated lower crust within the overriding plate. The depths of laminated lower crust varies across the NFZ, which is shallower in the southwest than in the northeast.

In the southwestern part of study area, the top of the PSP estimated from travel time tomography is shallower than the lower limit of the laminated lower crust. This result might suggest that the subducting PSP may contact with the bottom of the overriding crust beneath the study area.

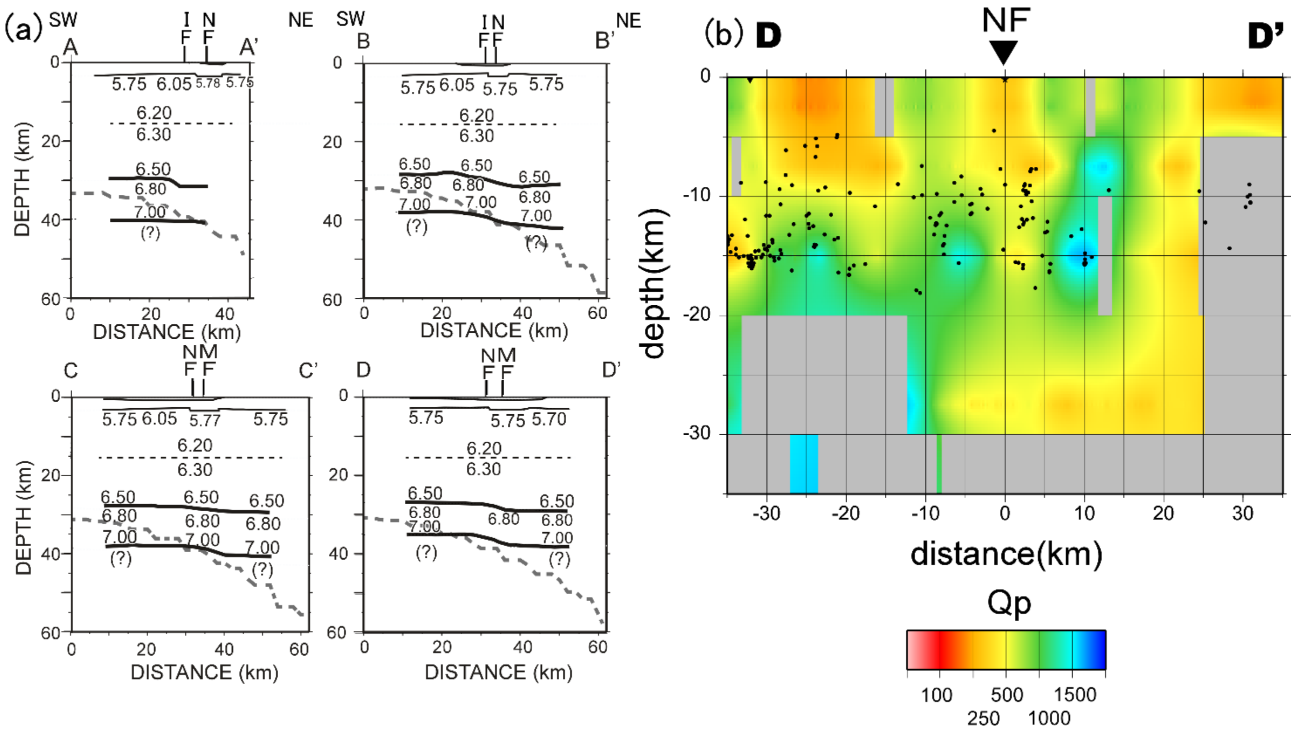

Fig.2 (a)Two-dimensional velocity structure models along lines AA’,BB’,CC’,and DD’ in Fig.1. Broken lines indicate the top of the Philippine Sea plate[Nakajima et al.(2009) , Hirose et al.(2008)].

(b) Depth cross section of Qp structure along line DD’. ▼show the surface location of Neodani fault.

From the results of attenuation tomography, we found that Q values also varies across the NFZ and Q values were higher in the southwestern side of the fault than those in the northeastern side at the depths of 5-10km. In the depth deeper than 10km, Q values just beneath the surface trace of the faults show lower than those at the outside of the faults. Q value of the area at the junction between Neodani, Ibigawa and Mugigawa faults has about 300, which is lower than those in the southeastern part of the faults. This low Q zone seems to continue from the surface to the lower crust.

Derived velocity and Q structures show that similar depth difference exists across the NFZ, implying that displacement along the Neodani faults extends to the deep crust and its configuration might be affected by the contacting PSP.

Conclusion

We estimated a velocity model and an attenuation structures beneath the NFZ, central Japan, where the largest inland Nobi earthquake occurred in 1891, using data recorded in linear arrays and dense seismic observation network. Depth difference of both structure, i.e. velocity and attenuation, exists across the NFZ and it may indicate that that displacement along the Neodani faults extends to the deep crust and its configuration might be affected by the contacting PSP.

Reference

Hirose et al., 2008, Jour. Seismo. Soc. Japan, 60, 3, 123-138
K. Kano, 2002, Jour. Geol. Soc. Japan, 108,591-605
Nakajima et al, 2009, Jour. Geophys. Res., 114, B08309, doi:10.1029/2008JB006101
Tsumura et al. , 2000, Tectonophysics, 319, 241-260.

O-24 **Tafilalt Ordovician Iron Formations (IFs) Discovery, Easter Anti Atlas of Morocco: Nomenclature and Classification**

Naoufal SAOUD*[(1)], Mohammed CHARROUD [(1)], Said HINAJ [(1)], Mohammed DAHIRE [(2)], Souhail MOUNIR [(1)].

[1)] Laboratory of Georesources and environment, Faculty of Science and Technology, Sidi Mohammed Ben Abdellah University, Fez-Morocco.
[2)] Laboratory of Geodynamics and natural resources, Faculty of Science Dhar el Mehrez, Sidi Mohammed Ben Abdellah University.

Correspondence contact:
Naoufal SAOUD, Laboratory of Georesources and environment (LGE), Faculty of Science and Technology, Sidi Mohammed Ben Abdellah University, B.P 2002, Imouzzer street, Fez Morocco. Mail address: saoud.naoufal@gmail.com

Abstract

The Tafilalt iron deposit is located in the east part of the Moroccan Anti Atlas structural domain. It is a sedimentary iron ore, deposited during upper ordovician, in shallow sea environment , occasionally influenced by waves, and forwarded to the especial climatic conditions characterizing the Ordovician "earth snowball" event (Fig.1. A) (Saoud et al., 2015 ; El Maazouz, 2007 ; Hamoumi, 1988). However the Ashgill deglaciation process allows the melting snow on continental areas, which causes an important contribution of sedimentary siliciclastic detrital supply, and a considerable increase of the sea level thus allowing medium oxygenation (Fig.1.B).

In fact, this contributed to the liberation of oxygen which is an essential chemical element for establishing combinations with reduced iron, and giving birth to complex iron oxides, able to gather with the sedimentary siliciclastic fraction. The latter is the phenomenon which promotes the iron oxides precipitation in the Bani2 sandstones, as a form of Hematite (Fe_2O_3) and Magnetite (Fe_3O_4) (Fig.1.C) in giving rise to IFs (Iron Formations).

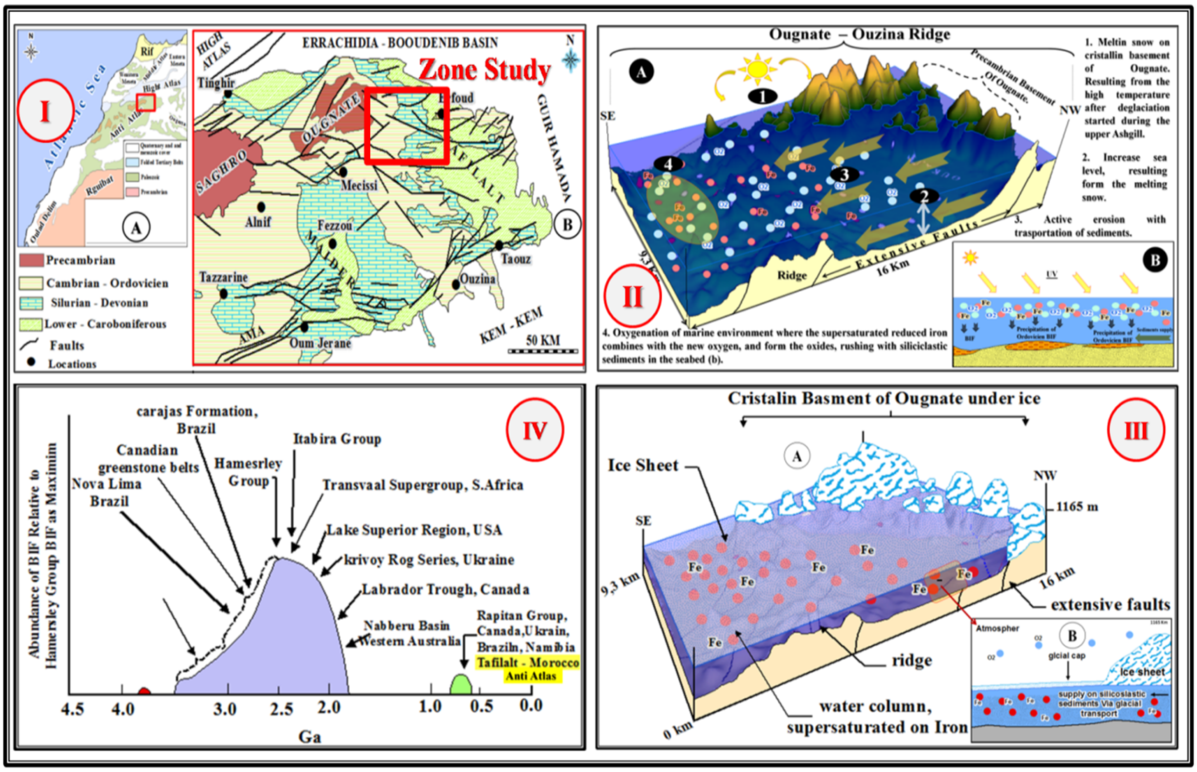

Fig.1: (I) the Moroccan geological map with localization of zone study (A and B); (III) Geodynamic model showing the appearance of ice cap during Caradoc; (II) Geodynamic model of Tafilalt basin with the super saturated sea environment on reduced iron (Fe) accompanied with oxygenation sea level and formation of iron oxides (IV) BIF Classification and position of Tafilalt BIF Kind.

The discovery of IF deposit in the Ordovician basin of Tafilalt at the level of the Anti Atlas Moroccan, and their description, illustrates an extension and local character because of its relation with typically geodynamic phenomenon which is the passage from sub-continental glacial medium to marine platform environment. This change is linked to the beginning of the Gondwana migration from an ice polar position to more northern situation (Berry et al., 1990; Destombes et al., 1963, 1966, 1967; Babin et al., 1993; Hamoumi, 1988; EL Mazouz, 2007). The iron content in the Tafilalt IFs is in fact an exploitable ore body, since the tenors exceed 40% (Fe). This syn-sedimentary iron ore is linked to the siliciclastic detrital phase characterizing the Ashgill. It corresponds to an iron deposit of Rapitan type (Fig.12), formed during Upper Ordovician, where the deglaciation is the engine trigger of the iron mineralization establishment.

The petrographic studies and mineralogy of thin sections polished surfaces, prepared from the taken samples (Fig.2), indicate that the mineralization is evolving in a progressive way of the Middle Cambrian, to reach its peak during the upper Ordovician, and it is usually represented in the form of hematite and magnetite, concentrated around the oidales particles, giving rise to a granular or Oolitic iron oxides form.

This iron represented as granular form, is probably caused by the process of super saturation on reduced iron in water column, which can generates a massive extinction of micro-organisms producing the oxygen required for the oxidation of ferrous fraction, and finally precipitates of ferric oxides as an oolitic form.

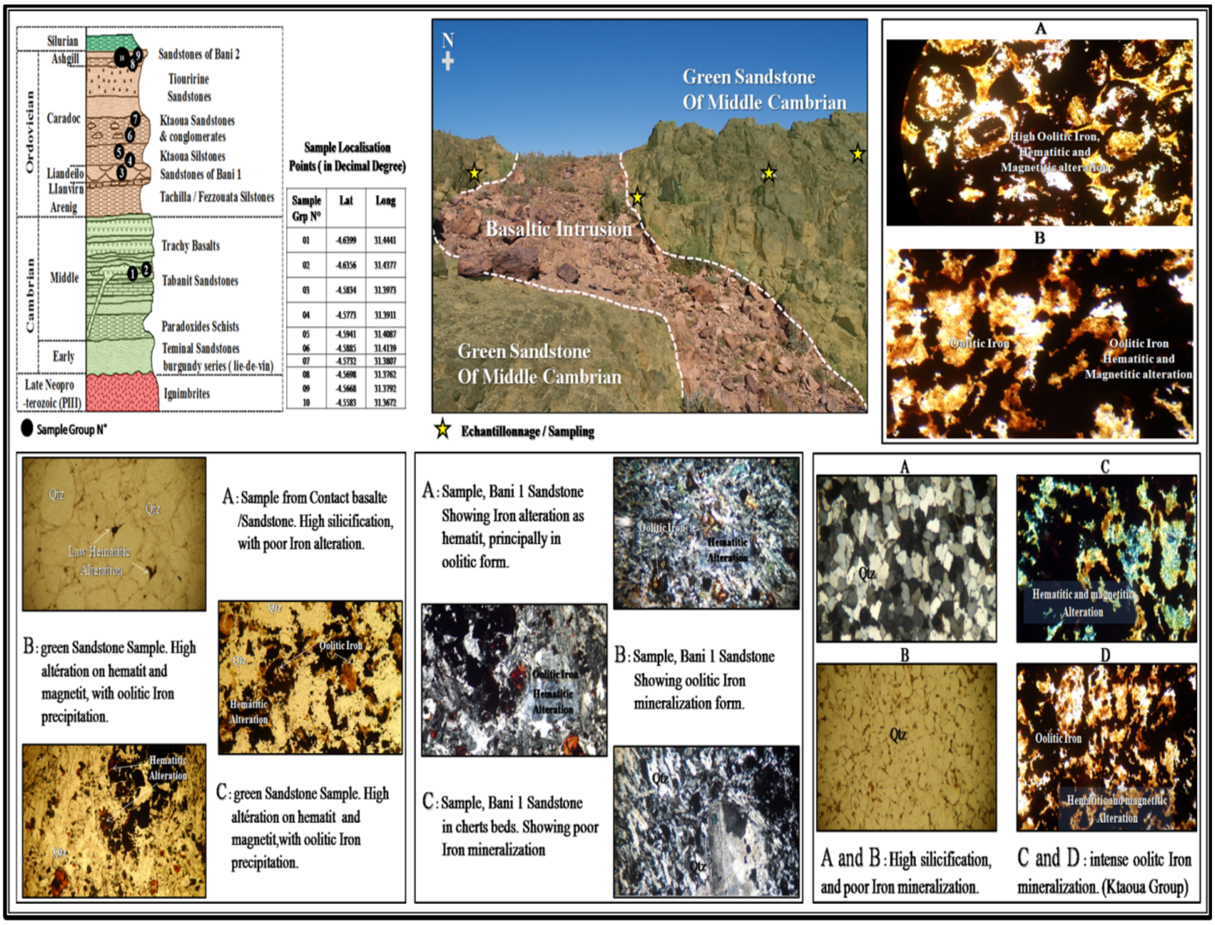

Fig.2 : Localization of studied samples, with petrographic description of iron mineralization, using the thin sections and polished surfaces.

Through the Tafilalt IFs studies, we have highlighted the distribution of iron mineralization which is, mainly represented as granular or oolitic form. That leaves us classify these formations as "Granular Iron formations" or GIF (Trendal, 2002), which are removed during Neoproterozoic. The Ordovician," earth snowball" climatic event presents the key factor which had brewed of a very exceptional geographical geodynamic conditions, responsible for the formation of an iron deposit of Type GIF, both assigned to Rapitan kind deposits (Saoud et al. ,2015).

References:

- Berryn.B.W. & Wilde P. 1990: Graptolite biogeography: implications for paleogeography and paleoceanography. Paleogeography and Biogeography, Geological Memoir n°12, pp.129-137.
- Destomes J. 1963 : Quelques nouveaux Phacopina (Trilobites) de l'Ordovicien supérieur de l'Anti-Atlas (Maroc). Notes et Mem. Serv. Geol. Maroc, n° 172, 23, pp.47-65,
- Destomes J. 1966 : Quelques Calymenina (Trilobitae) de l'Ordovicien moyen et supérieur de l'Anti- Atlas (Maroc). Notes et Mem. Serv. Geol. Maroc, n° 26, 188, pp. 33-53.

- Destomes J. 1967 a : Distribution et affinités des genres de Trilobites de l'Ordovicien de l'Anti-Atlas (Maroc). C. R. Somm. Soc. Géol. Fr., 4, pp. 133-134.
- Hamoumi N. 1988 : La plate forme Ordovicienne du Maroc: dynamique des ensembles sédimentaires. Thèse d'Etat. Univ. Louis Pasteur. Strasbourg 225p.
- El Maazouz B. & HamoumiI N. 2007: Différenciation paléogéographique à l'Ordovicien supérieur dans le Tafilalt (Anti-Atlas oriental, Maroc) sous l'interaction de la glaciation et de la tectonique. C. R. Geoscinces, doi: 10.1016/j.crte.2007.07.002.
- Saoud N., Charroud M., Hinaje S., Dahire M., Mounir S. 2015: "A New Banded Iron formations deposit Discovery in the eastern Anti Atlas of Morocco". *International Journal Of Multidisciplinary sciences and engineering, Volume 6 issue 7, July 2015.*
- Trendall, A.F. (Ed.), 2002. The significance of iron-formation in the Precambrian stratigraphic record. Precambrian sedimentary Environments: A Modern Approach to Depositional Systems. IAS Special Publication, 44. Blackwell, Oxford, 33-66 pp.

O-25 **Inherited Landscapes, Tectonics, Eustasy and Basin Fill**

Bilal U. Haq

NSF, Washington, DC, USA, and Pierre & Marie Curie University, Paris, France

Sea level variations control marine productivity as well as sedimentary accommodation and thus the nature of the basin fill. Understanding the causal mechanisms of these changes and deciphering their history is therefore fundamental to exploration for hydrocarbons. The role of *eustatic* (global) vs *eurybatic* (local/regional) sea-level fluctuations in tuning the quasi-cyclic sedimentary record of transgressions and regressions along continental margins and in the interior basins has been a controversial issue for several decades. However, recent years have seen a convergence of views among several geological subdisciplines and here the geodynamicists have come to the aid of stratigraphers in clarifying the controls on long-term sea level variations. With this has come the realization that without understanding inherited topographies reconstructions of the past land- and seascapes will remain unconstrained.

Sequestrations of seawater on land (as ice or soil moisture) or its subduction-related entrainment in the mantle are two direct means of lowering global sea level. Sea-level changes can also be affected by modifications in the container capacity of the ocean through numerous interconnected solid-Earth processes. Some of these processes can only refashion landscapes regionally, thus affecting local measures of sea-level change.

In a new in-depth appraisal of this topic Cloetingh and Haq (2015) have reviewed the various recent developments that have led to this convergence of opinions between stratigraphers and geophysicists. This includes advances in seismic tomography and high-speed computing that allow detailed forward and inverse modeling. In stratigraphy new concepts permit envisioning large-scale transfers of material among depocenters, which have brought us closer to understanding factors that influence landscapes and sea levels, their complex feedbacks, and the resultant basin fills, and thus of importance for exploration geology. As a result estimates of the amplitude of long-term eustatic changes are now converging using different datasets. We have learned that solid-Earth processes operating on decadal to multi-million year time scales are all responsible for retaining lithospheric memory and its surface expression. These include glacial isostatic adjustments that cause local topographic anomalies (on shorter 10^1-10^2 years time scales) while post-glacial rebound can be enhanced by viscous mantle flow (on somewhat longer time scales of 10^3-10^5 years). On extended time scales of millions of years, oceanic crustal production variations, plate reorganizations and mantle-lithosphere interactions (e.g., dynamic topography) become more influential in altering the longer wavelength surface response that obviously affects local measures of sea-level rises and falls. These regional surface anomalies explain why *eustatic* expression of sea level, when measured stratigraphically in different places, yields variable amplitude values.

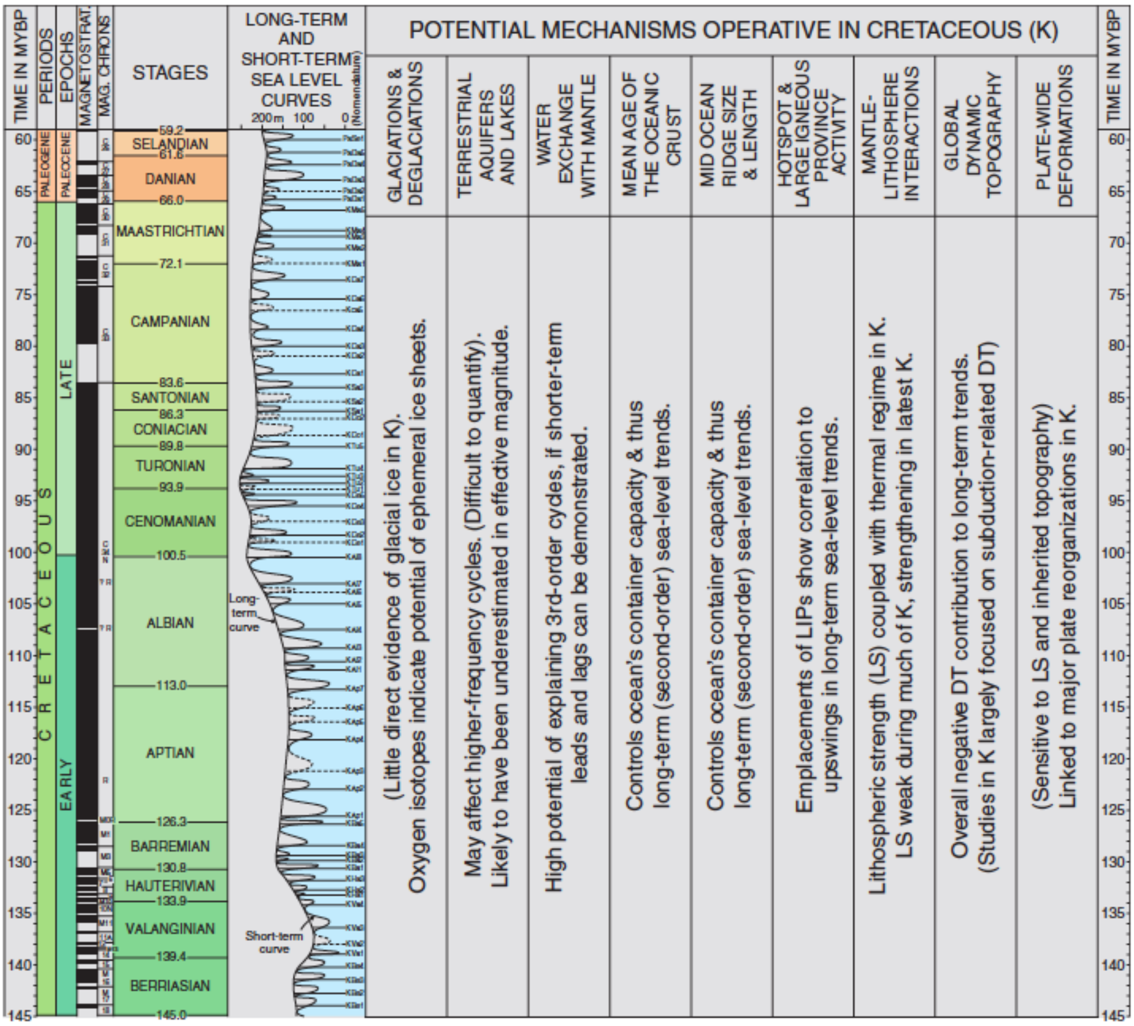

Figure 1: An updated sea-level curve for the Cretaceous (after Haq, 2014) plotted against potential mechanisms that could have been operative collectively in this period to produce the long-term (and possibly also contribute toward the short-term) sea level trends. The reasons for shorter-term (third-order) quasi-cyclic changes remain elusive.

In spite of many remarkable advances, we are no closer to resolving the causes for exploration-scale depositional sequences, i.e., those based on third-order quasi-cyclic sea-level changes (0.5-3.0 Myr in duration). Ascertaining whether ice-volume changes were responsible for these will require discerning the potential for extensive glaciation at higher altitudes on Antarctica in the deep past by modeling topographic elevation involving large-scale mantle processes. Another promising avenue of inquiry is the *leads* and *lags* between entrainment and expulsion of water within the mantle on third-order time scales.

References:

S. Cloetingh, B. U. Haq, Inherited Landscapes and Sea level Change. Science, 347, 1258375 (2015). DOI: 10.1126/science.1258375.

B.U. Haq, Cretaceous Eustasy Revisited. Global and Planetary Change 113, 44-58 (2014). DOI: 10.1016/j.gloplacha.2013.12.007.

O-26 **Rifting, Spreading and Inversion in the South China Sea Basin; Map View**

Manuel Pubellier, *CNRS, UMR-8538, 16 rue P&M Curie, 75005, Paris*
GRI, (*Group Research and Industry, ENS/CNRS/TOTAL*)

The South China Sea, is presented here as a case example of the evolution of basins developed at convergent boundaries.

Like most of the basins of SE Asia, it opened inside the Cretaceous Sundaland (a promontory of SE Eurasia) since the Late Cretaceous in a manner that may be correlated to the conditions of the subduction around it. Because of its narrow V shape oceanic crust, the wide extension of its rifted continental crust, and the various styles of rifting is an interesting object to study the formation of passive margins developed above former subduction zones. In addition, the South China Sea has been the focus of scientific interest in the past decade including ODP and IODP drillings, oil and gas exploration, and projects from several international teams onshore and offshore, which supplied a great deal of seismic and other geophysical and geological data. We present hereafter a synthesis of the main characteristics of the SCS on a structural map focused on the Late Mesozoic and Cenozoic features, as a support for depicting the birth and the decay of the basin.

Geological features linked to extensional history.

The basement, similar in China, Vietnam and part of the western Philippines is undifferentiated on the map. During Mesozoic times, the area was sitting on the upper plate of a subduction zone, resulting in an impressive coverage of Cretaceous granites sometimes separated by narrow Cretaceous molasse basins. These granitic bodies, widespread offshore in the extended crust conditioned the location of the extension via large detachments and normal faults; later cut by steeper faults. The geometries of the faults vary from E-W to NE-SW indicating that the rifting underwent several stages with different stretching directions. The extension therefore started during Late Cretaceous before the rifting *sensu stricto* which is clearly documented since the Early Eocene only. Stretching and thinning were important and resulted in a wide "Basin and Range" like province which was sustained near sea level during the entire duration of the rifting process. This province is seen on both margins of the SCS and ultimately exhumed the mantle like offshore Vietnam and SE of Taiwan. Some faults are low angle detachments and therefore surround the granitic and metamorphic basement. The structure of the margin by the end of the rifting is dominated by a strong boudinage of a thin crust (~12 Km), on which the low-angle normal faults are either the granitoids boundaries or the short limbs of Cretaceous folds. Because the thinned margin was sustained at shallow depth, platform and reef carbonates occupy some of the bathymetric highs. They developed mainly during Late Oligocene to Mid Miocene times and during Late Miocene times.

The SCS basin also raises questions about the time of the breakoff and the time of cessation of the extension. The spreading of oceanic crust started by 33Ma in the northern and central part of the basin although rifting continued until at least 15.5 Ma,

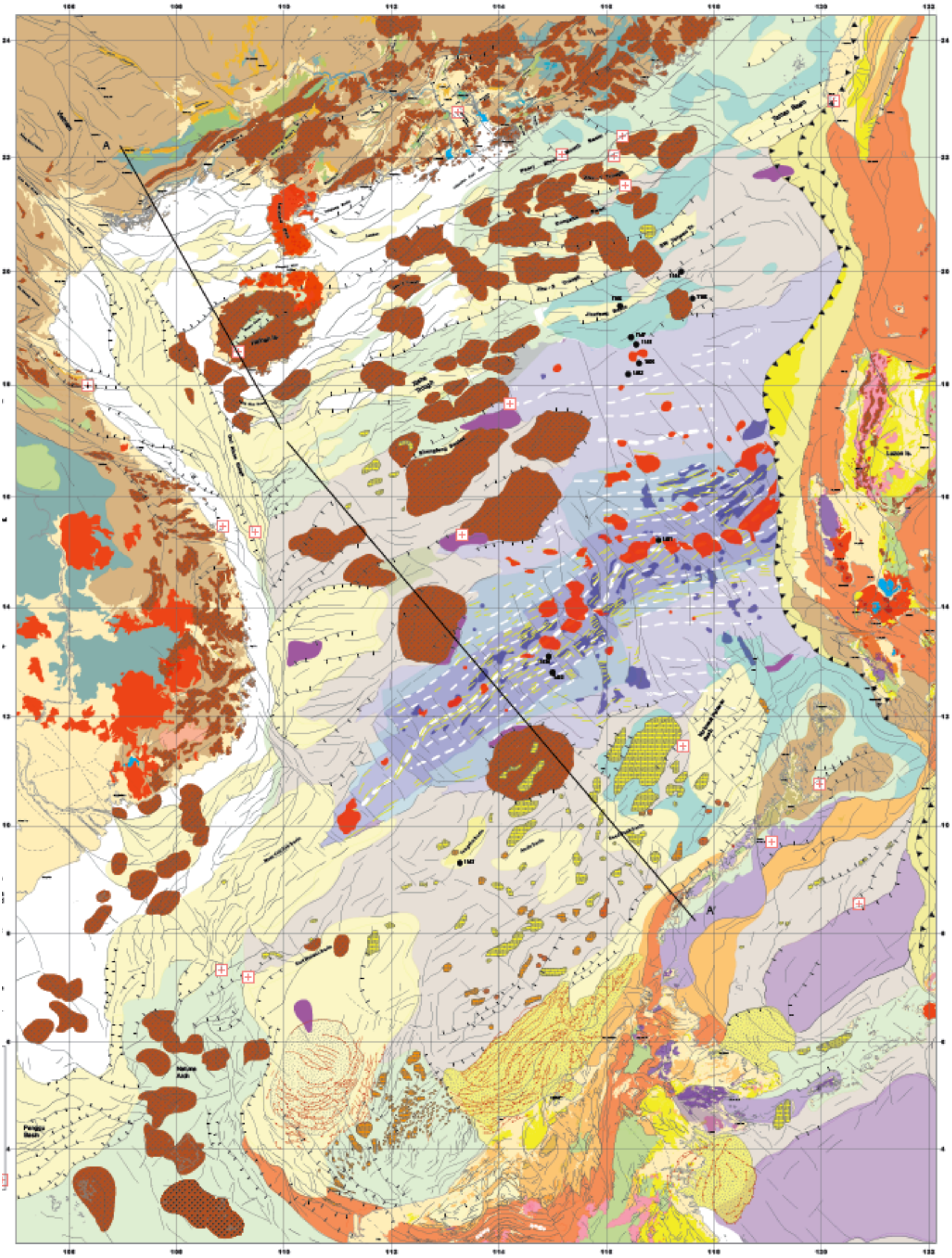

Figure 1: Structural Map of the South China Sea (Pubellier et al., in press). Original scale 1/1.5000.000, Commission for the Geological Map of the World, 2015. Emphasis is put on the basement morphostructures (e.g. Mesozoic granitoids) which control the rifting, and the accretionary wedges where shortening occurred in the late stages of the extension and trigger both deltas and gravity tectonics

The SCS basin also raises questions about the time of the breakoff and the time of cessation of the extension. The spreading of oceanic crust started by 33Ma in the northern and central part of the basin although rifting continued until at least 15.5 Ma, at a time when spreading was already finishing. Furthermore extension is also observed in the midst of the oceanic crust as indicated by low angle normal faults. It is only during early Late Miocene times (*circa* 12Ma) that extension ceased and regional subsidence was triggered, and marked by a well know Mid Miocene unconformity (MMU). The unconformable Late Miocene series are indicated on the map; they also seal the late structures of the collision along the NW Borneo Wedge.

The oceanic crust of the South China Sea has been represented with the main generally accepted magnetic anomalies. The areas where the crust is younger but the age of the anomalies is controversial is shown with a different color according to recent models. The geometry of the ocean floor basin has "V" shape which terminates to the SW as a propagator, implying that the age of the crust (and therefore the breakup) may be diachronic. It is likely that part of the NW Sulu Sea is actually floored by an oceanic crust which could represent a relic of the Proto South China Sea, to be correlated with the Palawan ophiolite.

<u>Geological features linked to shortening history</u>.

When the South China Sea basin subsided, the NW Borneo wedge started to raise quickly resulting in a subsequent erosion which actually develops offshore in the SE SCS and shifts to the NW of the Sulu Sea. Onshore Borneo, the sub-aerial conditions for the NW Borneo wedge resulted in intense erosion and deltas formation. It has been documented that the compression which marks the end of the subduction of the Proto South China Sea is responsible for the thrusting of the NW Borneo wedge onto the S Margin of the SCS by the Middle Miocene. This wedge is dominated by two large tectonic units (on the map) which represent the distal sedimentary series (Rajang wedge) and the proximal series (Crocker Wedge) deposited on the shelf of the conjugate block of the South China Sea (Palawan-Luconia Block).

The consequence of the probable slab detachment of the subducted Proto South China Sea slab, and the thrusting of the NW Borneo wedge on this later block induced thickening and uplift, which in turn generated sub-aerial conditions for the NW Borneo wedge. The resulting erosion created the large well-known deltas of Champion, Balingan, and Baram, starting from the end of the Early Miocene. Excess of sediment loading in the deltas induced gravity tectonics. The resulting gravity provinces are marked with red faults which include growth faults and toe-thrusts affecting generally the Mid-Miocene to Recent sedimentary pile.

<u>Lessons learned from the SCS Case study</u>.

Detailed study of this type of basins indicates that some accepted concepts of rifted basins must be handled with care. Among those are 1) the varying age of the breakup, the extension which may start before the rifting (orogenic collapse of former topography), and may continue long after the rifting has ceased, 2) the long lasting continental or shallow marine conditions without regional subsidence, 3) and the late crustal rebound associated with the end of the neighboring subduction, which may trigger high vertical motion and develop large deltas prone to gravity tectonics.

O-27 **Rock-Fluid interactions: Numerical modelling and future perspectives**

F. H. Nader

IFP Énergie nouvelles, 1-4 avenue de Bois-Préau 92852 Rueil-Malmaison, France

The onset of the worldwide interest in "Diagenesis" – especially for carbonate rocks – could be traced back to 1975, when R. Bathurst published the book entitled "Carbonate Sediments and their Diagenesis" including the famous statement: "*Carbonate rocks are as much the products of diagenesis as they are of primary deposition*". Alteration of sedimentary rocks after sediment deposition due to various processes of diagenesis is crucial in reshaping their mineralogical and petrophysical properties. The petroleum industry since that early time needed workflows and means to understand and predict the heterogeneous flow properties of reservoir rocks. Henceforth, a huge amount of research work has been dedicated to the investigation of diagenetic processes, environments, and products. Diagenesis processes are inherently related to the rock-fluid interactions and attract multi-disciplinary researchers. This is quite demonstrated by the wide spectrum of the nature of published work on diagenesis, and by the difficulty in integrating all aspects related to diagenesis research.

Sedimentologists have described the results of diagenetic processes ("diagenetic phases") in an extensive amount of surface-exposed rocks and subsurface well-cores across the planet. The aim was set at matching processes and products, and being able to come up with conceptual models that would allow at least to constrain the geometry/dimension as well as the fluid-flow history of the altered rocks. In addition, since the 1970s and the original paper of Choquette and Pray (1970) – entitled "Geologic nomenclature and classification of porosity in sedimentary carbonates" – efforts were spent to understand the impact of diagenesis on porosity and permeability of sedimentary rocks.

Classical diagenesis studies make use of a wide range of descriptive methods and analytical techniques converging into conceptual models that explain specific, relatively time-framed, diagenetic processes, and deduce their impacts on reservoir rocks. Currently used techniques combine petrographic (conventional, cathodoluminescence, fluorescence, and scanning electron microscopy with energy dispersive spectrometer – SEM/EDS), geochemical (major/trace elements, stable oxygen and carbon isotopes, strontium isotopes, Mg- and clumped-isotopes) and fluid inclusion analyses (microthermometry, Raman spectrometry, crush-leach analysis, laser ablation), providing independent arguments to support or discard any of the proposed models. More recently, the use of basin modelling is employed to support the burial history evolution (including temperature and pressure boundary data) and the proposed paragenesis (i.e. the sequence of diagenetic phases in chronological order). Still, conceptual models are qualitative and do not yield quantitative data to be directly used by reservoir engineers for rock-typing and geological modelling.

Today, the operational workflow that aims at predicting the impact of relevant diagenetic processes on reservoir properties consists of three main stages: i) constructing a conceptual diagenesis model, ii) quantifying the related diagenetic phases, and iii) modelling (numerically) the diagenetic processes (Fig. 1).

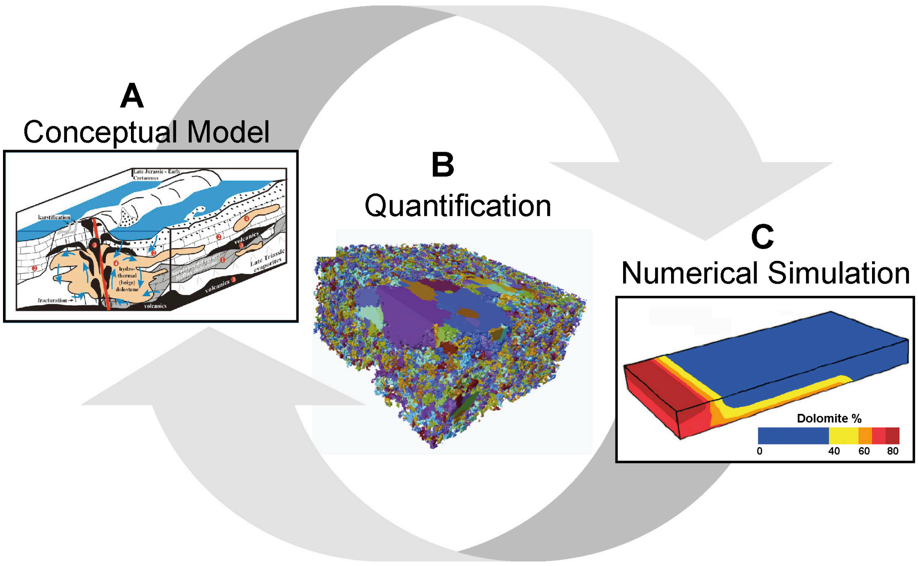

Figure 1. From conceptual to numerical modelling of diagenesis, quantifying diagenetic phases remains essential. (A) Conceptual studies of diagenesis – for example hydrothermal or high temperature dolomitization (HTD; Nader et al., 2004, 2007). (B) Quantification methods – e.g. micro-computed tomography (μ-CT) image analyses (De Boever et al., 2012). (C) Numerical simulations of diagenetic processes such as reactive transport modelling of dolomitization (e.g. Consonni et al., 2010).

While most of the concepts of diagenetic processes operate at the larger, basin-scale, the description of the diagenetic phases (products of such processes) and their association with the overall petrophysical evolution of sedimentary rocks remain at reservoir (and even outcrop/ well core) scale. Hence, "upscaling" becomes another major challenge for sedimentologists and reservoir engineers in the coming decades.

At present, the geoscience community has a variety of operational workflows for proposing conceptual models of diagenetic processes based on studying surface-exposed rocks and well cores. We are able to quantify the diagenetic products with various techniques and on varying scales (e.g. point-counting, 2D and 3D image analysis, micro-CT and pore network models). In addition, we have the possibility to use distinct software packages for numerical modelling.

Techniques for characterizing diagenesis and assessing quantitatively its impact on sedimentary rocks have been made quite available. Numerical modelling of diagenesis remains under development and the near future will certainly witness concrete innovations in this field. A numerical model is expected to deliver better constraints with respect to the understanding and predictability of the diagenetic processes, and their impacts on the petrophysical properties of the sedimentary rocks. Here, the key objective must not be limited to the capability of simulating the exact process under investigation. It should rather provide a tool able to test certain scenarios and to draw concluding statements that could enforce or dismiss the proposed conceptual model.

Modelling diagenesis has been used to unravel and constrain the heterogeneity of carbonate reservoirs (e.g. Whitaker et al., 1997a,b; Jones and Xiao, 2005; Barbier et al., 2012). Forward modelling to simulate early meteoric diagenesis occurring on an isolated platform have been used by Whitaker et al. (1997a, b). Reactive transport model to simulate dolomitization has been used by Jones and Xiao (2005) and Consonni et al., (2010). Only a few published articles make use of geostatistical methods to model diagenesis and associated reservoir heterogeneity (e.g. Barbier et al., 2012).

Two major numerical approaches for modelling diagenesis processes have been used so far, and these are going to be presented here: i) geostatistical, and ii) geochemical, reactive-transport modelling. Geostatistical methods are usually used for reservoir-scale modelling and make use of considerable amount of data. A golden rule states that the more data are available the more precise the modelling results will be. In any case, geostatistical modelling aims to fill in (via *intelligent* extrapolation) the space between control points with known 'exact' data. Hence, the resulting simulation consists of a having cells filled with the most probable facies/phase. This is not a predictive approach but rather an extrapolation workflow based on probability. It certainly helps in illustrating a probability-based heterogeneity. Geochemical modelling makes use of thermodynamic and kinetic rules and data-bases to simulate chemical reactions and fluid-rock interactions. This can be through a 0D model, whereby a certain process is tested and analyzed. It can also consist of changing parameters through time (e.g. thermal/flux variations) while remaining in the same dimensional configurations. The results are usually in two groups, those related to the fluids and those related to the mineral phases. They could be used as arguments to support or refute proposed outcomes of fluid-rock interactions. Coupling geochemical modelling with reactive-transport allows the simulation of fluid-flow and associated processes. Geochemical RTM are attractive as they provide forward simulations of diagenetic processes and resulting phases. Yet, they need to be validated since most of these processes occurred in different temporal and physico-chemical conditions. This remains a weak point for the geochemical approach in modelling diagenesis.

The way forward, seems evident as the integration of workflows at different scales (Fig. 2). Improving such integration could be achieved by planning research projects that go from a basin-scale (using seismic data, outcrop-analogues, well cores, etc.) to a reservoir-scale, and eventually the plug-scale. Such integration will bring more constrains on the boundary data, better validation for models, and less uncertainty.

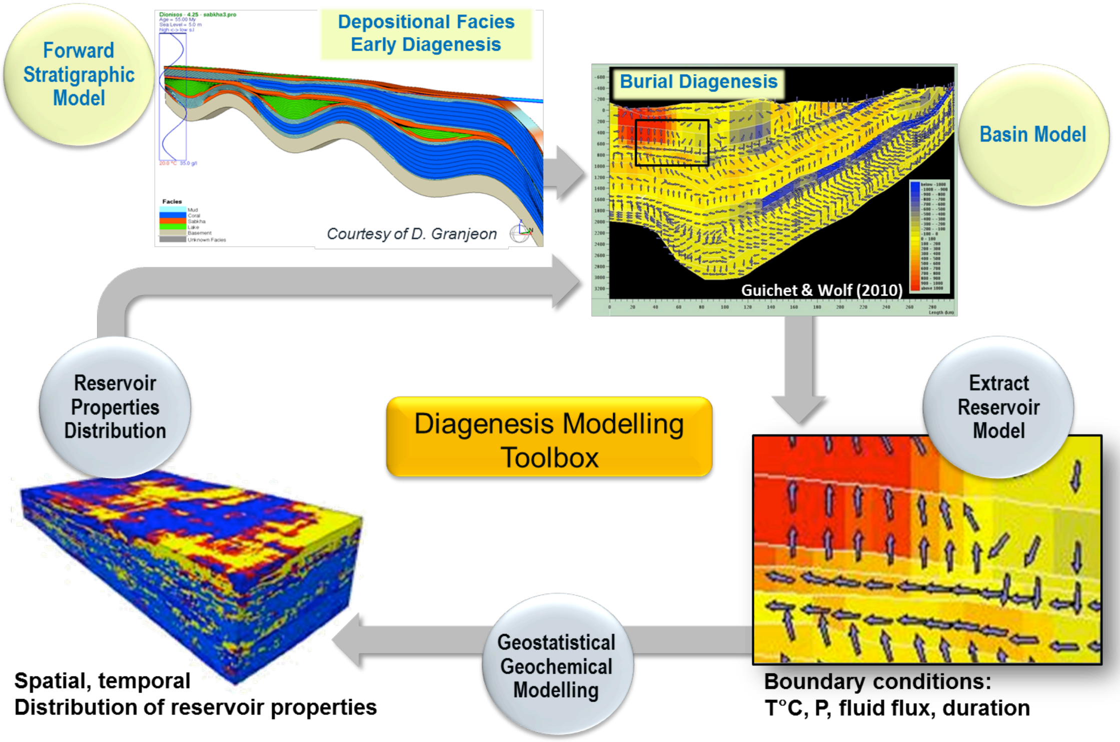

Figure 2. Towards integrated basin/reservoir numerical models in order to achieve better constraints, validation and less uncertainty. The central feature is a "Diagenesis Modelling Toolbox" with numerical procedures to simulate roc-fluid interactions at various scales.

References

Barbier, M., Hamon, Y., Doligez, B., Callot, J.-P., Floquet, M. and Daniel, J.-M., 2012. Stochastic joint simulation of facies and diagenesis: a case study on early diagenesis of the Madison Formation (Wyoming, USA). Oil and Gas Science and Technology (OGST), 67(1): 123-145.

Bathurst, R.G.C., 1975. Carbonate sediments and their diagenesis. Elsevier Science Publ. Co.

Choquette, P.W. and Pray, L.C., 1970. Geologic nomenclature and classification of porosity in sedimentary carbonates. AAPG Bulletin, 54: 207-250

Consonni, A., Ronchi, P., Geloni, C., Battistelli, A., Grigo, D., Biagi, S., Gherardi, F., and Gianelli, G., 2010. Application of numerical modelling to a case of compaction-driven dolomitization: a Jurassic palaeohigh in the Po Plain, Italy. Sedimentology, 57: 209-231.

De Boever, E., Varloteaux, C., Nader, F.H., Foubert, A., Bekri, S., Youssef, S and Rosenberg, E., 2012. Quantification and prediction of the 3D pore network evolution in carbonate reservoir rocks. Oil and Gas Science and Technology – OGST, 67(1): 161-178.

Jones, G.D. and Xiao, Y., 2005. Dolomitization, anhydrite cementation, and porosity evolution in a reflux system: Insights from reactive transport models. AAPG Bulletin, 89 (5): 577-601.

Nader, F. H., Swennen R. and Ellam, R., 2004. Stratabound dolomite versus volcanism-associated dolomite: an example from Jurassic platform carbonates in Lebanon. Sedimentology, 51 (2): 339-360.

Nader, F.H., Swennen, R. and Ellam, R., 2007. Field geometry, petrography and geochemistry of a dolomitization front (Late Jurassic, central Lebanon). Sedimentology, 54: 1093-1110.

Whitaker, F.F., Smart, P.L. (2007a). Geochemistry of meteoric diagenesis in carbonate islands of the northern Bahamas: 1. Evidence from field studies. Hydrological Processes, 21, 967-982.

Whitaker, F.F., Smart, P.L. (2007b). Geochemistry of meteoric diagenesis in carbonate islands of the northern Bahamas: 2. Geochemical modelling and budgeting of diagenesis. Hydrological Processes, 21, 967-982.

O-28 **Quantifying the evolution of sedimentary basins by coupling sedimentary fluxes with orogenic evolution**

Liviu Matenco

Tectonics Group, Department of Earth Sciences, Utrecht University, Budapestlaan 6 3584 CD Utrecht, The Netherlands

Tectonic, surface and external forcing processes are responsible for the growth and decay of continental topography and sedimentary basins, i.e. the interplay between sediment supply and mass (re)distribution with the full range of deep Earth to surface processes. These are important to assess the impact of tectonics and sediment distribution in highly populated areas, affected by flooding events, regional landslides and active seismicity. The mechanisms that link exhumation, formation of topography and sedimentation are poorly understood because of a lack of insight into the variability of the rates and scales of the underlying processes. The dynamics of these processes is explored by quantifying the link between tectonics and sedimentation with a multi-scale approach that combines field studies and basin-wide observations with analogue and numerical modelling. To this end, lateral variations of tectonic, climate and erosion/sedimentation evolution through time are incorporated into dynamic models of topography evolution by coupling deposition in sedimentary basins with topography formation and evolution in nearby source areas. This provides new opportunities to analyse and quantify the interplay between deep Earth and surface processes, critical for understanding geo-resources and natural hazards.

Current research by combining field observations in a selected number of European natural laboratories with analogue and numerical modelling has demonstrated a large variability of the mechanics driving mountain build-up and sedimentary basins formation. The associated formation of sedimentary basins is strongly influenced in zones of such interaction by more than one mechanical process. These studies suggest the existence of large-scale zones of interaction between individual mountain chains, inferring a number of outstanding questions of orogenic mechanics related to factors that control the localization of intense deformation in continental lithosphere. We study such complex interactions by employing a multi-scale and multi-disciplinary strategy passing from field studies, observations at the scale of sedimentary basins and process-oriented analogue and/or numerical modelling. Novel tectonic modelling concepts and their implementation in numerical and analogue modelling have opened new approaches to study the thermo-mechanical behaviour of the Earth's lithosphere and to assess the role and interaction of parameters such as intraplate stress, rock rheology and lithosphere structure. We couple such advanced methods for the quantitative analysis of dynamic models that address the link between lithosphere deformation processes and vertical and horizontal motions in space and time.

O-29 Messinian Event in the Deep Eastern and Western Mediterranean Sea: Interaction between deep processes and global sea level change

Christian Gorini

I Institute of Earth Sciences, Paris (IsTEP), Université Pierre et Marie Curie, Paris

The Messinian salinity crisis in the Mediterranean (5.96 to 5.33 million years ago) was caused by reduced water inflow from the Atlantic Ocean to the Mediterranean Sea resulting in widespread salt precipitation and a decrease in Mediterranean sea level of about 1500 m due to evaporation. Prior to this event active dynamics in the Mediterranean had controlled created the preconditions for the deposition of deep saline series that now form a natural laboratory in which we can study the interactions between various deep-seated and surficial processes.

A long-wavelength mantle-sourced tectonic uplift of the Betic and/or Rif mountains and global sea-level change, seem to have conspired to isolate of the Mediterranean from the Atlantic, by controlling the inflow of water required to compensate for the hydrological deficit of the Mediterranean, as well as the competition between uplift and erosion. New seismic images allow us to propose a Mediterranean Messinian depositional episode that can be divided into two megasequences (the lower MLM and the upper MUM) with distinctive seismic facies and corresponding system tracts deposited during the Salinity crisis : 1) a falling stage system tract including forced regressive clinoforms, mass transport deposits and marked depocenter shift towards the deep basins; 2) a lowstand system tract characterized by massive clastic input from major Messinian rivers (Rhone, Nile, and Antalia Gulf rivers) or smaller river systems (e.g., offshore south Lebanon). These clastics were deposited in an oversaturated basin, evidenced by interfingering of evaporites and clastic facies. 3) a late lowstand phase, starting with rapid deposition of massive halite, without detrital input into the deep basin. Its upper part is clearly transgressive on the margins. This third system tract is identified as the Messinian Upper Megasequence (MUM). The transition between the two megasequences is interpreted as the peak of the “salinity” crisis. A transgressive system tract is well developed in the eastern Mediterranean in front of the Nile River. The large amount of salt precipitated during a few hundred thousand year duration of the MSC that requires the evaporation of about 50, times more than the volume of the Mediterranean. A long period of continuous inflow and limited outflow may have been caused by a shallow connection between the Mediterranean and the Atlantic. The sequence stratigraphy of the deep Messinian basins and the geodynamics at that time, imply that the Mediterranean sedimentation was sustained by a competition between uplift and erosion, allowing for limited but uninterrupted Atlantic inflow. Tear propagation of a hanging lithospheric slab underneath the Gibraltar Arc provides a mechanism of westwards propagation of both uplift and subsidence. Recent seismic tomography and seismic stratigraphy of the west Alboran basin supports the presence of such lithospheric tearing. The location of this tear point between the last pre-Messinian corridor and the strait of Gibraltar could explain the uplift and closure of the Betic seaways, and a later subsidence in Gibraltar, leading to the Zanclean flooding. The ongoing tectonic convergence between Europe and Africa (about 4 mm/yr since the Paloegene) could also have contributed to uplift rates through faulting or doming. Dynamic topographic considerations and modeling could eventually lead to better understanding of the longer wave-length warping of the lithosphere and the tectonic causes for the Mediterranean's sequestration and reconnection to the world ocean.

O-30 Possible constraints on hydrate dissociation in sedimentary basin: Sedimentation, compaction, deep-source fluid and diffusion

Masa Kinoshita[1)] Tomohiro Toki[2)]

1) R&D Center for Ocean Drilling Science, JAMSTEC

2) Faculty of Science, University of the Ryukyus

The state and properties in sedimentary basins, such as the stress, temperature, pressure, fluid flow, chemical composition, keep changing throughout their sedimentation or erosion processes that are significantly affected by repeated earthquakes and consequent tilting of the hanging wall block. Compaction of buried sediments generates a differential movement between the subsiding solid matrix and the pore fluid. In addition, deep-source fluid flow will affect the thermal as well as chemical state in the sediment formation.

Kumano forearc basin is located above the seismogenic fault zone of the Tonankai great earthquake, with its water depth about 2000 meters (Fig. 1). The seismic profile (Fig. 2) exhibits a clear Bottom-Simulating Reflectors (BSRs) that is considered as a boundary between the methane-hydrate stability zone above and a zone containing free-gas beneath. Further down at ~900 m below sea floor (mbsf) is an unconformity, beneath which the strata is significantly deformed.

Since 2007 a series of scientific drilling have been conducted as a part of International Ocean Drilling Program (IODP), including a deep hole (Site C0002) targeting the seismogenic portion of the plate boundary thrust fault (e.g. Kinoshita et al., 2014). Biostratigraphy for Site C0002 was determined based on nannofossil and foraminifers. The age-depth curve indicates a hiatus between 5.6 Ma and 1.7 Ma, followed by a very rapid sedimentation between 1.7 Ma and 1.0 Ma, with its accumulation rate about 1300 m/Ma that is estimated from the porosity vs. depth profile (Expedition 315 Scientists, 2009; Harris et al., 2013) (Fig. 2). After that the accumulation rate drastically decreased to 110 m/Ma. The formation below the hiatus (~unconformity) is defined as the old accretionary prism that is inactive at present. Salinity and Chlorinity, measured on the pore fluid squeezed from core samples, show significant nonlinear characteristics with depth.

Upon taking cores with Advanced Piston Corer (APC), formation temperature is obtained with the APC-T tool, a temperature logger attached to the APC shoe. The temperature vs. depth profile is linear and its extrapolated line is consistent with the temperature at the BSR. Therefore we assess that the formation down to BSR depth is basically in thermal equilibrium, in spite of recent rapid sedimentation.

On the other hand, the nonlinear Chlorinity profile suggests that ions in the pore fluid are not equilibrated. It can be reconciled that the thermal diffusivity (1e-6 ~ 1e-7 m2/s) is larger than ion diffusivity (2e-9 m2/s) by more than an order of magnitude, and that the time constant of fluid advection is longer than the thermal diffusion time constant, but shorter than the ion diffusion time constant.

Accepting the time-varying state in sediments, we attempt whether we can find a best-fit solution for the nonlinear Cl profile. For simplicity (but with a reasonable basis), we assume that the thermal field is static (always equilibrated) and that there is no overpressure. By noticing that the BSR depth is controlled by the thermal regime and that hydrate-containing sediments above BSR are continuously ‘deepening’ across the BSR. It leads to a continuous dissociation of hydrate just beneath the BSR, and to a continuous freshening of pore water decreasing the Chlorinity there. Such anomalies will remain in the formation while deformed and decayed by compaction-driven or advection-origin fluids. Thus finding a best-fit solution can be used to infer the past Cl concentration as well as past fluid advection history. In this study we attempt to reproduce the observed Cl vs. depth profile by varying 4 important parameters through 1-D finite-difference method numerical simulation, based on the method described in Davie and Buffet (2001). Unfortunately equations in Davie and Buffet (2001) contain some errors, so we modified them for our use.

Although Davie and Buffet (2001) treated the hydrate saturation as a variable to be solved, we set the hydrate saturation value as independent of time. It is because we do not have enough information about hydrate saturation vs. depth at this site. Instead we treat the hydrate saturation as one of 4 parameters. Other parameters are; initial Chlorinity at 5.6 Ma, darcy velocity of fluid flow from depth, and the time when hydrate dissociation starts beneath BSR (Fig. 3).

The best-fit result is obtained with the initial Chlorinity of 350 mM and the darcy velocity of 10-12 m/s (Fig. 4). Also, dissociation should start at ~1.4 Ma, when the newly deposited basin-fill cut across the BSR. We are working on their geological and geochemical interpretations, but at least the observed Cl profile requires continuous hydrate dissociation for the recent 1.4 Ma.

References

Davie, M. K., B. A. Buffett (2001), A numerical model for the formation of gas hydrate below the seafloor, J. Geophys. Res., 106, 497-515.

Expedition 315 Scientists, 2009. Expedition 315 Site C0002. In Kinoshita, M., Tobin, H., Ashi, J.,Kimura, G., Lallemant, S., Screaton, E.J., Curewitz, D., Masago, H., Moe, K.T., and the Expedition 314/315/316 Scientists, Proc. IODP, 314/315/316: Washington, DC (Integrated Ocean Drilling Program Management International, Inc.). doi:10.2204/iodp.proc.314315316.124.2009

Harris, R., M. Yamano, M. Kinoshita, G. Spinelli, H. Hamamoto, and J. Ashi (2013), A synthesis of heat flow determinations and thermal modeling along the Nankai Trough, Japan, J. Geophys. Res. Solid Earth, 118, 2687–2702, doi:10.1002/jgrb.50230.

Kinoshita, M., G. Kimura, and S. Saito (2014), Chapter 4.4.2 Seismogenic Processes revealed through The Nankai Trough Seismogenic Zone Experiments: Core, log, geophysics and observatory measurements, In Ruediger Stein, Donna K. Blackman, Fumio Inagaki, Hans-Christian Larsen (eds) Developments in Marine Geology Vol 7 - : Earth and Life Processes Discovered from Subseafloor Environment, Elsevier, 641-670.

Moore, G.F., et al. (2009). Structural and seismic stratigraphic framework of the NanTroSEIZE Stage 1 transect. In Kinoshita, M., Tobin, H., Ashi, J., Kimura, G., Lallement, S., Screaton, E.J., Curewitz, D., Masago, H., Moe, K.T., and the Expedition 314/315/316 Scientists, Proc. IODP, 314/315/316: Washington, DC (Integrated Ocean Drilling Program Management International, Inc.). doi:10.2204/iodp.proc.314315316.102.2009.

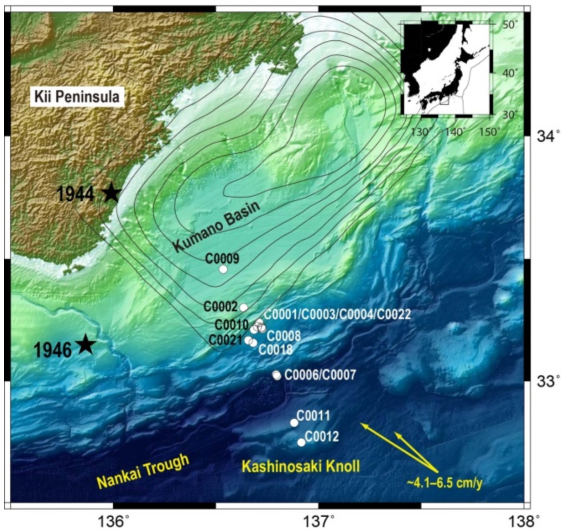

Figure 1. Bathymetry of the Kumano Basin and the location of IODP NanTroSEIZE drillsites. Contours represent the coseismic slip are during the 1944 Tonankai earthquake.

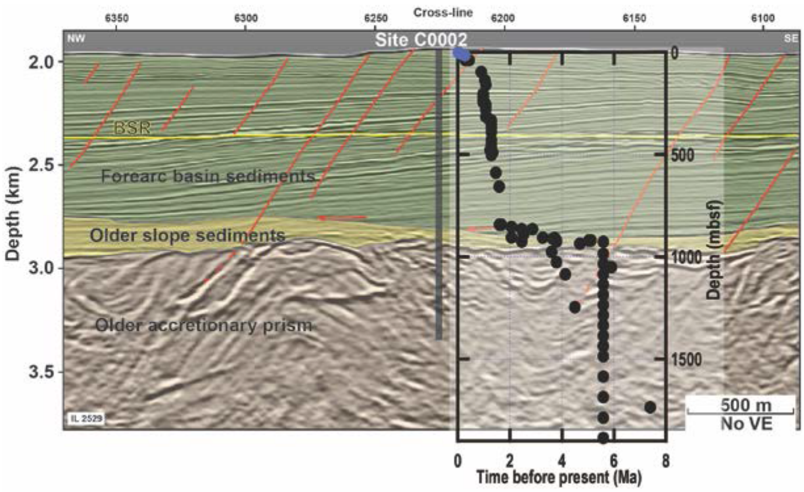

Figure 2. Inline seismic section around IODP Site C0002 (Modified from Moore et al., 2009). Age-depth plot is overlain.

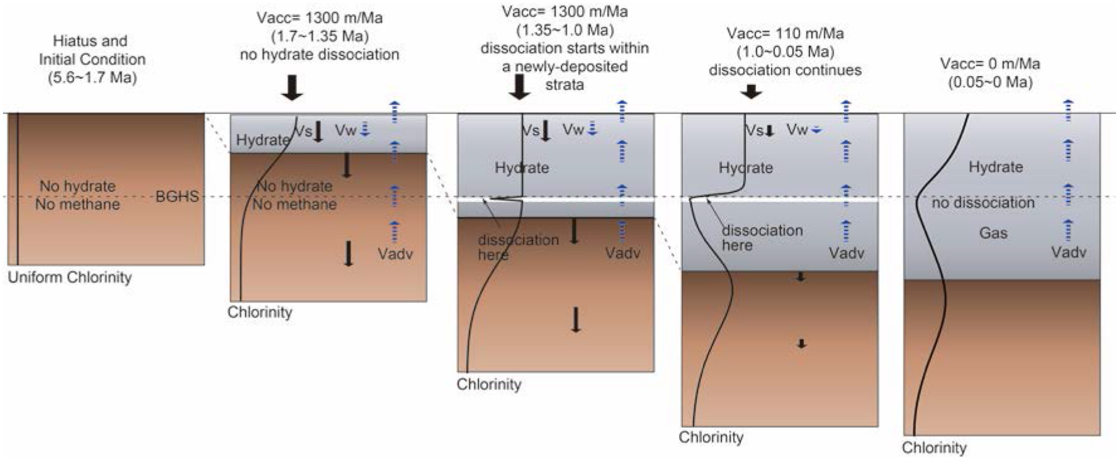

Figure 3. Model description for rapid-sedimentation and fluid flow.

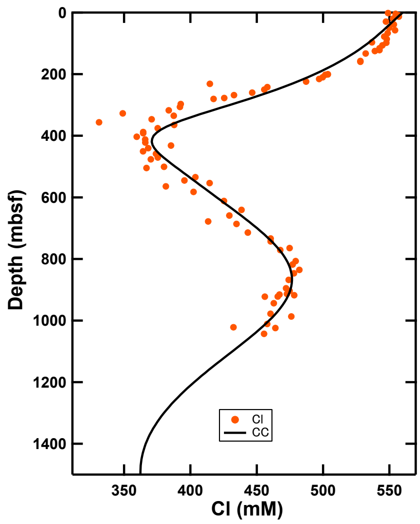

Figure 4. Example of best-fit results of Cl concentration vs. depth.

O-31 **Estimation of pre-Neogene basement in Niigata-area Japan using gravity anomalies and velocity model based on reflection and refraction seismic surveys**

Motonori Higashinaka*, Susumu Abe (JGI),
Hiroshi Sato, Tatsuya Ishiyama, Naoko Kato (University of Tokyo)

1. Background

Niigata Region locates the rifting zone in the eastern margin of the Japan Sea, and the post Neogene thick sediments overlies the basin. The thicknesses of these sediments are in maximum over six kilometers, to form the thickest sedimentary basin in Japan. After Pliocene, up to the present, the region has been under compressive stress field. Since large-scale folds with many reverse faults have developed, the underground structure is highly complex.

In such geological background, several large-scale reflection and refraction seismic surveys has carried out in recent days (Sato et al. 2010). These survey line length were over fifty kilometers. These seismic surveys have been providing detailed sections and velocity structures. But the number of survey lines is small and line distribution is sparse, then the three-dimensional structure of the region is not yet clear.

On the other hand, a large number of gravity measurement have been carried out. In this paper those gravity data have been used to estimate the three-dimensional pre-Neogene basement with velocity sections, which has been obtained in the seismic surveys.

2. Method

To Estimate pre-Neogene basement, we have processed gravity data as below.

(1) Extract residual gravity anomaly.

We calculated the residual gravity anomaly, excluding the effects of deep density structures (10km deeper) by frequency analysis.

(2) Two-dimensional gravity forward modeling

We made two-dimensional initial density model using seismic section and its interpreted horizons with P-wave velocity model, which is obtained by travel time tomographic method. Model density value is converted from P-wave velocity value using Gardner's Law (Gardner et al. 1974). Then we modified density model iteratively to fit the model gravitational response to observed value. Fig.1 is the result of gravity forward modeling, color section shows P-wave velocity model. We use the result of this two-dimensional modeling as the constraint for making other density model sections.

(3) Three-dimensional gravity inversion

Three-Dimensional density initial model was made by interpolating density model sections. From the initial model, the final density model is calculated using layer inversion method (Parker, 1972)

3. Result

Figure 2 is the Obtained pre-Neogene basement. It shows there is a major structure deformation, its strike direction is NE-SW, and the results suggests that some transverse fault exist in the region, which seismic surveys in NW-SE direction cannot image.

Gravity modeling methods with detailed seismic survey information, especially P-wave velocity, as the constraint will be effective to extract the deeper three-dimensional structures.

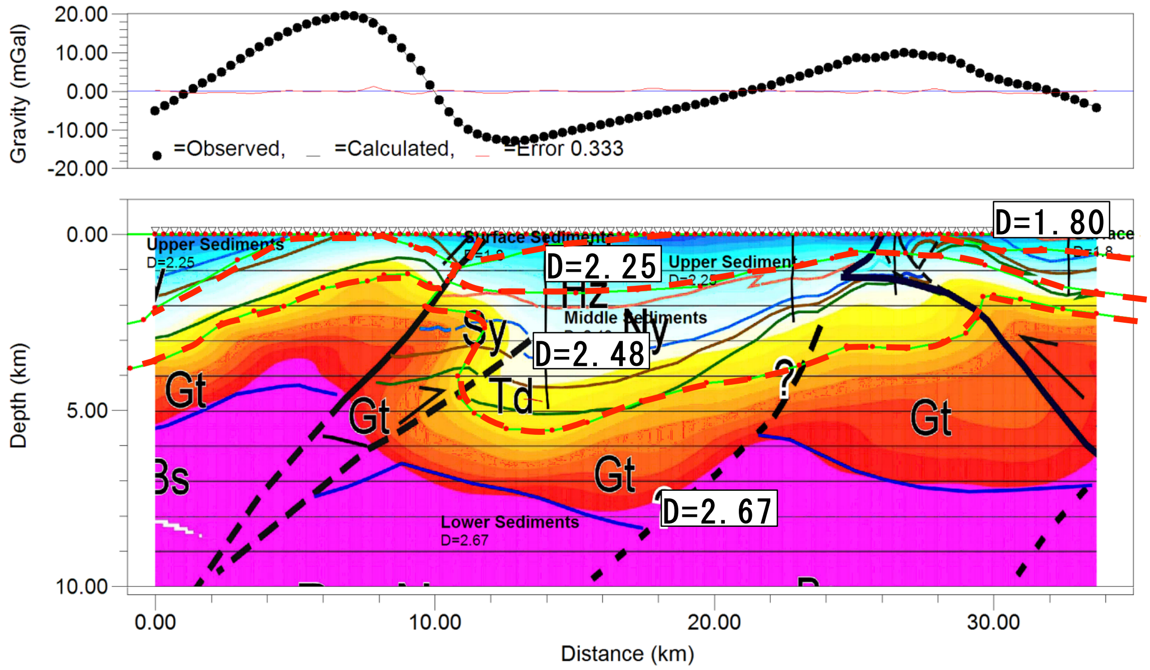

Figure 1. A two-dimensional density forward modeling result using P-wave velocity model. The density model consists of four layers, which densities are $1.80 g/cm^3$, $2.25 g/cm^3$, $2.48 g/cm^3$ and $2.67 g/cm^3$.

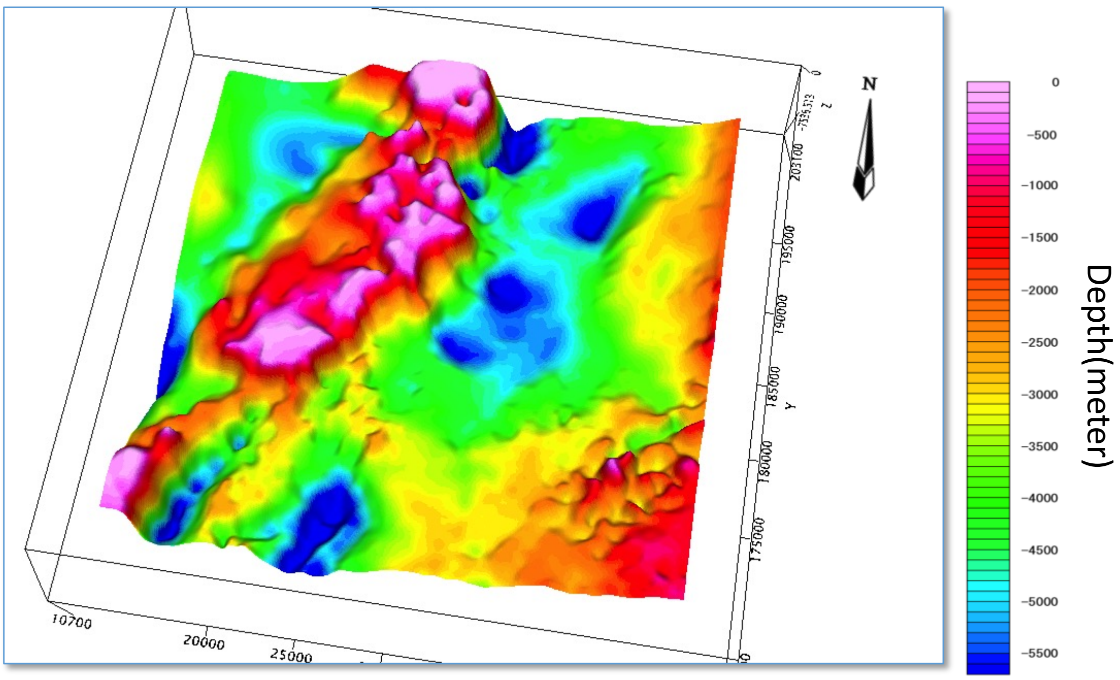

Figure 2. Inversion result, pre-Neogene Basement

References.

SATO, Hiroshi, ABE, Susumu, KAWAI, Nobuo, KATO, Naoko, IWASAKI, Takaya, ISHIYAMA, Tatsuya, SAITO, Hideo, SHIRAISHI, Kazuya, INABA, Mitsuru, FUKASAWA, Hikaru (2010), Deep seismic profiling across the Niigata basin, central Japan: 2008 Sanjo-Yahiko seismic survey, Chikyu Monthly Vol32, pp403-410

Gardner, G. H. F., Gardner, L. W. and Gregory, A.R. (1974), FORMATION VELOCITY AND DENSITY—THE DIAGNOSTIC BASICS FOR STRATIGRAPHIC TRAPS, GEOPHYSICS Vol. 39, pp. 770-780

Parker, R.L., (1972), The rapid calculation of potential anomalies: Geophysical Journal of the Royal Astronomical Society, v.42: 315-334.

O-32 Strategic seismic data processing for extraction of deep crustal reflectors through reconstructed velocity heterogeneity

Susumu Abe(1), Motonori Higashinaka(1), Hiroshi Sato(2), Tatsuya Ishiyama(2)

(1) JGI, Inc., (2) Earthquake Research Institute, the University of Tokyo

Introduction

In recent years, the quest for increased precision and channel capacity of receiver system led to the combination of telemetry and autonomous recorders with the deployment of dense seismic array for 100-250km long 2D survey. Furthermore, multi-scale and multi-mode survey layout has been realized by the simultaneous data acquisition of regional refraction, low-fold wide-angle reflection and standard reflection survey for the several targets on the same seismic line (Figure 1). In our study, multilateral approach beyond the conventional CMP stack was applied to the multi-scale, multi-mode seismic data for extraction of deep crustal reflectors through the reconstruction of velocity heterogeneity.

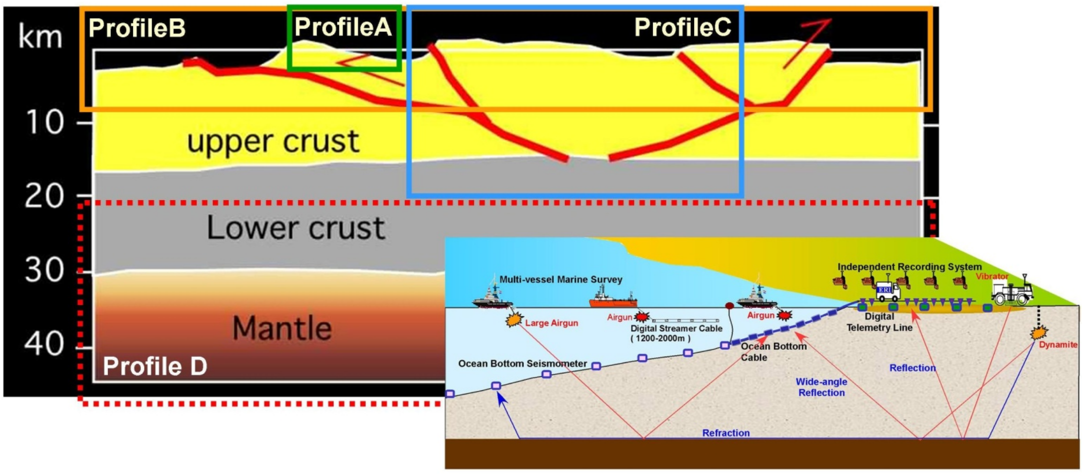

Figure 1 Schematic description of multi-scale, multi-mode seismic reflection survey
Profile A: High-resolution shallow reflection profile
Profile B: Basin-scale reflection and regional refraction profile
Profile C: Crustal-scale wide-angle reflection profile with large-energy sources
Profile D: Receiver function and seismic interferomeric profile using teleseismic and regional earthquake data

Extraction of deep crustal reflectors through reconstructed velocity heterogeneity

In order to build high-resolution velocity structure, we developed a processing workflow based on the hybrid approach of reflection velocity analysis and turning-ray tomography followed by full-waveform inversion (Figure 2). The uncertainty of the tomography solutions was estimated using a nonlinear Monte Carlo approach (Shiraishi et al., 2010) with randomized initial models, and the velocity structure of sedimentary basin was constrained by the short-wavelength structural heterogeneity estimated by the combination of CRS(Common reflection Surfaces)-driven velocity attribute and full-waveform inversion.

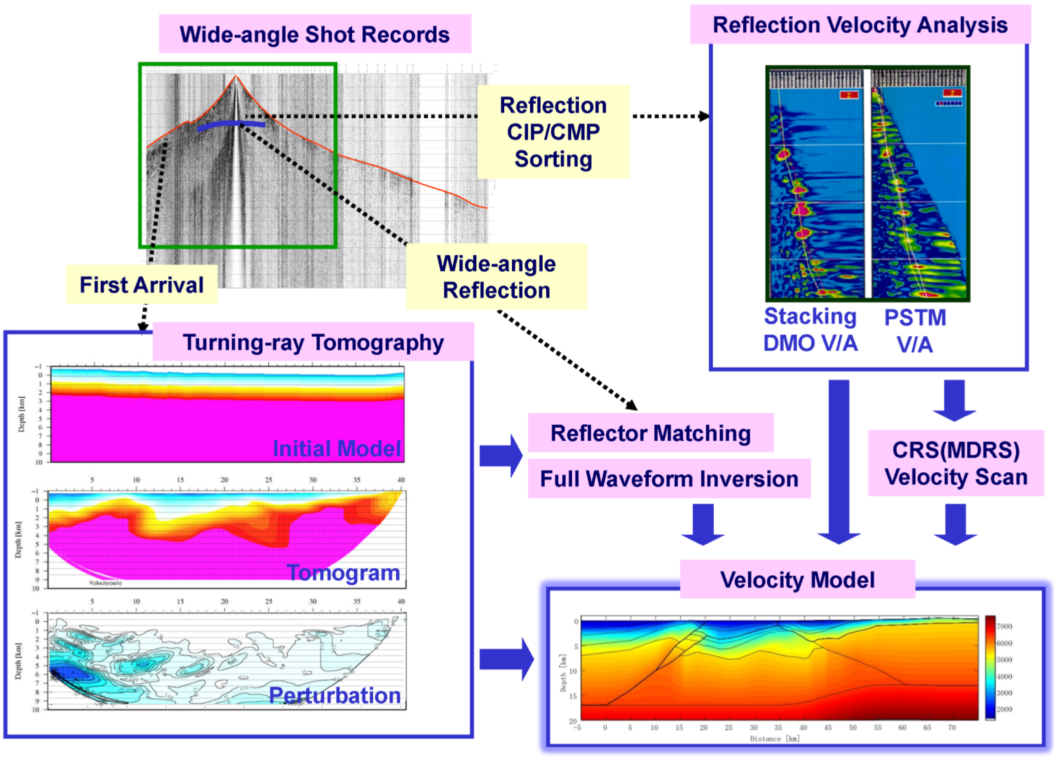

Figure 2 Workflow for the integrated velocity estimation based on grid-based refraction/reflection tomography, prestack reflection velocity analysis and full waveform inversion.

Application to 2D land seismic data

Offshore-onshore deep seismic profiling were conducted in 2008-2012 across a back arc rift basin, which formed during the Miocene opening of the Japan Sea, now uplifted and exposed in Niigata, central Japan (Sato et al., 2012). In these seismic experiments, the data acquisition of regional refraction, low-fold wide-angle reflection and standard reflection survey for the several targets on the same seismic line has been optimized based on the integration of air-gun, vibrator, and explosive sources focused on effective low-frequency bandwidth of seismic signature. Furthermore, the combination of telemetry and autonomous recording system including ocean-bottom cable has provided the deployment of wide-angle survey line with dense seismic array. We evaluated the relation between reconstructed velocity heterogeneity and the resolution of deep reflection patterns using typical multi-scale deep reflection data acquired in 2008 Sanjo-Yahiko seismic line (63.0 km).

The P-wave velocity structure estimated by turning-ray tomography, clearly demonstrates the basic structure of Niigata basin composed of previously undifferentiated syn-rift volcanics and pre-rift basement rock. Multi-dip CRS reflection profile indicates the process of fault reactivation in the current compressional regime documented by deformation patterns of post-rift sediments and the geometry of Miocene rift structure created during the extensional phase. The detailed geometry of reverse fault with short-wavelength velocity heterogeneity was obtained by acoustic full-waveform inversion (Figure 3).

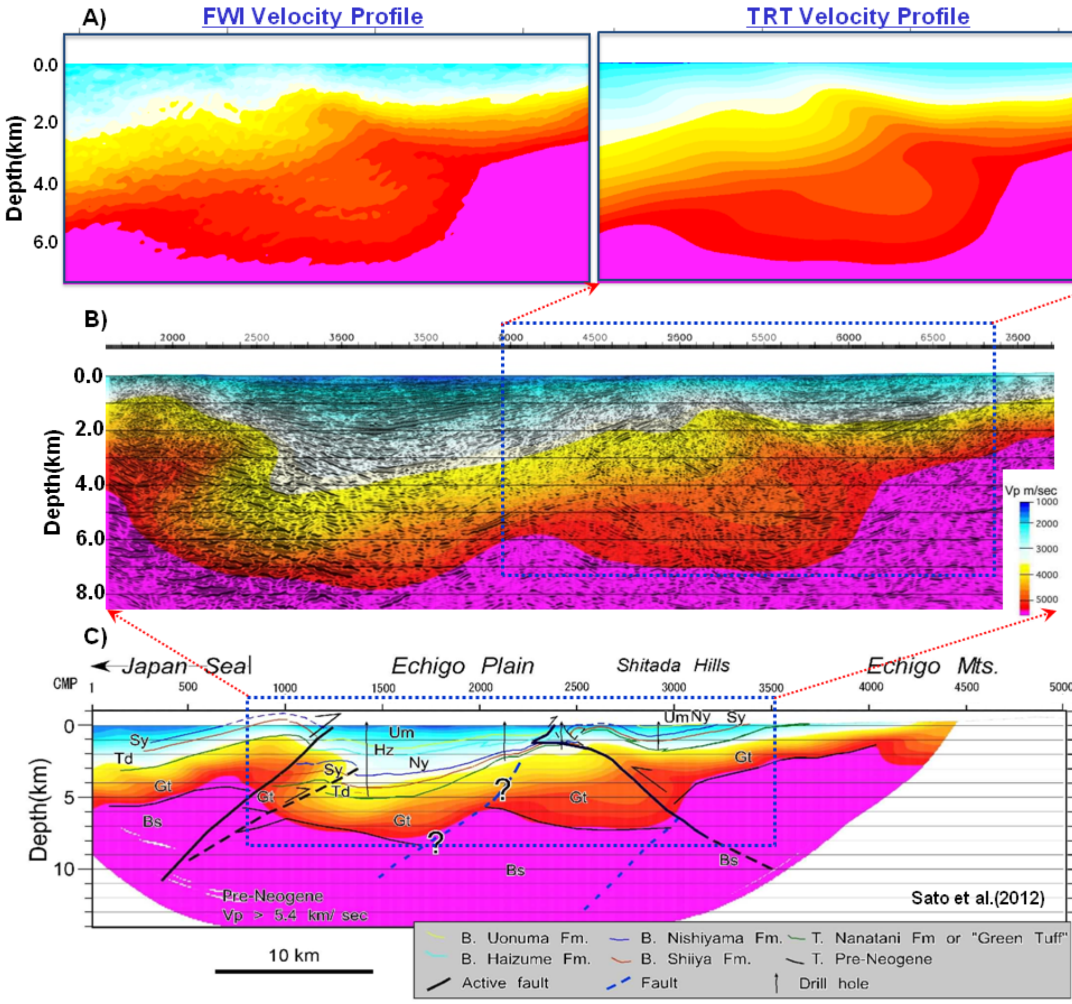

Figure 3 A) Comparison of estimated velocity structure between turning-ray tomography and full waveform inversion across the eastern boundary of the Niigata plane.
B) Superposition of multi-dip CRS profile and the turning-ray tomography model.
C) Turning-ray tomography model with geologic interpretation (Sato et al., 2012)

Conclusions

The combination of CRS-driven velocity attributes, turning-ray tomography and full-waveform inversion retrieves the detailed velocity structure of back arc rift basin in Niigata using multi-scale and multi-mode seismic data. Deep seismic reflection-refraction profile portrays the Miocene rift structure and processes of basin inversion.

References

Sato, H., Abe, S., Kawai, N., Saito, H., Kato, N., Ishiyama, T., Iwasaki, T., Kurashimo, E. and Inaba, M., 2012: Crustal architecture of an inverted back arc rift basin, Niigata, central Japan, EGU-10822.

Shiraishi, K., Abe, S., Iwasaki, T., Saito, H., Sato, H., Koshiya, S., Kato, N., Arai, R. and Kawanaka, T., 2010: Reliability evaluation by initial model randomization for refraction traveltime tomography, Geophysical Exploration (BUTSURI-TANSA), 63, 345-356.

O-33 Advanced workflows for fluid transfer in faulted basins

M. Thibaut, I. Faille, F. Willien

IFPEN 1-4 avenue de Bois-Préau, 92852 Rueil-Malmaison Cedex, France

INTRODUCTION

In view of the current context of oil and gas exploration, the discovery of new prospects in under explored areas or residual reserves in mature areas will depend on our ability to work on deeper and structurally more complex targets such as deep offshore or deeply-buried reservoirs. All these new opportunities stretch the capabilities of currently available 3D basin exploration software, which can not provide accurate structural reconstruction of the basin coupled with the controlling physical processes that lead to the generation and migration of hydrocarbons.

Since 2006, IFPEN has been developing a new basin simulator designed to handle moderately to highly deformed geometries and to better account for the impact of faults on fluid flow through time. This new simulator computes compaction, heat transfer, and fluid flow migration. It is designed to be used after the definition of the present day basin architecture validated by restoration and section balancing techniques.

In the first part of this abstract, the basin modelling workflow adapted to such 3D approaches is described in three steps: firstly how to reconstruct the present day 3D geometry from structural interpretation, secondly how the paleogeometries are generated, and finally how faults are described in the new simulator.

Then two applications are presented. The first case study presents a simplified thrust belt with thrust layers and faulted geometries. The second case is derived from an extensional gravity basin focusing on fault kinematics and its impact on fluid flow. In the new basin simulator, efforts have been made to develop a solution that takes better into account the physical characteristics for the fault representation.

A 3D ADVANCED BASIN MODELLING WORKFLOW

Our workflow separates the structural reconstruction from the forward basin modelling analysis. The advantage of this decoupled approach is that it is possible to use specific tools to perform each part of the workflow. The drawback of this decoupling is the lack of integration between the various steps of the workflow.

Our workflow is composed of steps represented by a sequence of successive and discrete stages. These steps are closely connected even if these are not assembled in the same software.

Step1: Present day 3D geometry of the sedimentary basin

The first step of the workflow is the building of the present day 3D model. In case of faulted geological structures, an important issue is the estimation of the correct layer and fault geometry in the depth domain. Efficient depth imaging and time to depth conversion of seismic data are obtained by an accurate velocity model through advanced inversion techniques and application of pre-stack depth migration.

Step 2: Basin history from palinspastic reconstruction

The second step is the structural reconstruction through time. The structural model is built through successive backward geological deformations which is called restoration. In the traditional 3D basin modelling workflow, backstripping is the algorithm to automatically compute the paleo-geometries. It is suitable for geologic settings dominated by normal deposition and erosion or for moderately extended basins with a limited structural complexity such that vertical shear is justified. But in areas with faulted basin architectures, the assumption of vertical decompaction is too restrictive, especially for describing lateral movements due to fault gliding. In this case, we have to consider a volume restoration which renders the integration more complex.

Step 3: Forward simulation and fault description

The last step of the workflow is the coupling of the time-dependent and evolutive grid of the basin with its fluid flow through dynamic fault property modelling. Another point to mention is that, the forward simulation is based on an evolutive grid with specific requirements.

In the new forward simulator, the basin is represented by a dynamic mesh which is described by step-by-step topologic (modification of the structure) and geometric (modification of coordinates) increments. Each layer is described by a set of cells of arbitrary shape, preferentially with hexahedral cells of reasonable aspect ratio. The mesh is a non structured mesh which evolves with the field of displacement in every spatial direction. This mesh can be continuous via deposition or erosion, or discontinuous for fault gliding and it is derived from volumetric restoration. The restoration builds an dynamic grid based on a discrete number of successive time steps, and the forward simulator operates a linear interpolation between these time steps to get a gradually deformed grid. In conclusion, the time-dependant mesh is more realistic, and physical properties are continuous through time.

In addition, the fault is geometrically represented as a boundary surface, with a left and right side and described by a set of faces. This representation is compatible with the paleo-re-construction of the model, as the two fault boundaries can slip relative to each other to follow fault kinematics and rock displacements through time. For the hydraulic behaviour, the fault is represented by a volume with a thickness, a spatially and temporally variable permeability, in which fluid flow can occur along and across the fault.

The fault width is taken into account as a parameter of the fluid flow model and is given as a property attached to the fault faces. Fault network is defined as a set of connections between surface meshes. With this definition, faults are zones of deformed rocks with flow properties. They are represented by a porous media and could act as a barrier or a conduit for fluid migration. Their lithologic characteristics differ from the surrounding host rock.

On this mesh with dynamic fault property modelling, the forward simulator computes multiphase flow coupled with compaction and heat transfer.

In the following examples, the dynamic mesh is obtained by two different approaches: the first by volumetric restoration, and the second by geometric modelling.

3D BASIN MODELLING WORKFLOW APPLIED TO A SIMPLIFIED THRUST BELT WITH THRUSTED LAYERS AND FAULTED GEOMETRIES

The first case study is inspired by the Gaspé Peninsula located in the northern part of the Canadian Appalachians which presents a structurally complex geology characterized by two imbricate thrust belts.
The central part of the Gaspé Peninsula delimits our study area. The structure “Lac des

Huits-Miles” is a large open syncline 35 km wide that reaches 6.5 km depth at its core. It is limited to the North by the Shickshock Sud fault and to the south by the Causapscal fault. Based on the interpretation of 2D depth seismic images, a 3D block diagram of the central part of the Acadian Gaspé Belt has been constructed.

The paleo-geometry is given at the end of each time step. This 4D grid reproduces properly the different stages of the deformation of the simplified basin (deposition, erosion, gliding along the faults).

The last step of the workflow is the thermal forward modelling of the basin through geological time. A constant basal heat flow of 50mW/m2 at the bottom of sediments has been used and a paleo-surface temperature of 15°C is assumed.

At this stage, the results demonstrate the feasibility of the whole workflow, but there is no calibration against well data. The structural and stratigraphic geology of the area have been simplified to demonstrate the feasability of the workflow.

ADVANCED FAULT DESCRIPTION FOR FLUID FLOW MODELLING: EXAMPLE OF A BASIN DEFORMED BY GRAVITY

To illustrate the impact of a more accurate characterisation of faults in basin modelling and its impact on fluid flow paths, a synthetic example inspired by geometries observed in the Gulf of Mexico is presented in this part. It represents an extensional gravity system combining a listric fault in the shallow part of the slope with reverse faults at the toe of the slope.

The deformation history is described by layers undergoing flexural slip folding. The lithofacies distribution used for modelling is an alternation of sand and shale layers. The structural history is composed of a normal deposition of sand and shale between 100 and 60 Ma, a sliding phase along the fault surfaces between 60 and 50Ma, and lastly a thrust episode between 50 and 45 Ma.

This model is used to demonstrate the impact of the displacement on fluid flow, represented by the fault movement and how the impact is extended far from the faults into the surrounding host rock.

CONCLUSIONS

Targeting new resources in deeper and structurally more complex geological environments requires an advanced basin modelling workflow to describe fluid transfer due to fault activity. In this paper, we present an advanced basin workflow.

Using two greatly simplified examples from compressional and extensional settings, results have demonstrated that such a basin workflow can be well established and that a fault model is possible on unstructured grids at basin scale.

Beside the evaluation of the workflow, we have introduced an innovative 4D grid concept which is a major step forward that allows to follow continuously deforming basin architecture in faulted environments, including displacement along the faults, and accounting for fluid flow coupled with relative displacement of the fault walls.

More work needs to be done to cover a large range of complex structural situations on a continuously evolving grid. We are only at the beginning by using synthetic examples that have been inspired by real cases and many difficulties still exist to make this workflow fully operational in natural cases.

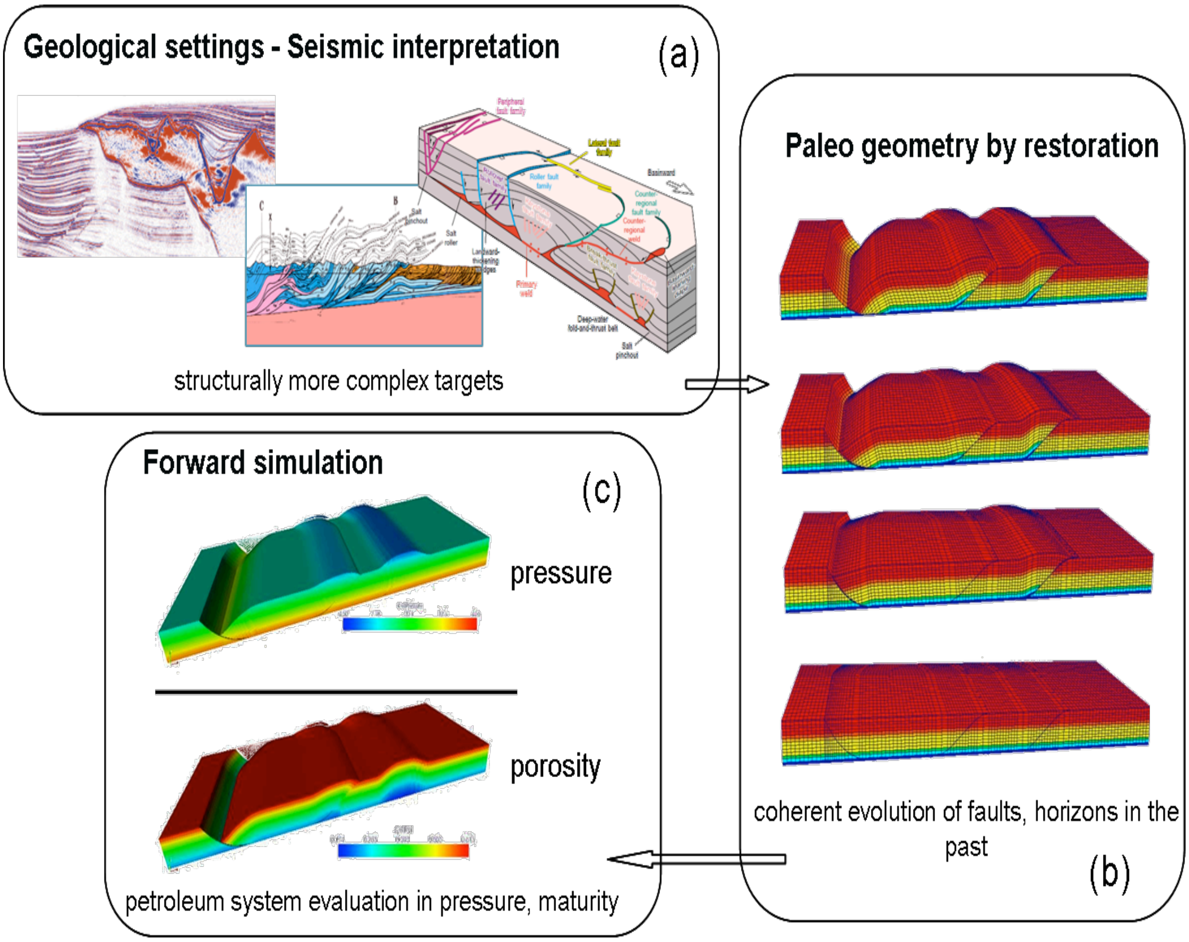

Figure Proposed 3D basin modelling workflow. (a) Present day 3D geometry of the sedimentary basin. Input data in structurally deformed environments: seismic cross sections, structural interpreted cross sections, 3D block diagrams with fault families. (b) Basin history from palinspastic reconstruction. Illustration of paleo-geometries at various time steps of deformation of thrust units over a fixed unit. (c) Forward simulation and fault description. Illustration of the coupling between paleo-geometries given in b) and forward simulations results of pressure and porosity at present day.

O-34 Challenges of the Levant Basin: a typical example of frontier, off-shore, deep-water hydrocarbon basins

Fadi H. NADER

IFP Énergie nouvelles, 1-4 avenue de Bois-Préau 92852 Rueil-Malmaison, France

Today, the Levant Basin – located in the East Mediterranean region – represents a new Frontier Gas Province. Offshore discoveries in this basin (e.g. Mari-B, Tamar, Dalit, Leviathan, Tanin, Karish, and Cyprus-A) have confirmed the presence of gas accumulations in subsalt Lower Miocene sandstones (exceeding 38Tcf of recoverable reserves). The East Mediterranean region remains, nevertheless, burdened with a complex geodynamic, tectono-stratigraphic history and high exploration costs (deep offshore drilling, sub-salt reservoirs).

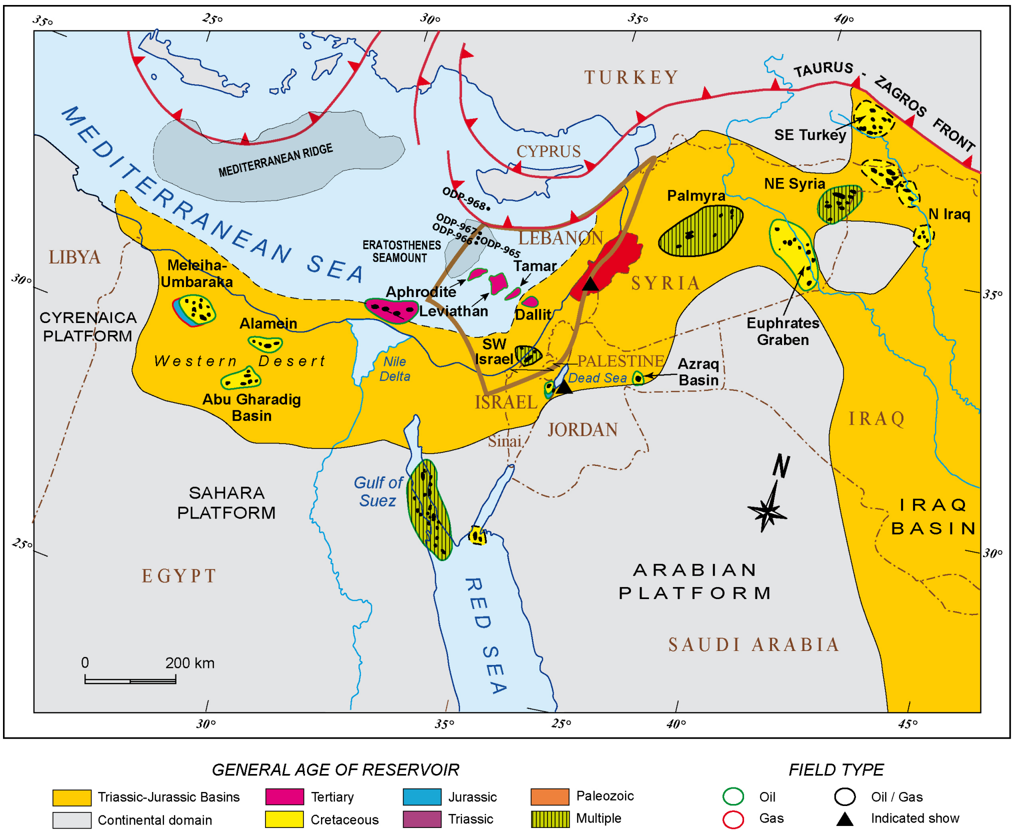

Figure 1. Schematic map showing the Levant Basin and the major oil/gas fields and discoveries in the East-Mediterranean region and northern Arabia (Nader, 2014).

Frontier hydrocarbon basins are commonly associated with risky and rather expensive exploration. A very limited number of wells generally exists and seismic data constitute the key information that is available for evaluating the basin's architecture and sedimentary filling history (and subsequently its prospectivity). Here, robust geological concepts and uncertainty analyses become crucial tools for sound economic assessment.

The origin of the Levant Basin (as a part of the NeoTethys) has been ascribed to the Permo-Triassic fragmentation of Pangea. Sedimentary filling therein was influenced by several tectonic events including the closure of the Neo-Tethys, pulsating compressive folding (previously called "Syrian Arc Deformation"), and strike-slip faults associated with the separation of the African and Arabian Plates. Impacts of such tectonic history on the distribution of sedimentary facies (source-, reservoir-, and sealing rocks) remain difficult to comprehend, and need appropriate numerical modeling before successful drilling. New seismic data confirm that the southern part of the Levant Basin (offshore Sinai, Israel) is significantly different from the northern part (offshore Lebanon, Cyprus). Indeed, the former could be associated to a western extension of the southern Palmyride zone, denoting thicker Upper Cretaceous – Cenozoic rock successions, and thicker underlying crustal segment invoking thin-skinned tectonics. Three distinct domains across the northern Levantine basin/ margin (Lebanon) have been illustrated in Nader (2011): deep basin offshore, margin offshore, and margin onshore. The latter domain being correlated with the inland Palmyride Trough (see Fig. 2). Such domains are well in-line with recent results of seismic interpretation and basin modeling provided by a series of academic projects (MSc and PhD theses; Hawie et al., 2013a and b; Bou Daher et al., 2014; Ghalayini et al., submitted).

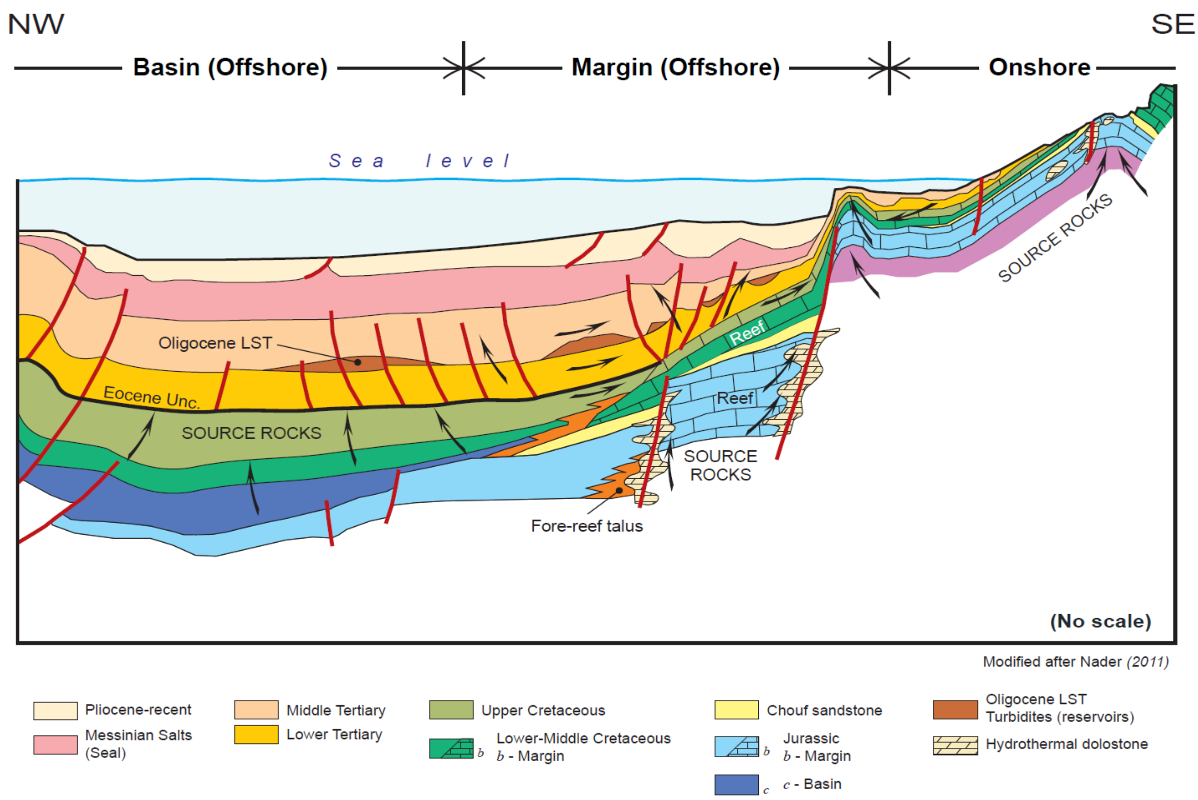

Figure. 2. Schematic petroleum system model for Lebanon (northern Levant Basin), with possible plays offshore, in the continental margin and onshore (modified from Nader, 2011).

New ideas have emerged from recent studies regarding source-to-sink approach for filling the basin with relatively thick sedimentary packages, in-depth structural investigation of the mechanisms and timing of observed faults and folds, and geochemical analyses of outcropping source rocks (Hawie et al, 2013; Ghalayini, submitted; Bou Daher et al., 2014;

and references therein). Integrating all such information in one geomodel will provide a powerful tool to test geological concepts and to de-risk the continuing exploration of such a frontier province.

Towards an Integrated Stratigraphic GeoModel

An emerging frontier hydrocarbon province, with risky off-shore subsalt exploration and production, presents numerous challenges. One of which, may be seen by far as the most important, concerns the lack of available data – especially in distal parts of the basin (offshore). Classically, the lack of data is met with adequate regional studies and comprehensive synthesis (Fig. 3) taking into account the scarce available information, which is then extended to unknown areas through extrapolation. This is based on the state-of-the-art concepts of geology and basin analysis. In frontier offshore basins, reflection seismic data (2D and 3D) among other geophysical techniques are often being used extensively. Yet even with relatively robust geologic concepts and reasonable seismic-stratigraphic correlations, the lack of data prohibits crucial validations to limit uncertainties.

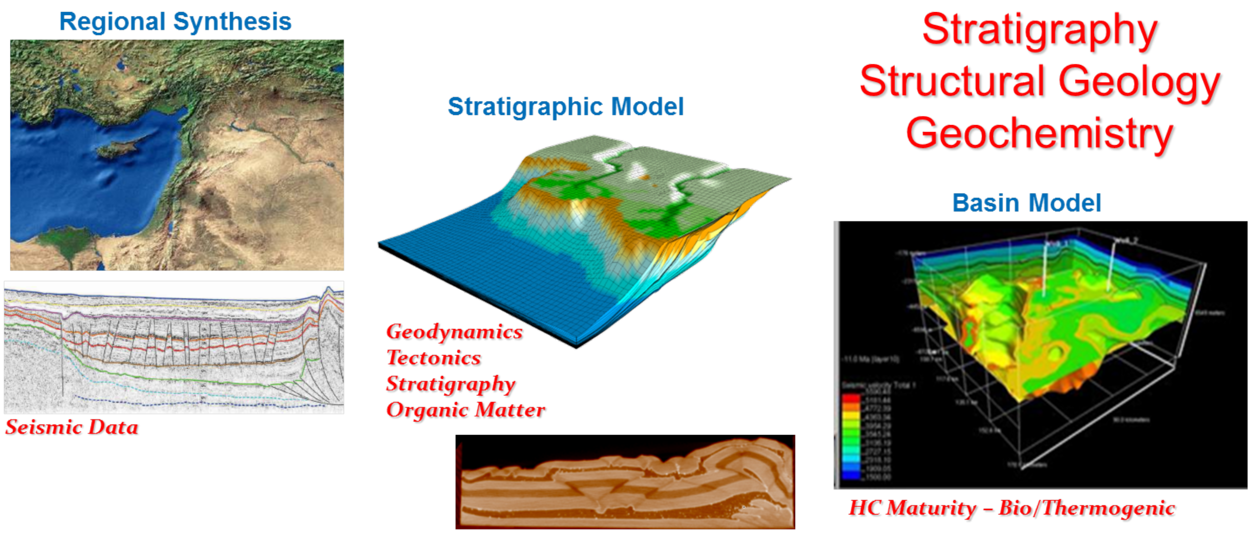

Figure 3. Regional geologic synthesis (including seismic data interpretations; e.g. Hawie *et al.*, 2013), stratigraphic and structural modeling (e.g. Gvirtzman *et al.*, 2014), and petroleum systems basin modeling. Tools often used to test scenarios and limit exploration uncertainties.

Various types of modeling have been therefore used in order to test a broad range of hypotheses. For instance, Gvirtzman et al. (2014) make use of IFPEN’s Dionisos software package in order to constrain the major sediment sources responsible for filling the southern part of the Levant Basin (Fig. 3). Other types of numerical modeling at the basin-scale attempt to understand the distribution of organic matter, to apply structural restoration, or to infer about the evolution of basinal fluids. Analog modeling (sand-box experiments) have also been used in order to constrain boundary conditions for the effects of tectonics on the basin architecture and geometries (Fig. 3).

An integrated stratigraphic geomodel includes the application of the above mentioned approaches and tools (Fig. 3). Hence, workflows are designed to make use of the regional synthesis of a frontier basin in order to construct a forward stratigraphic model. Then such model is used aiming to achieve best fit simulations associated to tests with other tools (e.g. sand-box experiments). Integrating a stratigraphic model with a petroleum system basin model will be the final stage, whereby the produced geomodel scenarios could be used in optimal conditions to better understand the investigated frontier hydrocarbon basin.

PACTS-Basins R&D Approach

Today, the academic and industrial realms are faced with the needs to further upgrade research and development tools and workflows. Numerical modeling software packages are being continuously improved, and yet new needs keep on emerging. Under the PACTS-Basins Research Program, IFPEN proposes to develop a methodology for evaluating source rocks maturity in frontier hydrocarbon basins with complex geodynamic tectono-sedimentary history, based on integrated stratigraphic basin geomodeling. The Levant Basin is believed to be an excellent application for the proposed approach.

In addition to the workflow presented above, this proposed research program will include uncertainty numerical modeling. Such tool will be used to constrain uncertainties where validation and calibration are lacking (namely in frontier hydrocarbon provinces). Uncertainty analysis may be considered as an adequate way to value the integrated geomodels in under-drilled frontier basins, paving the way for a less risky exploration.

References

Bou Daher, S., Nader, F.H., Strauss, H., and Littke, R. (2014). Depositional environment and source-rock characterization of organic-matter rich upper Santonian - upper Campanian carbonates, northern Lebanon. Journal of Petroleum Geology, 37 (1): 5-24.

Ghalayini, R., Daniel, J.-M., Homberg, C., Nader, F., and Comstock, J. (*submitted*). Impact of the Cenozoic strike-slip tectonics on the evolution of the northern Levant Basin (offshore Lebanon).

Gvirtzman, Z., Csato, I., and Granjeon, D. (2014). Constraining sediment transport to deep marine basins through submarine channels: The Levant margin in the Late Cenozoic. Marine Geology, 347: 12-26.

Hawie, N., Gorini, C., Deschamps, R., Nader, F.H., Montadert, L., Granjeon, D. Baudin, F. (2013). Tectono-stratigraphic evolution of the northern Levant Basin (offshore Lebanon). Marine and Petroleum Geology, doi: 10.1016:j.marpetgeo.2013.08.004.

Montadert, L., Nicolaides, S., Semb, P.H., and Lie, O. (2010). Petroleum systems offshore Cyprus. AAPG Annual Convention and Exhibition, New Orleans, Louisiana, April 11-14, 2010.

Nader, F. H., 2011. The petroleum prospectivity of Lebanon: an overview. Journal of Petroleum Geology, 34 (2): 135-156.

Nader, F.H. (2014) Insights into the Petroleum Prospectivity of Lebanon. *In*: Marlow, L., Kendall, C., and Yose, L. (eds): Petroleum systems of the Tethyan region. AAPG Memoir 106: 241-278.

O-35 **The Japanese island arc: geological structures and its formation processes**

Tanio Ito, Satoshi Yamakita and Hiroshi Sato

1 Teikyo Heisei University, 2 Miyazaki University, 3 Earthquake Research Institute, University of Tokyo

The formation of the Japanese island arc occurred through a long but drastic series of events. Since the middle Paleozoic, the structure of present Japanese island arc has built its basement at the border of the Asian continent mainly by successive accretionary process and subordinately by huge strike slip faultings. Longitudinal zonal structures then grew nearly parallel to the continental margin in the basement. In the middle Miocene, a big event, the opening of the Japan Sea occurred, forcing the basement to be separated from the Asian continent and constructed an island arc, the Japanese island arc. The event also bent the newly formed arc into three large segments, Northeast Japan, Southwest Japan and Ryukyu islands by collisions against the Izu-Bonin island arc and the Kyushu-Palau aseismic ridge in the Pacific side. These movements drastically deformed the original structures in the bending regions and established the present structures of the Japanese island arc, which have been controlling the tectonics in the Japanese island arc since the middle Miocene.

In this talk, we present recent developments in the research as well as controversial and unsettled problems for discussion.

O-36 **Determination of the tectonic evolution from fractures, faults and calcite twins on the south-western margin of the Indochina Block**

Francesco Arboit [a]*, Khalid Amrouch [b], Alan S. Collins [a], Rosalind King [a] and Christopher Morley [c]

[a] Centre for Tectonics Resources and Exploration (TRaX), Department of Earth Sciences, The University of Adelaide, SA 5005, Australia.
[b] The Australian School of Petroleum, The University of Adelaide, SA 5005, Australia.
[c] Chiang Mai University, 239 Huaykaew Road, Tumbol Suthep Amphur Muang, Chiang Mai, Thailand.

Abstract
In polyphase tectonic zones, integrating a study of fault and fracture with calcite twin analysis can determine the evolving paleo-stress magnitudes and principle stress directions that affected the area. This paper presents the results of the analyses of fractures, striated faults and calcite twins collected within the Khao Khwang Fold-Thrust Belt (KKFTB) in central Thailand (SE Asia). Here we attempt to reconstruct the orientation of the principal stresses that developed during the tectonic evolution of this highly deformed, polyphase orogen. Tectonic data were collected in the Permian carbonates of the Khao Khad Formation of the Saraburi Group, and five successive tectonic stages are determined that are interpreted to have developed before, during, and after, the Triassic Indosinian Orogeny. The first three stages pre-date the main deformation event: the first stage is interpreted as a pre-Indosinian N-S extensional stage, the second stage described a N-S strike-slip and compressional regime, largely perpendicular to the fold axes of the main structures, while the third stage is associated with an E-W compressional strike-slip phase. A further two stages took place after, or during, the main folding event and correspond to N-S compression and to an E-W composite strike-slip/contractional stage, the latter which is interpreted to represent Cenozoic deformation related to the India-Asia collision.

P-1 **Detrital zircon age, Hf isotopic analysis and tectonic reconstruction of the Khao Khwang Fold-Thrust Belt, south-western margin Indochina terrane, central Thailand**

Francesco Arboit [a]*, Alan S. Collins [a], Christopher Morley [b], Rosalind King [a] and Khalid Amrouch [c]

[a] Centre for Tectonics Resources and Exploration (TRaX), Department of Earth Sciences, The University of Adelaide, SA 5005, Australia.
[b] Chiang Mai University, 239 Huaykaew Road, Tumbol Suthep Amphur Muang, Chiang Mai, Thailand.
[c] The Australian School of Petroleum, The University of Adelaide, SA 5005, Australia.

Abstract
In situ U-Pb detrital zircon ages and Hf isotope analyses from Permian Triassic clastic units in central Thailand constrain the provenance, maximum depositional ages and depositional environment of the south-western margin of the Indochina terrane through the Late Palaeozoic Early Mesozoic. The key lithological units: the Sap Bon, Pang Asok and Nong Pong formations are part of the Saraburi Group and have feasibly spread age spectra. The entire dataset have a common most relevant peak at about 450 Ma and all samples are also characterised by zircons that aged about 0.2-0.3, 0.4-0.6, 1.0-1.3, 1.7-1.8, 2.2-2.7, spreading in few cases over 3.0 Ga. These data - combined with the available sedimentological and detrital zircon ages data - allow interpreting the siliciclastic formations within the Saraburi group as the distal and the proximal deposits of the deposit filling the Indosinian foreland basin on the south-western margin of the Indochina terrane. Detrital zircons as young as ± 205 Ma show that previously considered Mid-Late Permian deposits of the Saraburi Group is no older than Early Jurassic. Further, the entire detrital zircon age spectra of the Sap Bon, Pang Asok and Nong Pong formations bear a resemblance to those of the Permian-Triassic sequence within the Khorat Plateau, Truong Song and NE Vietnam, indicating a possible source from the NE at the time of the deposition.

P-3 **Deformation and paleo-geothermal structure of the Neogene forearc basin in the Boso Peninsula, central Japan**

Nana KAMIYA (Nihon Univ., JAMSTEC), Yuzuru YAMAMOTO (JAMSTEC), Takato TAKEMURA(Nihon Univ.)

Geologic structures (i.e. fold, faults, etc.) in forearc basins have clues to understanding tectonic processes related to plate-subduction, since their capacities should formed associated with development of accretionary prisms. However, structural analyses for forearc basin deposits and studies on their tectonic history related to plate subduction have been limited. We performed structural analyses of the post-Middle Miocene forearc basin in the Boso Peninsula, central Japan, to examine the relationship between the basin evolution and plate-subduction processes.

The geology of the Boso Peninsula is controlled by plate subduction phenomena and is subdivided into three parts; 1) Early Miocene and Late Miocene to Pliocene accretionary prisms in the southern part, 2) the Hayama-Mineoka tectonic belt mainly composed of ophiolite in the middle part, and 3) post-Middle Miocene forearc basin in the northern part. The southern rim of the forearc basin in central-western part of the Boso Peninsula, located close to the trench-slope-break (Mineoka ophiolite), expected to represent the most active deformations related to the forearc-basin formation. We therefore conducted the geologic survey and geothermal analyses. As the results, characteristic geological and geothermal structures in the forearc basin were identified. The forearc basin deposit in this region is composed of conglomerate, sandstone, alternation of sandstone and mudstone, mudstone and many tuffaceous marker beds. These deposit correspond to the post Middle Miocene Miura Group and Pliocene and late Pleistocene Kazusa Group. Boundary of two groups is the Kurotaki Unconformity formed approximately 3Ma, when the convergent direction of Philippine Sea Plate has been changed (Takahashi, 2006). Bedding attitudes in the study area are controlled by the E-W trending fold axes (Fig.1). Predominant normal and transversal faults trend N-S. Reverse faults trend E-W or NE-SW in the Miura Group (below the Kurotaki Unconformity) while NE-SW in the Kazusa group (above the unconformity). This variation has relationship with the tectonic event: direction of plate subduction (Philippine Sea Plate) changed from northward to NW-ward when Kazusa Group started to deposit. Microstructural analyses of the fault zones revealed rounded shapes of sand grains and their size reduction indicative of that these faults formed syn-sedimentary.

Vitrinite reflectance (Ro) analyses were conduced to examine geothermal structure and revealed that variation of maximum paleo-temperature between the Miura and Kazusa groups (below and above the Kurotaki Unconformity). The maximum paleo-temperature in the former is estimated as 70-95˚C, whereas in latter is less than 10-35˚C. Given 20˚C/km paleo-geothermal gradient (Sakai et al, 2011), about 2000 m uplifting/erosion of the Miura Group associated with the formation of the unconformity is expected. To verify this, we are performing consolidation tests for mudstone.

References

Masaki Takahashi (2006), Tectonic Development of the Japanese Islands Controlled by Philippine Sea Plate Motion, *Journal of Geography*, 115, 116-123.

Sakai R., Munakata M., Kimura H., Ichikawa Y., and Nakamura M., 2011, Study on Validation Method of Regional Groundwater Flow Model : Case Study for Boso Peninsula, JAEA-research 2010(66), 1-20, 1-2.

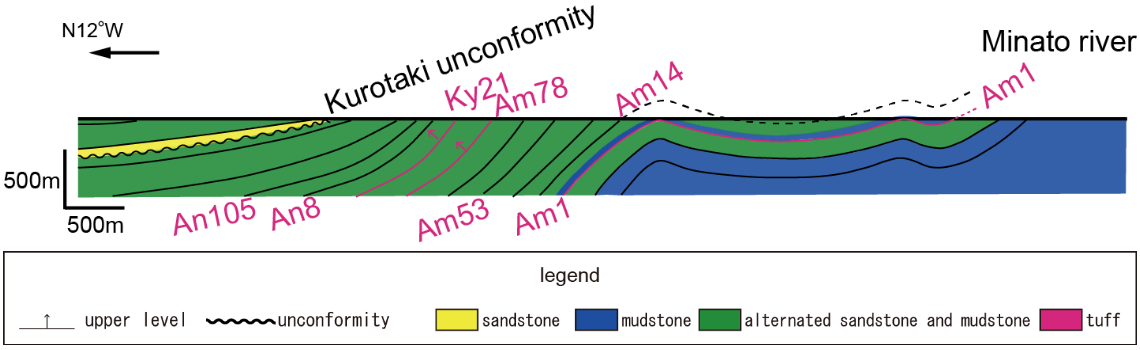

Fig.1 Cross-sectional view of forearc basin in Boso Peninsula

P-4 **The problem with the plate boundary in the Sea of Japan**

Anne Van Horne[1,2], Hiroshi Sato[1], Tatsuya Ishiyama[1], Naoko Kato[1]

[1] *Earthquake Research Institute, The University of Tokyo, Tokyo, Japan*
[2] *Department of Geology and Geophysics, University of Wyoming, Laramie, Wyoming USA*

Plate boundaries that are defined by spreading ridges, subduction trenches, or large transform faults are easily recognizable, but those that lack such obvious tectonic features are more difficult to define. The Japan Sea plate boundary has been treated since the mid-1980’s as a well-defined dividing line between Eurasia and North America, extending from Sakhalin south through the Japan Sea, then cutting east through central Japan along the Itoigawa-Shizuoka Tectonic Line (ISTL). Its location has been inferred from geodetic models which suggest that NE Japan moves independently from Eurasia, but geologically and seismologically, it cannot be constrained. Available published data show a nuanced picture. A series of destructive (M>7) intraplate earthquakes in the Japan Sea, with E-thrusting focal mechanisms, was once taken to be evidence of nascent subduction, but they appear to be occurring at the boundary between thick ocean crust in the Japan Sea and the island-arc crust of central Japan, on inherited structures, formed during back-arc opening, that are being reactivated. Seismic images for this region show no crustal discontinuities that could be interpreted as a plate boundary. As for the ISTL, available geological and seismological evidence indicates that the southern ISTL marks a W-dipping deformation boundary related to the collision of the Izu-Bonin arc with SW Japan (15 Ma). Although indented by the collision, the geological structure and basement of SW Japan are continuous across the ISTL, making it an unlikely plate boundary. The northern ISTL has a completely different origin as an E-dipping boundary fault for a Neogene rift basin. It has been inactive in the late Quaternary and, again, does not constitute a major geological discontinuity in the basement. Hence, while geodetic models imply a plate boundary between Japan and Eurasia, published geological and seismological data cannot support its location in the Japan Sea or at the ISTL. If, as studies show, almost half of the convergence between North America and Eurasia is taken up in Hokkaido and across N Japan, the small amount of remaining convergence may be difficult to discriminate given the large elastic response in the upper plate (N Honshu) after the 2011 Tohoku-oki (M9.0) earthquake, and strong coupling at the megathrust.

P-5 Migration of active contractional deformation estimated from fold topographic developments along the eastern margin of the Japan Sea, northeast Japan

Makoto Otsubo (otsubo-m@aist.go.jp), Ayumu Miyakawa

Geological Survey of Japan, AIST Tsukuba Central 7, Higashi-1-1-1, Tsukuba, 305-8567, JAPAN

The eastern margin of the Japan Sea (Fig. 1), northeast Japan arc, lies in a strongly compressional area, and contractional deformation in the region is ongoing. The Tohoku district, on the eastern margin of the Japan Sea, lies within a strongly compressive area that has been experiencing large, contractional, crustal deformations, since the late Pliocene (Sato and Amano, 1991; Sato, 1994). In the region, Fold-and-thrust structures (Sato, 1989) and fold-topographic structures with distributed reverse-type faults (e.g., Okamura et al., 1995) have developed in response to this contractional deformation. Geodetic surveys in the Tohoku district have detected zones with a high rate of horizontal strain (Sagiya et al., 2000). Within the high strain rate zones, a number of large, reverse-type faulting earthquakes have occurred in the upper crust over the past 10 years (Fig. 1; e.g., Sibson, 2009). When the contractional deformation continues to the present, the high strain rate zones at the geodetic and geological scales should be overlapped. However, the high horizontal strain-rates recognized at geodetic and geological time-scales are spatially heterogeneous. Rates are consistent in the Niigata region, in the southwestern part of the Tohoku district, but not in the Akita region in the northwestern part of the district. There is a need to constrain the spatial differences in the horizontal strain-rate between the geodetic and geological timescales, in order to understand regional tectonic differences across the district.

In this study, we focus on the topographic and erosional evolution of folded structures developed since the late Pliocene in the Akita and Niigata regions (Fig. 2). Based on the degree of fold activity, the balance between surface uplift and erosion controls the topographic development (Ellis and Densmore, 2006). The geomorphic analysis of erosional features has $10^{3–4}$ yr time-scales (e.g., Lavé and Avouac, 2000). We measured the horizontal distance between the fold hinge lines and the mountain ridge lines. We treated 44 folds that were activated since the late Pliocene, comprising 12 and 32 folds in the Akita and Niigata regions, respectively (Fig. 2). We used a 50 m grid meshed digital elevation model (DEM) published by the Geospatial Information Authority of Japan and 1:200,000 geological maps published by the Geological Survey of Japan.

Spatial variations in the horizontal deviations are consistent with the systematic eastward migration of fold growth in the study area (Fig. 2). The topographic behavior indicates that the eastward migration (landward migration) of the fold growth is generally constant. The results are concordant with fold developments inferred from geological researches (Awata and Kakimi, 1985; Kishi and Miyawaki, 1996). Awata and Kakimi (1985) and Kishi and Miyawaki (1996) showed that fold development in this region is migrating from west (back-arc) to east (volcanic front), which is consistent with the history of crustal active faulting in the area (e.g., Doke et al., 2012). Our results indicate that the fold growth occurred over a time-scale of $10^{3–4}$ yr. This time scale may constrain the model of stress accumulation and release on the crustal fault reactivation.

The spatio-temporal distribution of volcanism in the Tohoku district shows a recent (5–0 Ma) migration of volcanism from the back-arc region to the volcanic front (Honda and Yoshida, 2005), which might be correlated with dynamics in the mantle wedge beneath the Tohoku district (Yoshida et al., 2013). The distribution of geodetic high-strain-rate regions is broadly coincident with the area of high heat flow in the Tohoku district (Hasegawa et al., 2005; Townend and Zoback, 2006). The high crustal temperatures may be the key control factor on upper plate strength (Townend and Zoback, 2006). Therefore, we suggest that the gap between geodetic and geological high-strain-rate regions reflects the migration of strong contractional deformation, which followed the landward migration of the geothermal spatial heterogeneity.

The study was supported by MEXT KAKENHI (26109003).

References

Awata, Y., Kakimi, T., 1985. Quaternary tectonics and damaging earthquakes in northeast Honshu, Japan. In: C. Kisslinger and T. Rikitake (Eds.), Practical Approaches to Earthquake Prediction and Warning. Springer, Netherlands, pp. 231–251.

Doke, R., Tanikawa, S., Yasue, K., Nakayasu, A., Niizato, T., Umeda, K., Tanaka, T., 2012. Spatial patterns of initiation ages of active faulting in the Japanese Islands. Katsudanso Kenkyu (Active Fault Research) 37, 1–15 (in Japanese, with English Abstract).

Ellis, M.A., Densmore, A.L., 2006. First-order topography over blind thrusts. Geological Society of America Special Papers 398, 251–266.

Hasegawa, A., Nakajima, J., Umino, N., Miura, S., 2005. Deep structure of the northeastern Japan arc and its implications for crustal deformation and shallow seismic activity. Tectonophysics 403, 59–75.

Honda, H., Yoshida, T., 2005. Application of the model of small-scale convection under the island arc to the NE Honshu subduction zone. Geochemistry, Geophysics, Geosystems 6, 1–22, Q01002, http://dx.doi.org/10.1029/2004GC000785.

Kishi, K., Miyawaki, R., 1996. Plio-Pleistocene fold development in the Kashiwazaki Plain and vicinity, Niigata Prefecture. Journal of Geography Tokyo 105, 88–112 (in Japanese, with English Abstract).

Lavé, J., Avouac, J.-P., 2000. Active folding of fluvial terraces across the Siwaliks Hills, Himalayas of central Nepal. Journal of Geophysical Research: Solid Earth 105 (B3), 5735–5770.

Okamura, Y., Watanabe, M., Morijiri, R., Satoh, M., 1995. Rifting and basin inversion in the eastern margin of the Japan Sea. Island Arc 4, 166–181.

Sagiya, T., Miyazaki, S., Tada, T., 2000. Continuous GPS array and present-day crustal deformation of Japan. Pure and Applied Geophysics 157, 2303–2322.

Sato, H., 1989. Degree of deformation of late Cenozoic strata in the Northeast Honshu Arc. Memoirs of the Geological Society of Japan 32, 257-268 (in Japanese, with English abstract).

Sato, H., 1994. The relationship between late Cenozoic tectonic events and stress field and basin development in northeast Japan. Journal of Geophysical Research: Solid Earth 99

(B11), 22,261–22,274.
Sato, H., Amano, K., 1991. Relationship between tectonics, volcanism, sedimentation and basin development, Late Cenozoic, central part of Northern Honshu, Japan. Sedimentary Geology 74, 323–343.
Sibson, R.H., 2009. Rupturing in overpressured crust during compressional inversion—the case from NE Honshu, Japan. Tectonophysics 473, 404–416.
Townend, J., Zoback, M.D., 2006. Stress, strain, and mountain building in central Japan. Journal of Geophysical Research: Solid Earth 111 (B3), B03411, doi:10.1029/2005JB003759.
Yoshida, T., Kimura, J.-I., Yamada, R., Acocella, V., Sato, H., Zhao, D., Nakajima, J., Hasegawa, A., Okada, T., Honda, S., Ishikawa, M., Prima, O.D.A., Kudo, T., Shibazaki, B., Tanaka, A., Imaizumi, T., 2013. Evolution of late Cenozoic magmatism and the crust-mantle structure in the NE Japan Arc. Geological Society, London, Special Publication 385, doi:10.1144/SP385.15.

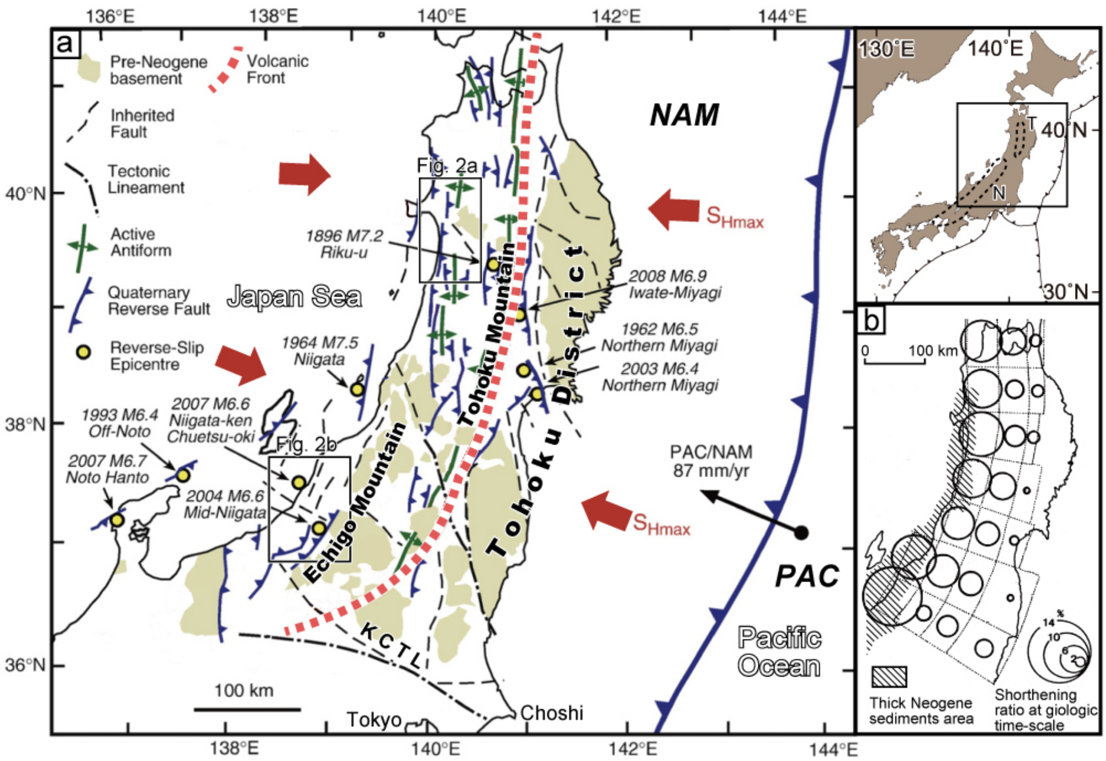

Fig. 1. Active tectonics of the eastern margin of the Japan Sea. (a) Seismo-tectonic sketch map showing the epicenters of recent reverse-fault ruptures in relation to basin-bounding faults, exposed areas of pre-Neogene basement, actively growing regional antiforms, Quaternary volcanoes, and the volcanic front (modified after Sato, 1994; Sibson, 2009). (b) Shortening ratios estimated from geological fold structures in each grid in the Tohoku district (modified after Sato, 1989). Shading indicates areas of thick Neogene sediments (Sato, 1994). In the area, the average amount of horizontal shortening at geological time-scales is estimated to be 10%–15% (Sato, 1989).

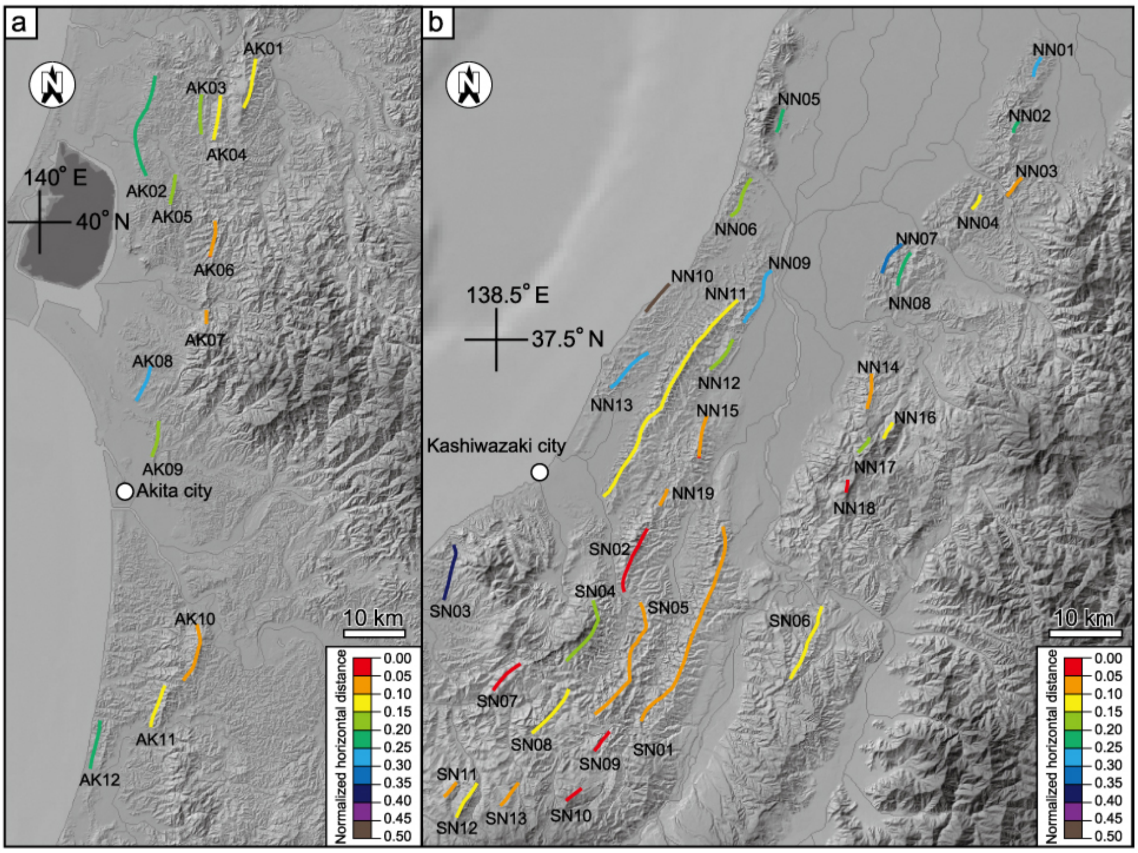

Fig. 2. Spatial distribution of the horizontal differences based on the hinge–ridge distances in the (a) Akita and (b) Niigata regions. Colors of the lines indicate the horizontal differences at 0.05 intervals. The horizontal differences in each fold are normalized by widths of each fold.

P-6 Evolution of fault activity in the northeast–central Japan: Insights from crustal stress and fault orientations

Ayumu Miyakawa*, Makoto Otsubo

Geological Survey of Japan, AIST Tsukuba Central 7, Higashi-1-1-1, Tsukuba, 305-8567, JAPAN

Corresponding author: Ayumu Miyakawa (miyakawa-a@aist.go.jp)

Understanding the intraplate fault activity is important for various fields of geoscience including the reconstructing geodynamic processes. A physical method based on Mohr–Coulomb criteria is effective for evaluating the activity of faults including fault reactivation. The slip tendency analysis (Morris et al., 1996) that is one of the physical methods based on Mohr–Coulomb criteria can evaluate the activity of active faults under the tectonic stress (e.g. Miyakawa and Otsubo, 2015; Yukutake et al., 2015). This method uses fault orientation data and the proximal stress field, meaning it can be applied in evaluating present-day and/or future fault activity without the need for data on the timing of fault activity. It is known that first-order tectonic stress is concordant in its principal orientations with relative plate motions (Zoback, 1992). The agreement of instantaneous plate motions and the long-term plate motions determined from marine magnetic anomalies seems to suggest that the stress field is as old as ~10^6 years (Argus and Gordon, 1990). If the given tectonic stress continues for a few million years under present tectonic setting, we develop a hypothesis that the slip tendency analysis can be applied to not only the active faults but also the non-active faults. Hence, we need to know the response of active and non-active faults under the continued tectonic stress.

We studied fault activity in northeast–central Japan (Fig. 1) by calculating the regional stress and the fault orientation field for active faults and inactive faults (here, an inactive fault is a fault for which Quaternary activity has not been observed). First, the regional stress field was calculated by using the damped inversion method (Hardebeck and Michael, 2006) applied to earthquake focal mechanisms in Japan. Second, we acquired the locations and orientations (i.e., strike and dip) of active faults in the study area from the Active Fault Database of Japan and inactive faults from a database compiled by Kosaka et al. (2011). Third, we calculated slip tendency (Morris et al., 1996) for the evaluation of the likelihood of fault slip.

Slip tendency is generally high along active faults, though the slip tendency is generally low along inactive faults (Fig 2). The gap between the slip tendencies of active and inactive faults is induced from the difference in their activities. However some inactive faults show high slip tendency. The high slip tendency observed for some inactive faults imply their high activity, although the inactive faults are not observed their recent activity. This discrepancy is explained that the high slip tendencies indicate their potential to become active fault in future. The potential to be active fault along inactive faults can be explained with the temporal evolution from inactive to active faulting during long-term crustal deformation. If we see a region undergoes the transition from inactive to active faulting, future active faults were observed as inactive faults with a high slip tendency. Furthermore, the average values of slip tendency for inactive faults gradually increases from northeast Japan to central Japan, because a relatively large number of inactive faults in central Japan have a high slip tendency. These spatial variations in the evolution from inactive to active faulting reflect the representative tectonic zones of the Japan. There is a clear difference between the types of deformation in the eastern margin of the Japan Sea (EMJS) and the Niigata–Kobe Tectonic Zone (NKTZ) (Okamura, 2002; Sagiya et al., 2000) (Fig. 1). The structures produced by deformation, such as reverse faulting and folding, are concentrated in the EMJS (Okamura, 2002), indicating that the crust in this region has undergone long-term deformation. In the NKTZ, crustal deformation is clearly observed in geodetic signals, but there are only weakly developed deformation structures. Therefore, the crust in the NKTZ may have undergone recent and/or short-term deformation. This observation suggests that different regions in Japan have been exposed to the present-day stress field for different lengths of time. The spatial variations in the evolution from inactive to active faulting reflect the different length of time to be exposed to the present-day stress filed.

This study was supported by MEXT KAKENHI (26109003).

References

Argus, D.F., R.G. Gordon (1990), Pacific−North American Plate motion from long baseline interferometry compared with motion inferred from magnetic anomalies, transform faults, and earthquake slip vectors. Journal of Geophysical Research, 95, 17315−17324.

Hardebeck, J. L., and A. J. Michael (2006), Damped regional-scale stress inversions: Methodology and examples for southern California and the Coalinga aftershock sequence, Journal of Geophysical Research, 111, B11310, doi:10.1029/2005JB004144.

Kosaka, K., Y. Kanaori, M. Chigira, and S. Yoshida (Eds.) (2010), Fault Map of Japan, Baifukan, Tokyo (in Japanese).

Miyakawa, A., and M. Otsubo (2015), Applicability of slip tendency for understanding long-term fault activity: a case study of active faults in northeastern Japan, Journal of JSCE, 3(1), 105–114, doi:http://doi.org/10.2208/journalofjsce.3.1_105.

Morris, A., D. A. Ferrill, and D. B. Henderson (1996), Slip-tendency analysis and fault reactivation, Geology, 24(3), 275–278, doi:10.1130/0091-7613(1996)024<0275:STAAFR>2.3.CO;2.

Okamura, Y. (2002), Deformation zones since the Neogene along the eastern margin of the Japan Sea (in Japanese), in Active Faults and Seismotectonics in the Eastern Margin of the Japan Sea, edited by M. Otake et al., pp. 111–121, Univ. of Tokyo Press, Tokyo.

Sagiya, T., S. Miyazaki, and T. Tada (2000), Continuous GPS array and present-day crustal deformation of Japan, Pure. Appl. Geophys., 157(11–12), 2303–2322, doi:10.1007/PL00022507.

Yukutake, Y., T. Takeda, and A. Yoshida (2015), The applicability of frictional reactivation theory to active faults in Japan based on slip tendency analysis, Earth and Planetary Science Letters, 411, 188–198, doi:10.1016/j.epsl.2014.12.005.

Zoback, M. L. (1992), First- and second-order patterns of stress in the lithosphere: the World Stress Map Project, Journal of Geophysical Research, 97, 11703−11728.

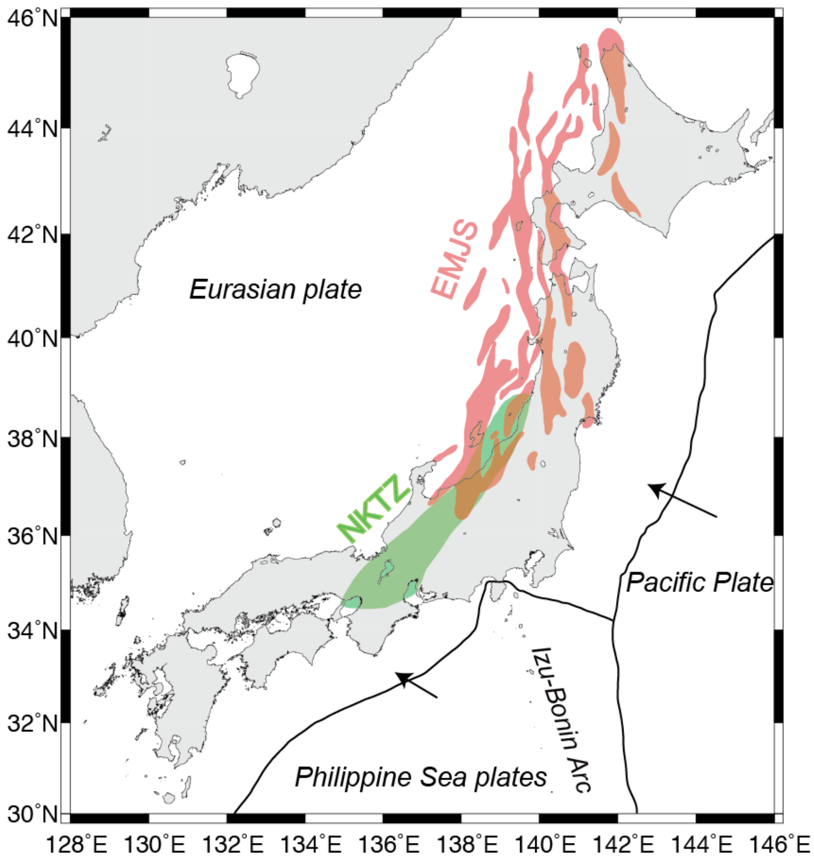

Fig. 1. Map showing the tectonic setting of the Japanese Islands. The Pacific and Philippine Sea plates are subducting beneath the Eurasian plate. Orange areas mark the eastern margin of the Japan Sea (EMJS) (Okamura, 2002). The green area marks the Niigata–Kobe Tectonic Zone (NKTZ) (Sagiya et al., 2000).

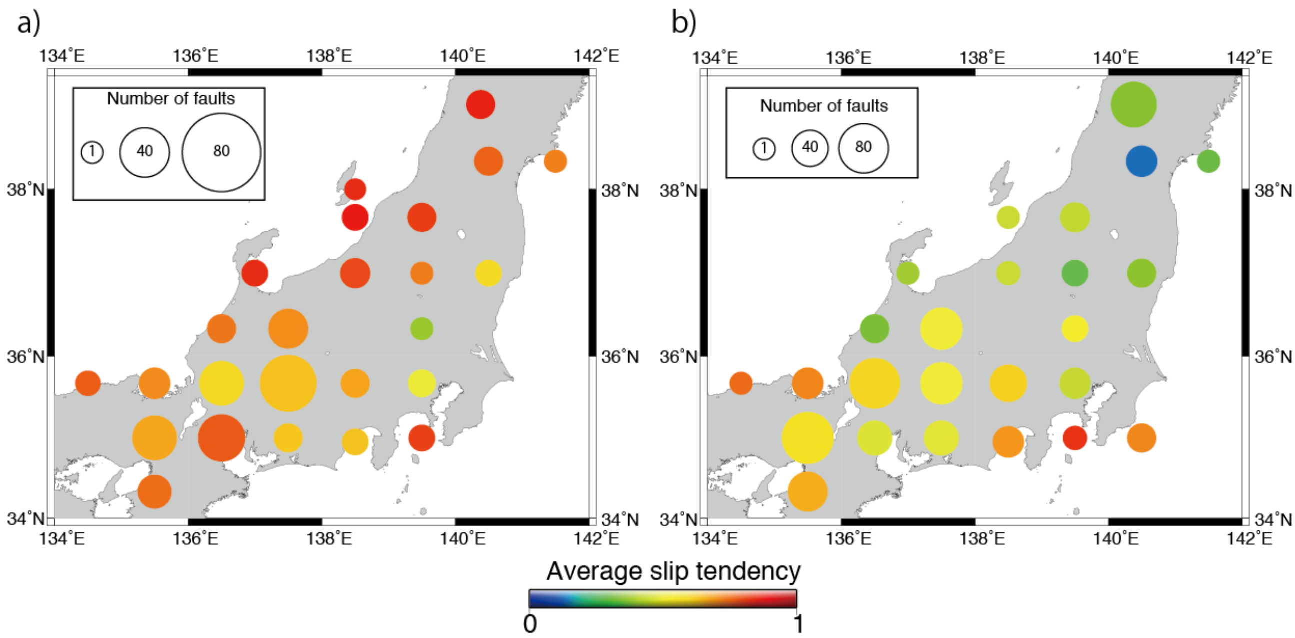

Fig. 2. Average slip tendencies for active faults (a) and inactive faults (b) in central–northeast Japan under the regional stress field calculated by using the damped inversion method (Hardebeck and Michael, 2006) applied to earthquake focal mechanisms in the study area. Circles indicate the average slip tendency in each region, and their color and size indicate the average slip tendency and the number of active faults, respectively.

P-7 **Active fault and fold systems from shallow to deep in the eastern part of Niigata basin, central Japan**

Naoko Kato (1), Hiroshi Sato (1), Tatsuya Ishiyama (1)

(1) Earthquake Research Institute, University of Tokyo, Tokyo, Japan

Northern Honshu rifted away from Eurasian continent ca. 25 Ma and backarc opening terminated at 15 Ma. By fault controlled subsidence and subsequent thermal subsidence (Yamaji, 1990), thick argillaceous sediments have been accumulated covering the Miocene submarine volcaniclastic rocks. Since the Pliocene, compressional stress has produced the shortening deformation in the Miocene back-arc rift basins. Fault reactivation of Miocene normal faults as reverse faults are prevailed and a fold-and-thrust belt is developed in the most stretched Miocene rift system (Sato, 1994; Kato et al., 2006).

The Niigata basin, central Japan, is one of such basins and filled by thick (< 7 km) Neogene sediments. The Niigata basin is frequently attacked by devastative earthquakes, due to reverse faulting. To reveal the crustal architecture, in particular geometry of source faults, onshore-offshore integrated deep seismic profiling was undertaken since 2008. The geometry of earthquake source faults is significant to estimate strong ground motions and tsunami heights. Seismic data were collected for CMP reflection imaging and refraction tomography. Offshore data were collected using two ships to obtain large offset reflection data. For the imaging of shallow part of on shore active structure, we performed high-resolution seismic reflection profiling using Minivib and Enviro vib (IVI). The resultant seismic profiles provide the image of a fold-and-thrust belt developed in the Miocene volcanic rift basin. Former syn-rift faults reactivated as reverse faults and thin-skinned deformation prevails in the post rift sediments forming detachment in the Miocene over pressured mudstone units. Fault-related folds and wedge thrusting is common feature of the shortening deformation. The lateral extension of source fault is strongly controlled by syn-rift faults, including transfer faults. Size and geometry of the present earthquake source faults strongly controlled by syn-rift fault systems.

References

Kato N., Sato H. and Umino N.. 2006. Fault reactivation and active tectonics in the for-arc side of the back-arc rift system, NE Japan. *Journal of Structural Geology*. **28**, 2011-2022.

Sato, H., 1994. The relationship between late Cenozoic tectonic events and stress field and basin development in northeast Japan. *Jour. Geophys. Res.*, **99**, 22261-22274.

Yamaji, A., 1990. Rapid intra-arc rifting in Miocene Northeast Japan, *Tectonics*, **9**, 365-378.

P-8 **Crust composition in the Hidaka Metamorphic Belt estimated from seismic velocity by measurements under the high P-T condition**

Koichi Yamauchi (Earthquake Research Institute, the University of Tokyo), Masahiro Ishikawa (Yokohama National University), Hiroshi Sato, Takaya Iwasaki (Earthquake Research Institute, the University of Tokyo), Tsuyoshi Toyoshima (Niigata University)

To understand the dynamics of the lithosphere in subduction systems, the knowledge of rock composition is significant. However, rock composition of the overriding plate is still poorly understood. To estimate rock composition of the lithosphere, it is an effective method to compare the elastic wave velocities measured under the high pressure and temperature condition with the seismic velocities obtained by active source experiment and earthquake observation.

Due to an arc-arc collision in central Hokkaido, middle to lower crust is exposed along the Hidaka Metamorphic Belt (HMB), providing exceptional opportunities to study crust composition of an island arc. Across the HMB, P-wave velocity model has been constructed by refraction/wide-angle reflection seismic profiling (Iwasaki et al., 2004). Furthermore, because of the interpretation of the crustal structure (Ito, 2000), we can follow a continuous pass from the surface to the middle-lower crust. We corrected representative rock samples from HMB and measured ultrasonic P-wave (Vp) and S-wave velocities (Vs) under the pressure up to 1.0 GPa in a temperature range from 25 to 400 °C (Fig.1).

For example, according to Fig.2, the Vp values measured at 25 °C and 0.5 GPa are 5.88 km/s for the granite (74.29 wt.% SiO_2), 6.02–6.34 km/s for the 129onalities (66.31–68.92 wt.% SiO_2), 6.34 km/s for the gneiss (64.69 wt.% SiO_2), 6.41–7.05 km/s for the amphibolites (50.06–51.13 wt.% SiO_2), and 7.42 km/s for the mafic granulite (50.94 wt.% SiO_2). And, Vp of 129onalities showed a correlation with SiO_2 (wt.%). Comparing with the velocity profiles across the HMB (Iwasaki et al., 2004), we estimate that the lower to middle crust consists of amphibolite and tonalite, and the estimated acoustic impedance contrast between them suggests an existence of a clear reflective boundary, which accords well to the obtained seismic reflection profile (Iwasaki et al., 2014). And, we can obtain the same tendency from comparing measured Vp/Vs ratio and Vp/Vs ratio structure model (Matsubara and Obara, 2011).

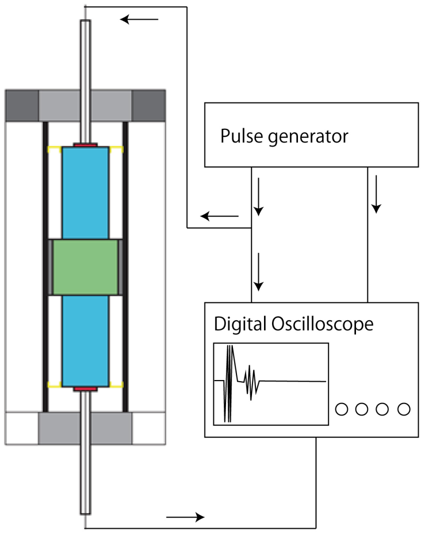

Fig.1 A schematic illustrateon of the high pressure cell assembly and the ultrasonic attachment.

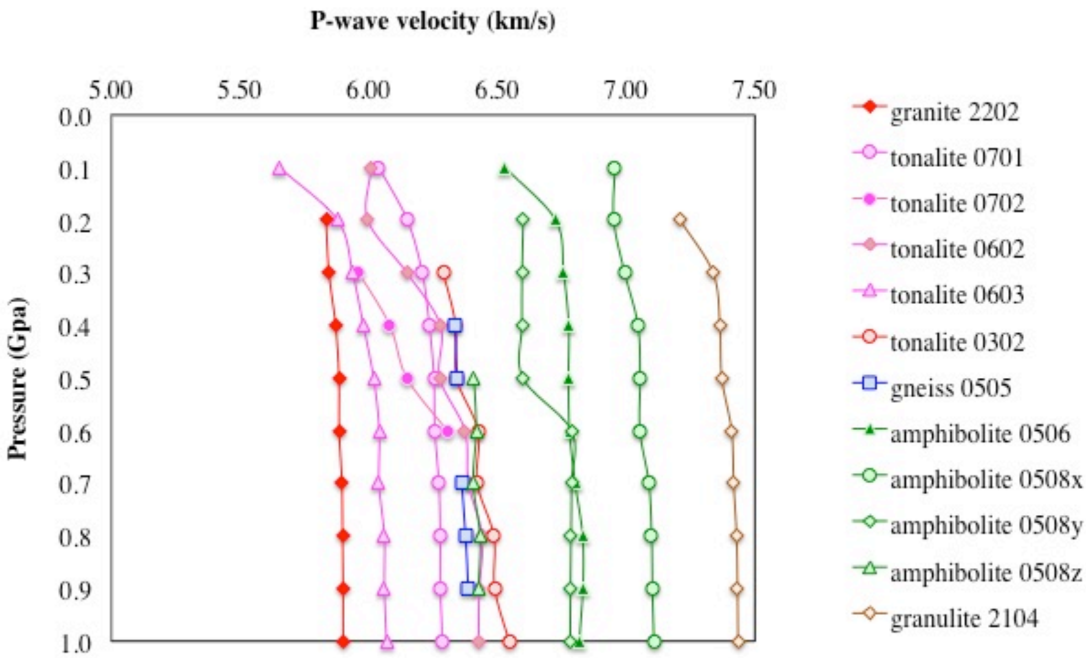

Fig.2 The values of the P-wave velocity measured at room temperature.

References
[1] Iwasaki, T. et al. Tectonophys, 388, 59–73, doi:10.1016/j.tecto.2004.03.025, 2004.
[2] Ito, T. Journal of the Japanese Association for Petroleum Technology, 65, 103-109, 2000
[3] Iwasaki, T. et al. AOGS, SE31-A012, 2014
[4] Matsubara and Obara, Earth Planets Space, 63, 663-667, 2011

P-9 High-resolution sequence stratigraphy of the subaqueous Nakdong Delta on the Korea Strait shelf during the Holocene transgression

Dong-Lim Choi

South Sea Research Institute, Korea Institute of Ocean Science and Technology (KIOST), Geoje 656-834, Korea
E-mail: dlchoi@kiost.ac.kr

ABSRACT

The Nakdong River delta is situated inner shelf off southeastern corner of the Korean Peninsula (Fig. 1). The offshore area of the Nakdong delta has an active depositional environment where river-supplied sediment is being deposited during the high-frequency glacio-eustatic sea-level cycle in Late Quaternary. The study area, along the southeast Korean Peninsular coast, has dominantly a microtidal range, which is semidiurnal, with amplitude ranging from 0.4 m during neap tides to 1.7 m during spring tides. An early study shows that ten million tons of fluvial sand and mud from the Nakdong River are annually supplied into the shelf (KMO, 1974). The Nakdong delta depositional system is recognized in detail through high-resolution 'Chirp' seismic profiles encompassing from the mouth of the river to offshore. The correlation of seismic profiles with a long core data is determined for lithology of bounding surfaces and systems tracts and their ages.

The sequence comprises a group of the transgressive and highstand systems tracts above the type I sequence boundary and their bounding surfaces of ravinement and maximum flooding surfaces (Fig. 2). The sequence boundary coincided with the transgressive surface is formed by erosional surface associated with an incised valley, indicating a possible former location of the Nakdong River during the last glacial maximum. The transgressive systems tract just above the sequence boundary consists of the lower and upper depositional sequences, bounded by a ravinement surface, during the early Holocene sea-level rising between 12.0 and 6.0 ka BP. The lower depositional unit mostly occurs in the incised valley area, comprising fluvio-estuarine sediments, whereas the upper one nearshore environments consisting of sand sheet and ridges. Stacking pattern of these sequences demonstrates overall retrogradation landward. During the late Holocene sea-level highstand of last 6.0 ka BP, the highstand systems tract overlying the maximum flooding surface established the deltaic system, formed as a seaward progradation pattern. The subaqueous Nakdong delta system has been evolved with the depositional sequence of the retrogradational transgressive and then the progradational highstand systems tract over a sequence boundary during the Holocene transgression.

References

KMC (Korea Ministry of Construction), 1974, Report on the Nakdong estuary: Industrial site investigation. Unpublication Report, 56 p. (in Korean).

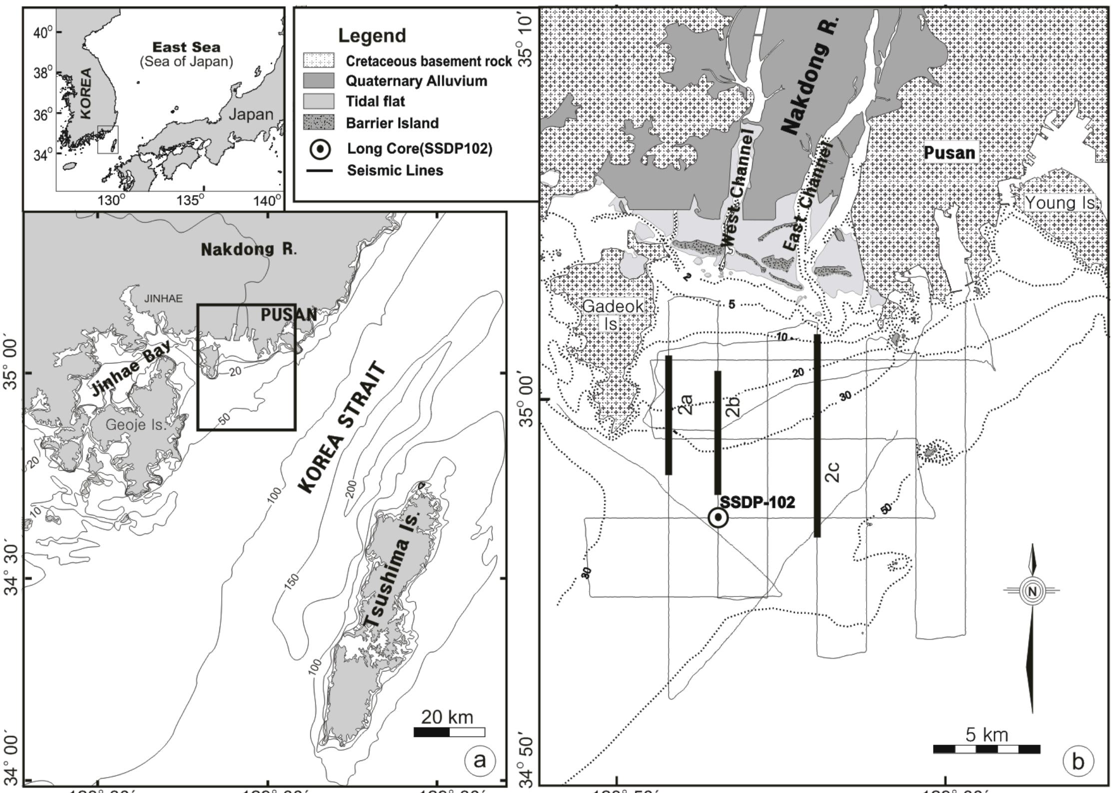

Fig. 1. Map of (a) bathymetry of the study area and its surrounding (depth in meter) and (b) locations of high-resolution 'Chirp' seismic tracklines and a long core (SSDP-102). Heavy lines with numbers denote the locations of seismic profiles shown in corresponding figures.

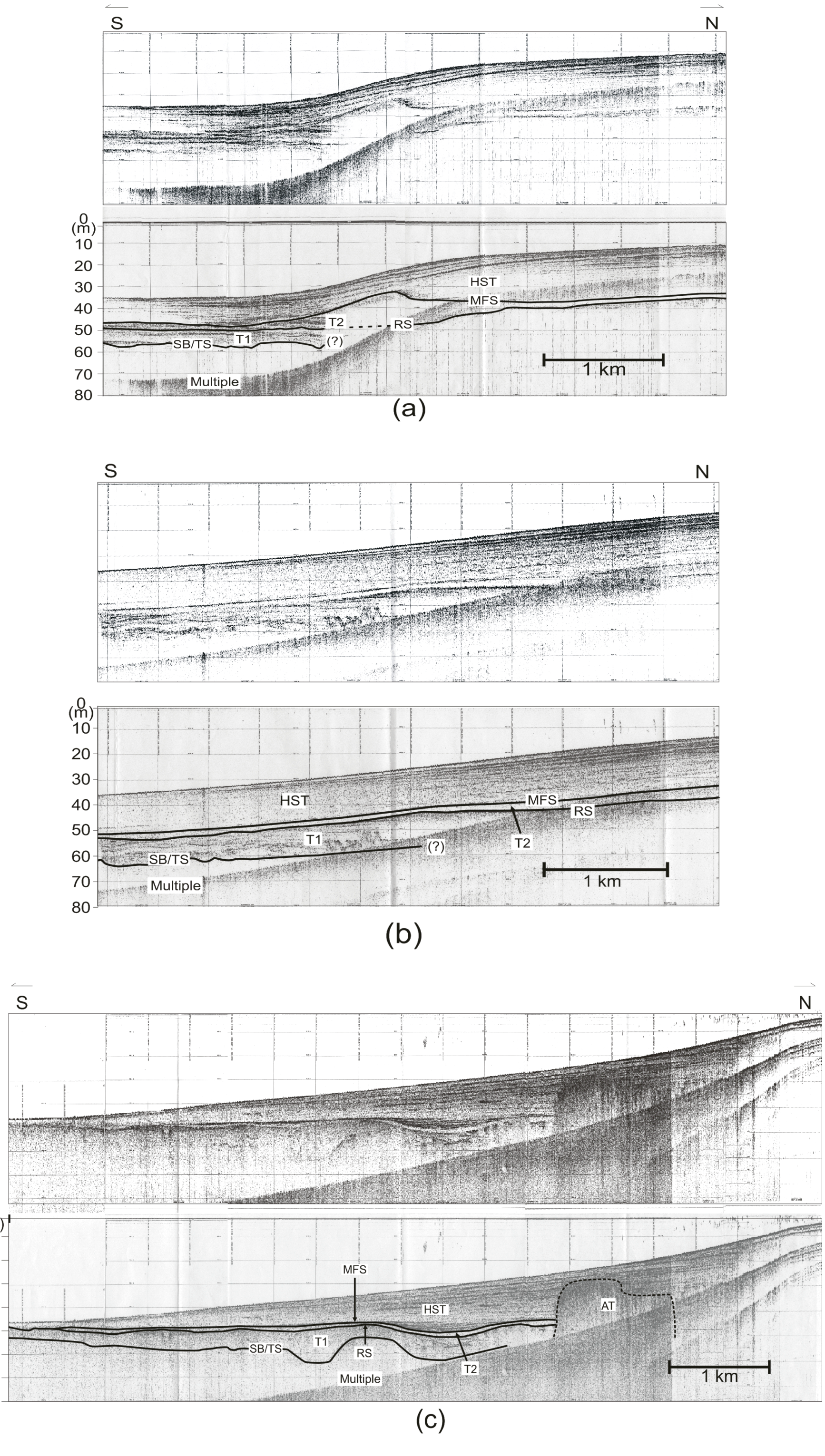

Fig. 2. Uninterpreted and interpreted high-resolution 'Chirp' seismic profiles.
HST, Highstand Systems Tract; MFS, Maximum Flooding Surface;
RS, Ravinement Surface; TS, Transgressive Surface;
SB, Sequence Boundary; AT, Acoustic Turbidity